CONTROL OF PNEUMATIC SYSTEMS FOR FREE SPACE AND INTERACTION TASKS WITH SYSTEM AND ENVIRONMENTAL UNCERTAINTIES

By

Yong Zhu

Dissertation

Submitted to the Faculty of the

Graduate School of Vanderbilt University

in partial fulfillment of the requirements

for the degree of

DOCTOR OF PHILOSOPHY

in

Mechanical Engineering

December, 2006

Nashville, Tennessee

Approved:

Dr. Eric J. Barth

Dr. Michael Goldfarb

Dr. Nilanjan Sarkar

Dr. Joseph A. Wehrmeyer

Dr. Robert E. Bodenheimer

To my parents and wife

AKNOWLEDGEMENTS

First and foremost, I would like to thank Dr. Eric Barth for being my mentor during the course of this work. Without his insightful, constructive and inspirational advice and guidance, this dissertation would never have been possible. I would also like to acknowledge the financial support from different sources: Dr. Barth's startup fund, the National Science Foundation, Festo Corporation, the National Fluid Power Association and a Teaching Assistantship from the Department of Mechanical Engineering.

I would like to thank Dr. Michael Goldfarb for his insightful comments and providing all necessary experimental devices and tools. I would also like to thank all other professors in my committee: Dr. Nilanjan Sarkar, Dr. Robert Bodenheimer and Dr. Joseph Wehrmeyer for contributing their precious time to this work.

I am very grateful to Dr. Kevin Fite and Dr. Thomas Withrow for always being there to help me with all practical matters. I also want to say thanks to all the current and past members at the Center for Intelligent Mechatronics during my stay. You have helped make this experience much more enjoyable.

Special thanks are due to my parents for teaching me the first, but the most important, lessons of my life when I was still a child and always believing in me and supporting me in every stage of my life. Last but not least, I am truly and deeply indebted to my wife Jing. Being away from you has never been easy, but luckily, you are always there for me. Thank you! I hope I can also be there for you in seeing you through your own Ph.D. at Maryland.

TABLE OF CONTENTS

LIST OF TABLES

LIST OF FIGURES

MECHANICAL ENGINEERING

CONTROL OF PNEUMATIC SYSTEMS FOR FREE SPACE AND INTERACTION TASKS WITH SYSTEM AND ENVIRONMENTAL UNCERTAINTIES

YONG ZHU

Dissertation under the direction of Professor Eric J. Barth

This dissertation presents three control methodologies for pneumatic applications in both free space and constrained environment with system and environmental uncertainties.

First, a model reference adaptive controller (MRAC) is designed to achieve accurate free space position tracking of a pneumatic actuator by estimating and compensating for friction uncertainties. Three parameters of a static friction model are estimated. The controller consists of an inner and outer loop structure. The inner loop provides the desired actuation force through adaptive estimation and the outer loop achieves the desired actuation force through a sliding mode force controller. Both loops are based on Lyapunov stability. Experimental results verify the stability of the controller and show that adaptive control improves position tracking accuracy and reduces payload sensitivity without tuning the friction compensation manually.

Then, a passivity-based approach is taken to carry out stable and dissipative contact tasks with an arbitrary and unknown passive environment (unknown in terms of stiffness and location). A pseudo-bond graph model is developed to prove the passivity of

a pneumatic actuator controlled by proportional valves. Using this model, an open-loop pneumatic actuator can be proven to not be passive, but it can be passified under a simple closed-loop feedback control law. The passivity of the closed-loop system is verified in impact and contact force control experiments.

Finally, an energetically derived control methodology is presented to specify and regulate the oscillatory motion of a pneumatic hopping robot, which constantly switches between free space and a constrained environment (system and environmental uncertainties). The desired full hopping period and the desired flight time are predefined to solve for the static pressure in the upper chamber and the velocity immediately before lift-off. Therefore, during contact, the pressure in the upper chamber is controlled according to a position-based mapping to control the duration of contact, while controlling the total conservative energy of the system specifies the flight time. During flight, both chambers are sealed to preserve the passive dynamics of the system. This control methodology is demonstrated through simulation and experimental results to provide accurate and repeatable energetically efficient hopping motion.

Approved: _____ Date: _____

CHAPTER I

INTRODUCTION AND BACKGROUND

1. Introduction

Friction force is one of the most common system and environmental uncertainties in an electro-mechanical system. For pneumatic actuators, friction mainly exists between the contacts of the piston with cylinder wall. Uncertainty of friction has a direct impact on the dynamics of the system in all regimes of operation. When the system is operating close to zero velocity, friction has a dominant influence on the position tracking steady state error. Generally, direct measurement of friction is not possible, so an adaptive friction compensation method will be first presented for accurate position tracking of a pneumatic actuator in free space by compensating for friction uncertainties. To simplify the controller, an inner force control loop and outer position control loop structure will be implemented.

Interaction between a robot manipulator and an environment is inevitable for the successful execution of many industrial tasks such as polishing, assembly, or deburring, among others. The insertion of a piston into a motor-block is one industrial example where the use of a purely position controlled strategy is inadequate. One of the fastest growing interests in robot research is the interaction and co-existence of robots and humans for such uses as industrial applications, at home for entertainment and other home devices, and in hospitals for health care applications. Improvement in flexibility and compliance and the ability to deal with interaction forces are key aspects during the

interaction. This can be achieved either in a passive way, by using a suitably compliant mechanical device, or in an active way, by designing an interaction control strategy. Conventional industrial robots present contact stability problems when, in particular, the robot comes in contact with a hard, or stiff, environment. Pneumatic manipulators can provide unique flexibility during such interaction and offer the possibility of robots working in close cooperation with humans more feasible and natural. For interaction tasks, whether or not the robot is in contact with the environment is another major system and environmental uncertainty. Two approaches based on passivity and energy will be presented for interaction tasks using pneumatically actuated systems, respectively.

Pneumatic actuators present some unique dynamic features. They are very different from their incompressible fluid power counterparts, hydraulic actuators, due to the compressibility of gas. To carry out stable and dissipative interaction tasks with an arbitrary environment, one feasible approach would be to make the pneumatic system passive with respect to a supply rate consisting of the spool valve position input and the actuation force output. A passive system can interact stably with any strictly passive system. Given that almost all environments are strictly passive, the passivity-based approach should be able to provide a simple and straightforward controller design concept for interaction tasks.

A second energy-based control approach for interaction tasks is carried out on the control design of a pneumatic hopping robot. The conservative energy storage elements in a pneumatic hopping system are analyzed. Instead of tracking a desired trajectory in time, the oscillatory motion is generated by maintaining a desired total conservative energy level during contact. The resulting desired velocity, acceleration and jerk

trajectories are all position-based pre-generated trajectories. By specifying the quasi-linear stiffness of the pneumatic actuator, the duration of contact can be explicitly controlled. By specifying the desired total conservative energy of the system during contact, the flight time can be controlled. The compliance of the pneumatic system allows the difficulty of directly dealing with the transition between free space and a constrained environment (the ground) to be avoided. It also takes full advantage of the pneumatic system compressibility during impact by transforming most of the system kinetic energy (except the cylinder rod kinetic energy) into the internal energy of the compressed air in the lower chamber.

2. Literature Review

"An adaptive controller is a controller with adjustable parameters and a mechanism for adjusting the parameters [1]". Adaptive control has been widely used in research and industrial applications on electrically actuated systems. Armstrong and Canudas de Wit [2] offer a good summary by presenting some typical static and dynamic friction models. Direct and indirect adaptive controls for friction compensation were also discussed for general dynamic systems.

Little work on adaptive friction compensation for pneumatic system has been done because of pneumatic systems' inherent low stiffness and highly nonlinear dynamics. Wang et al. [3] proposed a modified PID controller for a servo pneumatic actuation system through time delay minimization and target position compensation. The mean value of position error is less than 1 mm. An experimental comparison between six different control algorithms including PID, Fuzzy, PID with pressure feedback, Fuzzy

with pressure feedback, sliding mode and Neuro-fuzzy control were presented in [4], but none of them focused on the accuracy of position control. Aziz and Bone [5] proposed an automatic tuning method for accurate position control of pneumatic actuators by combining offline model based analysis with online iteration. The steady state error accuracy is 0.2mm to a step input with some amount of overshoot. A highly accurate (low steady-state error) pneumatic servo positioning system was proposed by Ning and Bone [6] using both Position-Velocity-Acceleration (PVA) and PV control with friction compensation. Although the steady state error can be reduced to as small as 0.01mm, the performance is based on the manual tuning of PVA parameters. Accurate position control of a pneumatic actuator was also carried out through PWM algorithms using on/off solenoid valves by Varseveld and Bone [7]. A PID controller specifying the pulse-width of the on/off signal, with friction compensation and position feedforward control, can provide better than 0.21 mm steady-state accuracy with a rise time of 180 ms for step inputs as large as 64 mm.

Industrial robots perform well at free-space tasks like welding or spray painting, which involve precision positioning but little interaction with the environment. Pneumatic actuators, by contrast, are natural impedances with true mechanical compliance. Forces are controlled by manipulating the difference in pressure between the two chambers of the actuator, and compliance is provided by the compressibility of air. As properly noted by Pratt et. al. [8] in their work regarding series elastic actuators, “lower interface stiffness has advantages as well, including greater shock tolerance, lower reflected inertia, more accurate and stable force control, less damage during inadvertent contact, and the potential for energy storage.” Given their properties, pneumatic actuation

systems present a viable option for force controlled interaction tasks, especially in dealing with system and environmental uncertainties.

Tasks that require a high degree of interaction with the environment require the actuator to be an impedance [9]. Many approaches have been taken to have an actuator contact with an environment and maintain a certain contact force using electrical systems [10], hydraulic systems [11] [12] and pneumatic systems as well [13]. Most of these approaches divide the task into three modes: free space mode, constrained mode and transition mode. Different switching control strategies are used to guarantee stability and minimize bouncing.

One of the most widely used approaches for contact task control is impedance control [14] [15]. The key point of impedance control is that one controller deals with all stages of the contact tasks. Hogan [14] first proposed stable contact tasks using impedance control. Hogan [15] also showed that if a system has the behavior of simple impedance, then the stability of the manipulator is preserved when it is coupled to a stable environment. The limitation of impedance control approach is that it requires accurate environment location and stiffness information in order to *artificially* impose the desired impedance with a bandwidth high enough for stable interaction with stiff surfaces. In the language of impedance control, the advantage of a pneumatic system is that it is already an impedance, as opposed to an admittance, and does not require high bandwidth feedback to artificially impose this.

A passivity-based control approach for interaction tasks has been pursued by some researchers for hydraulically and electrically actuated systems. The directional control valve is the only non-passive device in a hydraulic actuation system. Li [16] has

proven that if appropriate first order or second order spool dynamics can be implemented, the spool valve can become passive. The same dynamic passive valve method has been used in bilateral teleoperation of a hydraulic actuator [17]. The passivity concept was also used to design a hydraulic backhoe/force feedback joystick system [18]. Other than hydraulic systems, some other passive systems, such as Cobots [19] and smart exercise machines [20], have also been designed for various human-robot interaction tasks. As will be shown, the fundamental energetic properties of pneumatic actuation can be exploited through passivity-based analysis to provide stable interaction forces with any passive environment.

The aim of the third part of the work is to design a control methodology that takes advantage of the passive dynamics of pneumatic actuation that will result in energetically efficient oscillatory motion when dissipation is present. Recent work [21] on high energy-density monopropellant power supply and actuation systems for untethered robotics motivates an energetically savvy approach to the control of such systems with application to legged robots.

Raibert was a pioneer in legged robot locomotion research. He first presented the design and control of a pneumatic hopping robot in [22]. The hopping is generated in an intuitive manner where the upper chamber is charged when the foot is on the ground and exhausted until it reaches a predefined low pressure (15 psi) as soon as it leaves the ground. There is a monotonic mapping between hopping height and thrust value, but this relationship can not be simply characterized. The hopping height can only be chosen based on a set of empirical experimental data. There is also a unique frequency associated with each thrust value.

Raibert used another leg actuation method for better efficiency [22] when the hopping machine works in three dimensions. The upper chamber works as a spring and the lower chamber works as an actuator. The upper chamber is connected to the supply pressure through a check valve. The lower chamber is charged when the foot is in flight and discharged when it is on the ground through a solenoid valve. By controlling the length of charging time during flight, the hopping height and frequency can be implicitly controlled.

For an electrically actuated robot, if no active force control is implemented to effectively absorb the energy during contact, oscillations and even instability can occur. For example, joint acceleration feedback was used to control the contact transition of a three-link direct-drive robot [10]. Aiming at control and energetics, a monopod running robot with hip and leg compliance was controlled by taking advantage of the "passive dynamic" operation close to the desired motion without any actuation [23]. It was shown that 95% of hip actuation energy was achieved passively at 3 m/s running speed. This idea is similar to the approach used in the work presented in this dissertation, except the compliance and hence passive dynamics will be specified by the compressibility of gas in a pneumatic actuator.

Suffering from highly nonlinear dynamics, varying environment conditions and frequent phase transitions between free space and constrained motions, legged robot researchers generally face the challenge of real-time motion planning and control simultaneously. Changing interactions with the environment present extreme challenges for such systems. Looking toward nature, the compliance of tendons show great advantages for the interaction tasks experienced in legged locomotion. Series elastic

actuators have been applied to walking robot applications [24]. A hopping robot "Kenken" with an articulated leg and two hydraulic actuators as muscles and a tensile spring as a tendon was studied, although stability problems remained for higher speeds [25]. Mckibben artificial muscles were used for a hopping robot to pursue higher power-to-weight ratio [26], but the end-effects of the McKibben actuators limited their application. A dynamic walking biped "Lucy" actuated by pneumatic artificial muscles was investigated in [27]. Although artificial muscles can be used as actuators for legged robots and provide high power-to-weight ratio and shock absorption, they have some challenging limitations, such as hysteresis and short stroke.

Pneumatic actuators can be used directly as legs to drive a legged robot, which provide much higher power-to-weight ratio than their electrically actuated competitors. A small six-legged pneumatic walking robot named Boadicea was designed using customized lightweight pneumatic actuators and solenoid valves [28]. The performance clearly showed high force and power density, which implies that the robot can walk faster with larger payloads. Other advantages such as energy storage, and natural compliance for shock absorption, provide appealing latitude for stable and energy efficient controller design with pneumatically actuated systems. The absorbed energy can be stored as the internal energy of compressed air and can be released again when the hopper is in flight. Fast real-time gaits are generated for the control of a pneumatically actuated robot in [29]. The control system generates the desired trajectories on line and generates proper control inputs to achieve the desired trajectories. An energy-based Lyapunov function was chosen to generate the controlled limit cycles. This is similar to the approach we are taking, except this work will generate a desired velocity based on the current position and

direction of motion. The compliance of pneumatic actuators has been proven to be of great importance when a robot interacts with unknown environment perturbations [30].

3. Contribution

In the first part of this work, a model reference adaptive controller (MRAC) for compensating friction and payload uncertainties in pneumatic system is designed. Experimental results show that adaptive control improves position tracking and reduces payload sensitivity without tuning friction compensation parameters manually. The positioning accuracy can be controlled within $\pm$ 0.1mm for a 60 mm step input (rise time is about 200 ms). For both step and sinusoidal inputs, the pneumatic actuator can reject a payload disturbance and maintain good position tracking.

In the second part of this work, a pseudo-bond graph model with the inner product between spool valve position input and actuation force output as a pseudo supply rate is developed. Using this pseudo-bond graph model, an open-loop pneumatic actuator controlled by a four-way proportional valve can be proven to not be passive with respect to the pseudo supply rate. More importantly, it can also be proven to be passive with respect to the pseudo supply rate under a closed-loop feedback control law. The passivity of this closed-loop pneumatic actuator is verified in dissipative impact and force control experiments when the actuator interacts with an unknown environment. The pseudo-bond graph model can be used in other passivity analyses and controller designs for pneumatic actuation systems.

In the third part of this work, the kinetic and potential energy of a pneumatic actuator is first analyzed. Then an energetically efficient hopping control methodology

for pneumatically actuated robots is developed. The control strategy is energy based and takes advantage of the natural passive dynamics of the system to provide much of the required actuation forces, while the remaining forces needed to overcome the energy dissipation present in a non-ideal system with losses are provided by a nonlinear control law for the charging and discharging of the actuator. Both the hopping period and the flight time can be specified explicitly by specifying the natural stiffness of the cylinder and the total conservative energy. This control methodology is demonstrated experimentally to provide accurate and repeatable oscillation in the presence of dissipative forces.

4. Organization of the Document

The dissertation is organized as three independent journal article manuscripts for the three control methodologies. In Chapter II (manuscript 1), the adaptive control based position control in free space is presented. In Chapter III (manuscript 2), the passivity-based control strategy to carry out stable interaction tasks is presented. In Chapter IV (manuscript 3), the energy-based control strategy for a pneumatic hopping robot is presented. Each section includes an addendum section for additional details not covered in the article.

References

[1] Astrom, K. J. and Wittenmark, B., *Adaptive Control*, Pearson Education Inc, 1995.

[2] Armstrong, B. and Canudas de Wit, C., "Friction Modeling and Compensation," *The Control Handbook* (by William S. Levine), CRC Press, pp. 1369-1382, 1996.

[3] Wang, J, Pu, J. and Moore, P., "Accurate Position Control of Servo Pneumatic Actuator Systems: an Application for Food Packaging," *Control Engineering Practice*, vol. 7, pp. 699-706, 1999.

[4] Chillari, S., Guccione, S. and Muscato, G., "An Experimental Comparison between Several Pneumatic Position Control Methods," *Proceedings of the 2001 IEEE Conference on Decision and Control*, pp. 1168-1173, 2001.

[5] Aziz, S. and Bone, G. M., "Automatic Tuning of an Accurate Position Controller for Pneumatic Actuators," *Proceedings of the 1998 IEEE/RSJ International Conference on Intelligent Robots and Systems*, pp.1782-1788, 1998.

[6] Ning, S. and Bone, G. M., "High Steady-state Accuracy Pneumatic Servo Positioning System with PVA/PV Control and Friction Compensation," *Proceedings of the 2002 IEEE International Conference on Robotics and Automation*, pp. 2824-2829, 2002.

[7] Van Varseveld, R. B. and Bone, G. M., "Accurate Position Control of a Pneumatic Actuator Using On/Off Solenoid Valves," *IEEE/ASME Transactions on Mechatronics*, vol. 2, no. 3, pp. 195-204, 1997.

[8] Pratt, G. A., Williamson, M. M., Dillworth, P., Pratt, J., Ulland, K., and Wright, A., "Stiffness Isn't Everything," *The 4th International Symposium on Experimental Robotics*, Stanford, California, 1995.

[9] Hogan, N., "Impedance Control: An Approach to Manipulation: Part I - Theory," *Transactions of the ASME in the Journal of Dynamic Systems, Measurement, and Control*, vol. 107, pp. 1-7, 1985.

[10] Wu, Y., Tarn, T., Xi, N. and Isidori, N., "On Robust Impact Control via Positive Acceleration Feedback for Robot Manipulators," *Proceedings of the 1996 IEEE International Conference on Robotics and Automation*, pp. 1891-1896, 1996.

[11] Niksefat, N., Wu, C. Q. and Sepehri, N., "Design of a Lyapunov Controller for an Electro-hydraulic Actuator During Contact Tasks," *Transactions of the ASME in the Journal of Dynamic Systems, Measurement and Control*, vol. 123, pp. 299-307, 2001.

[12] Sekhavat, P., Wu, Q. and Sepehri, N., "Impact Control in Hydraulic Actuators," *Transactions of the ASME in the Journal of Dynamic Systems, Measurement and Control*, vol. 127, pp. 197-205, 2005.

[13] Bobrow, J. E. and McDonell, B. W., "Modeling, Identification, and Control of a Pneumatically Actuated, Force Controllable Robot," *IEEE Transactions on Robotics and Automation*, vol. 14, pp. 732-742, 1998.

[14] Hogan, N., "Stable Execution of Contact Tasks Using Impedance Control," *Proceedings of the 1987 IEEE international Conference on Robotics and Automation*, pp. 1047-1054, 1987.

[15] Hogan, N., "On the Stability of Manipulators Performing Contact Tasks," *IEEE Journal of Robotics and Automation*, vol. 4, pp. 677-686, 1988.

[16] Li, P., "Toward Safe and Human Friendly Hydraulics: The Passive Valve," *Transactions of the ASME in the Journal of Dynamics, Measurement and Control*, vol. 122, pp. 402-409, 2000.

[17] Krishnaswamy, K. and Li, P., "Passive Teleoperation of a Multi Degree of Freedom Hydraulic Backhoe Using Dynamic Passive Valve," *Proceedings of the 2003 International Mechanical Engineering Congress and Exposition*, Washington D.C., pp. 149-156, 2003.

[18] Krishnaswamy, K. and Li, P., "Bond Graph Based Approach to Passive Teleoperation of a Hydraulic Backhoe," *Transactions of the ASME in the Journal of Dynamics, Measurement and Control*, vol. 128, pp. 176-185, 2006.

[19] Colgate, J. E., Wannasuphoprasit, W. and Peshkin, M. A., "Cobots: Robots for Collaboration with Human Operators," *Proceedings of the 1996 International Mechanical Engineering Congress and Exposition*, vol. 58, New York, NY, pp. 433-439, 1996.

[20] Li, P. Y. and Horowitz, R., "Control of Smart Exercise Machines: Part I. Problem Formulation and Non-adaptive Control," *IEEE/ASME Transactions on Mechatronics*, vol. 2, no. 4, pp. 237-247, 1996.

[21] Goldfarb, M., Barth, E. J., Gogola, M. A. and Wehrmeyer, J. A., "Design and Energetic Characterization of a Liquid-propellant-powered Actuator for Self-powered Robots," *IEEE/ASME Transactions on Mechatronics*, vol. 8, no. 2, pp. 254-262, 2003.

[22] Raibert, M., *Legged Robots that Balance*, MIT Press, Cambridge, MA, 1986.

[23] Ahmadi, M. and Buehler, M., "Stable Control of a Simulated One-legged Running Robot with Hip and Leg Compliance," *IEEE Transactions on Robotics and Automation*, vol. 13, no. 1, pp. 96-104, 1997.

[24] Williamson, M. M., *Series Elastic Actuators*, Master's thesis, MIT, Cambridge, MA, 1995.

[25] Hyon, S. H. and Mita, T., "Development of a Biologically Inspired Hopping Robot – 'Kenken'," *Proceedings of the 2002 IEEE International Conference on Robotics and Automation*, Washington DC, pp. 3984-3991, 2002.

[26] Delson, N., Hanak, T., Loewke, K. and Miller, D. N., "Modeling and Implementation of McKibben Actuators for a Hopping Robot," *Proceedings of the 12th Annual International Conference on Advanced Robotics (ICAR)*, Seattle, Washington, pp. 833-840, 2005.

[27] Verrelst, B., *A Dynamic Walking Biped Actuated by Pleated Pneumatic Artificial Muscles: Basic Concepts and Control Issues*, Ph.D dissertation, Vrije Universiteit Brussel, 2005.

[28] Binnard, M. B., *Design of a Small Pneumatic Walking Robot*, master's thesis, MIT, Cambridge, MA, 1995.

[29] M'sirdi, N. K., Manamani, N. and Nadjar-Gauthier, N., "Methodology based on CLC for Control of Fast Legged Robots," *Proceedings of the 1998 IEEE/RSJ International Conference on Intelligent Robotics and Systems*, Victoria, B.C., Canada, pp. 71-76, 1998.

[30] Guihard, M. and Gorce, P., "Dynamic Control of a Large Scale of Pneumatic Multichain Systems," *Journal of Robotic Systems*, vol. 21, no. 4, pp. 183-192, 2004.

CHAPTER II

MANUSCRIPT I

ACCURATE POSITION CONTROL FOR PNEUMATIC ACTUATORS USING MRAC

Yong Zhu and Eric J. Barth

Department of Mechanical Engineering
Vanderbilt University
Nashville, TN 37235

Submitted as a Full Paper to the *International Journal of Fluid Power*

Abstract

Adaptive control is a popular method of controlling the dynamic system with uncertainties or slowly changing parameters. Friction and payload are probably the most common uncertainties in mechanical systems. A model reference adaptive controller (MRAC) for compensating friction and payload uncertainties in a pneumatic system is presented in this paper. The parameters of a static friction model are estimated. Because of the asymmetric nature of the Coulomb friction in our pneumatic system, a two-direction Coulomb friction model is adopted using two parameters. Estimated actuation force is used as the command of the inner force control loop, which is controlled by a sliding mode controller. Both the force control loop and the adaptation law are Lyapunov stable. Experimental results verify the theory and show that adaptive control improves position tracking and reduces payload sensitivity without tuning friction compensation parameters manually. The positioning accuracy can be controlled within ± 0.1mm for a 60 mm step input with a rise time around 200 ms. Both step and sinusoidal inputs can reject the payload disturbance and maintain good position tracking.

1. Introduction

Although pneumatic actuators are highly nonlinear due to the compressibility of air, they still provide a better alternative to electric or hydraulic systems for some applications, such as assembly task, which requires the system to work in a constrained environment [1]. For pneumatic actuators, friction mainly exists between the contacts of the piston with cylinder wall. Friction and load mass have a direct impact on the dynamics of the system in all regimes of operation. Especially, when the system is

operating close to zero velocity, friction has a dominant influence on position control performance. Generally, the direct measurement of friction is not straightforward, so an adaptive friction compensation method will be proposed here.

Armstrong and Canudas de Wit [2] proposed several static and dynamic friction models. Direct and indirect adaptive controls for friction compensation were also discussed for general dynamic systems. Three adaptive controllers for a permanent magnet linear synchronous motor position control system were proposed in [3], including a backstepping adaptive controller, a self-tuning adaptive controller and a model reference adaptive controller. The position control performance of this paper was compared with their work on motor system, which proves that pneumatic actuators can provide as accurate position control as electric systems. Adaptive automatic voltage control in fusion arc welding is presented in [4], an adaptive controller is used to identify the arc sensitivity characteristic and adapt in real time for good welding response without priori knowledge of the system.

Because of pneumatic system's inherent low stiffness and unique direct drive capability, very little work about adaptive friction compensation for pneumatic system has been done. Wang et al. [5] proposed a modified PID controller for servo pneumatic actuator system, time delay minimization and target position compensation algorithm were used to achieve accurate position control. The position accuracy can be controlled within ± 1 mm. An experimental comparison between six different control algorithms including PID, Fuzzy, PID with pressure feedback, Fuzzy with pressure feedback, sliding mode and Neuro-fuzzy control were presented in [6], but none of them focused on the accuracy of position control. Aziz and Bone [7] proposed an automatic tuning method for

accurate position control of pneumatic actuators by combining offline model based analysis with online iteration. The steady state error accuracy is 0.2 mm and overshoot exists in step response. A high steady-state accuracy pneumatic servo positioning system was proposed by Ning and Bone [8] using PVA/PV control and friction compensation. Although the steady state error can be minimized as small as 0.01mm, the system is based on manual tuning of PVA parameters, and good parameter combination can easily generate big overshoot, or even jeopardize the stability of the system. The system also has a long rise time. Basically, this is a system based on high-resolution encoder position feedback and simple feedback control methodology. In [9], a nonlinear position controller for a pneumatic actuator with friction was proposed, nonlinear modification to the designed PI controller was introduced. Regulating errors less than $\pm$ 1 mm were achieved consistently. When the demanding reference tracking tasks covers 60% of the actuator stroke, the maximum steady state error increased to 4mm. Accurate position control of a pneumatic actuator was also carried out using on/off solenoid valves by Varseveld and Bone [10].

Accurate position control of a pneumatic system using a proportional valve will be presented in this work. The proposed controller has a partitioned control structure as shown in Figure 2-1. The inner force control loop deals with the highly nonlinear dynamics of compressed air using a first order sliding mode controller to achieve the desired actuation force. The outer loop provides the desired actuation force for the inner loop using a MRAC.

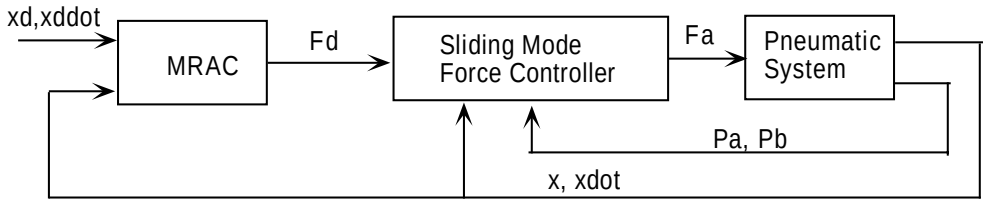

Figure 2-1. Position control structure for pneumatic actuators using MRAC.

The rest of this paper is organized as follows. In Section 2, the friction model will be first presented. In Section 3, the sliding mode force controller will be proposed and experimental results will be presented to show the fast and accurate force tracking up to 20 Hz. In Section 4, a MRAC will be designed to estimate the friction parameters. In Section 5, experimental results will be presented to show the accurate position control performance and the ability to accommodate payload uncertainty. Section 6 contains the concluding remarks.

2. Friction Model

In order to compensate friction and achieve precise position control, an accurate and feasible friction model needs to be chosen first. Although friction occurs in almost all mechanical systems, there is no universal friction model that can be used for any system. For different systems and control objectives, different friction models are adopted to ease the task. A simple Gaussian exponential static friction model can be represented in Equation (1) as a function of instantaneous sliding velocity $v(t)$, which captures three basic frictions: coulomb, viscous and Stribeck friction.

$$F[v(t)] = F_c \operatorname{sgn}[v(t)] + F_s e^{-[v(t)/v_s]^2} \operatorname{sgn}(v(t)) + F_v v(t) \qquad (1)$$

Where F_c is the coulomb friction, F_s is the magnitude of the Stribeck friction, which is the excess of static friction over coulomb friction, F_v is the viscous friction and v_s is the characteristic velocity of the Stribeck friction. By choosing different parameters, different friction models can be realized. This is one of the best models describing the zero velocity friction force. Figure 2-2a shows how friction force may evolve continuously from the static friction level. The Stribeck effect happens very close to zero velocity. Therefore, it is very hard to capture it using an adaptive law due to the lack of consistent excitation around zero velocity. A simpler friction model including only Coulomb friction and viscous friction, as shown in Figure 2-2b, will be used for adaptive friction compensation of the pneumatic system. It can be seen later in the experimental results that the tracking performance does not deteriorate obviously because of this simplified friction model. Because the Coulomb friction of the pneumatic system we are using is not symmetric, it is represented by two parameters for positive and negative direction, respectively. So the friction force F_f can be represented as,

$$F_f[v(t)] = F_v v(t) + F_{cpos}\, sat1[\mathrm{sgn}(v(t))] + F_{cneg}\, sat2[\mathrm{sgn}(v(t))] \tag{2}$$

Where F_v is the viscous friction parameter, F_{cpos} and F_{cneg} are the positive and negative direction Coulomb friction. $sat1(\cdot) \geq 0$ and $sat(\cdot) < 0$ are two saturation functions to capture the positive and negative direction velocity information, respectively, for the parameter adaptation of two Coulomb friction parameters.

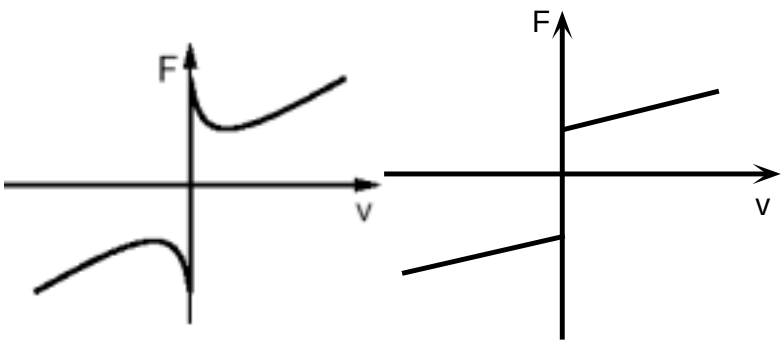

(a) (b)

Figure 2-2. Friction models. (a) with Stribeck effect and (b) without Stribeck effect.

3. Sliding Mode Force Controller

Sliding mode control can maintain stability and good performance for nonlinear control systems with modeling inaccuracies, which fits well with pneumatic control systems. The force provided by the pneumatic actuator with the pressures in each side of the cylinder P_a and P_b acting on their respective areas A_a and A_b along with atmospheric pressure P_{atm} acting on the area of the rod $A_r = A_a - A_b$ can be represented as:

$$F_a = P_a A_a - P_b A_b - P_{atm} A_r \tag{3}$$

Taking derivative of Equation (3) yields,

$$\dot{F}_a = \dot{P}_a A_a - \dot{P}_b A_b \tag{4}$$

The rate of change of pressure within each pneumatic chamber can be expressed as:

$$\dot{P}_{(a,b)} = \frac{\gamma RT}{V_{(a,b)}} \dot{m}_{(a,b)} - \frac{\gamma P_{(a,b)} \dot{V}_{(a,b)}}{V_{(a,b)}} \tag{5}$$

where γ is the thermal characteristic coefficient, with $\gamma = 1$ for isothermal case, R is the ideal gas constant, T is the temperature, V is the control volume, and P is the pressure. The nonlinear relationship between the valve orifice area and the mass flow rate is given by:

$$\dot{m}_a = A_v \psi_a (P_u, P_d) \tag{6}$$

$$\dot{m}_b = -A_v \psi_b (P_u, P_d) \tag{7}$$

where A_v is the high-bandwidth controlled orifice area of the valve and $\Psi(P_u, P_d)$ is the area normalized mass flow rate relationship as a function of the pressure upstream and downstream of the valve. By virtue of the physical arrangement of the valve, the driving pressures of $\Psi(P_u, P_d)$ are dependent on the sign of the "area". A positive area A_v indicates that the spool of the proportional valve is positioned such that a flow orifice of area A_v connects the high pressure pneumatic supply to one side of the pneumatic cylinder, and thereby promotes a positive mass flow rate into the cylinder chamber. A negative area A_v indicates that the spool of the proportional valve is positioned such that an orifice of area A_v connects one side of the pneumatic cylinder to atmospheric pressure, and thereby promotes a negative mass flow rate (exhaust from the cylinder chamber). Using this convention, the area normalized mass flow rate can be written as:

$$\Psi(P_u, P_d) = \begin{cases} \Psi(P_s, P) & \text{for } A \geq 0 \\ \Psi(P, P_{atm}) & \text{for } A < 0 \end{cases} \tag{8}$$

A common mass flow rate model used for compressible gas flowing through a valve is given by,

$$\Psi(P_u, P_d) = \begin{cases} \dfrac{C_1 C_f P_u}{\sqrt{T}} & \text{if } \dfrac{P_d}{P_u} \le C_r \text{ (choked)} \\ \dfrac{C_2 C_f P_u}{\sqrt{T}} \left(\dfrac{P_d}{P_u}\right)^{(1/k)} \sqrt{1 - \left(\dfrac{P_d}{P_u}\right)^{(k-1)/k}} & \text{otherwise (unchoked)} \end{cases} \tag{9}$$

where P_u and P_d are the upstream and downstream pressures, C_f is the discharge coefficient of the valve, k is the ratio of specific heats, C_r is the pressure ratio that divides the flow regimes into choked and unchoked flow and C_1 and C_2 are constants defined as:

$$C_1 = \sqrt{\frac{k}{R}\left(\frac{2}{k+1}\right)^{(k+1)/(k-1)}} \text{ and } C_2 = \sqrt{\frac{2k}{R(k-1)}} \tag{10}$$

The objective of the force control is to make the actuation force F_a to track a desired force trajectory F_d. The actuation force tracking error is defined as $e = F_a - F_d$. It can be seen from Equations (4)-(7) that $\dot{F}_a$ is directly related to the control input $u = A_v$ through pressure dynamics. Therefore, the dynamic model of the pneumatic actuator force control is a first order nonlinear system ($n = 1$) if the dynamics of the valve spool position control is neglected. This single input dynamic system can be put into standard form as:

$$\dot{F}_a = f(\mathrm{X}) + b(\mathrm{X})u \tag{11}$$

Where X is the state vector. The standard time varying surface is defined as $s = \left(\frac{d}{dt} + \lambda\right)^{n-1} e$, for $n = 1$, it becomes, $s = e = F_a - F_d = P_a A_a - P_b A_b - P_{atm} A_r - F_d$, Taking derivative of s and substituting Equation (5) into $\dot{s}$ yield the sliding mode equation:

$$\dot{s} = (\frac{RT}{V_a}\dot{m}_a - \frac{P_a\dot{V}_a}{V_a})A_a - (\frac{RT}{V_b}\dot{m}_b - \frac{P_b\dot{V}_b}{V_b})A_b - \dot{F}_d \tag{12}$$

Equating Equation (12) to zero yields,

$$(\frac{RT}{V_a}\dot{m}_a - \frac{P_a\dot{V}_a}{V_a})A_a - (\frac{RT}{V_b}\dot{m}_b - \frac{P_b\dot{V}_b}{V_b})A_b - \dot{F}_d = 0 \tag{13}$$

Substituting Equations (6) and (7) into Equation (13) gives,

$$[\frac{A_a}{V_a}\psi_a(P_u, P_d) + \frac{A_b}{V_b}\psi_b(P_u, P_d)]RTu - \frac{P_a\dot{V}_aA_a}{V_a} + \frac{P_b\dot{V}_bA_b}{V_b} - \dot{F}_d = 0 \tag{14}$$

Solving Equation (14) for equivalence control law:

$$u_{eq} = \frac{(P_aA_a^2V_b + P_bA_b^2V_a)\dot{x} + V_aV_b\dot{F}_d}{RT[A_aV_b\psi_a(P_u, P_d) + A_bV_a\psi_b(P_u, P_d)]} \tag{15}$$

Then a discontinuous robustness term is added across the sliding surface to achieve the complete sliding mode control law:

$$u = u_{eq} - \kappa sat(\frac{s}{\phi}) \tag{16}$$

where κ and ϕ are positive constants [11]. This control law can be easily proven to be Lyapunov stable. The actuation force tracking performance for 1 Hz and 20 Hz sinusoidal inputs is shown in Figure 2-3. Up to 30 Hz, the valve and controller can still provide good force tracking. In these experiments, the cylinder rod is fixed at the middle stroke position.

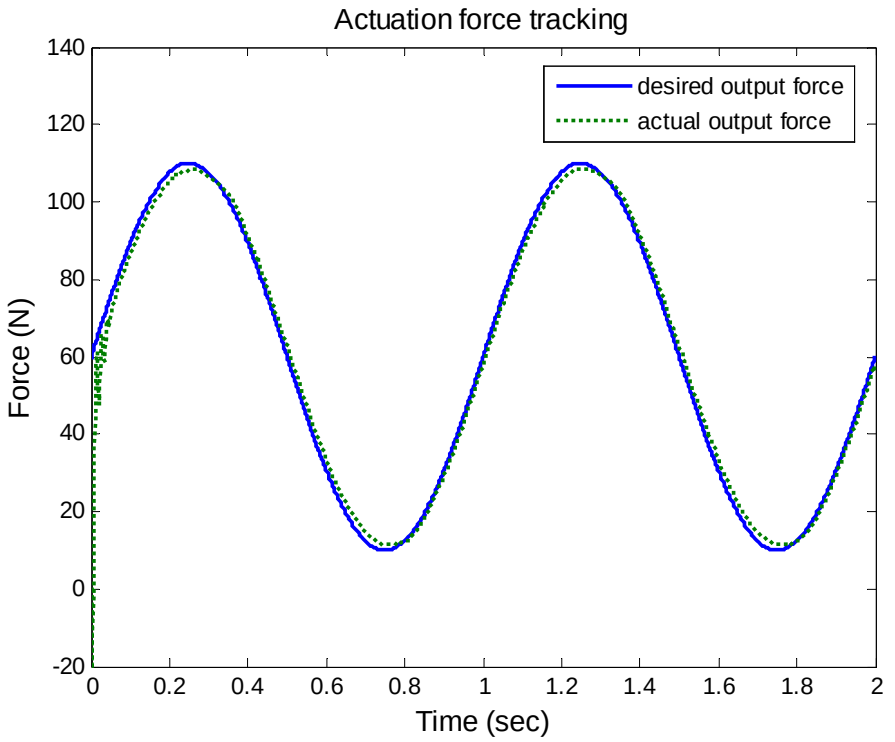

(a)

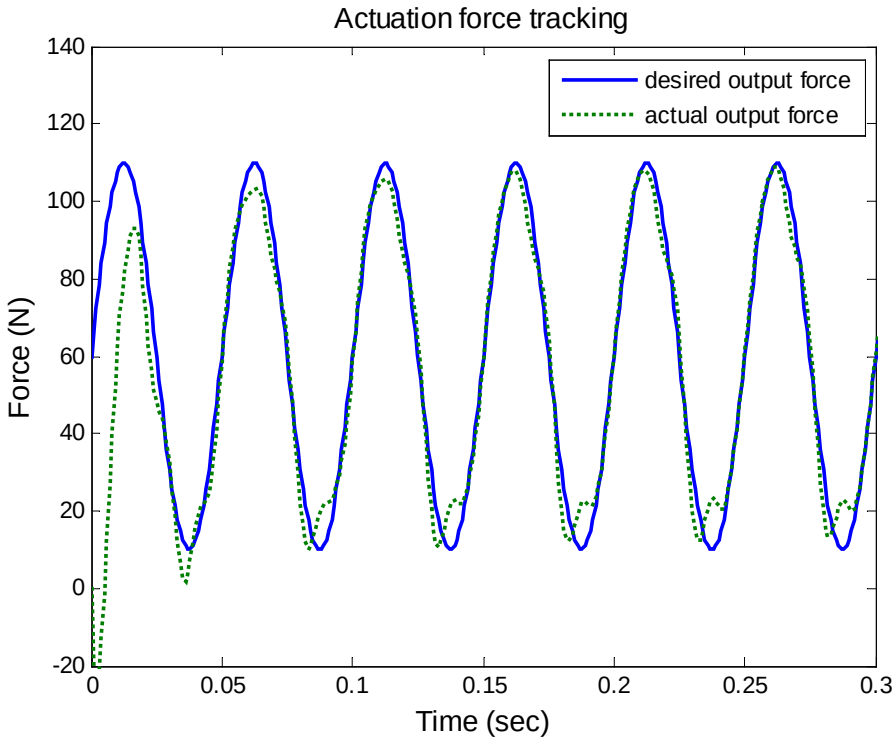

(b)

Figure 2-3. Experimental results of actuator force tracking for sinusoidal input with frequency: (a) 1 Hz and (b) 20 Hz.

4. Design of a MRAC for Adaptive Friction Compensation

A model reference adaptive controller will be designed for friction compensation in this section. In the previous research, the moving mass M is firstly chosen as one of the adaptive parameters. Experimental results show all the adaptive parameters could not converge. The reason is twofold: on one hand, M has little chance to converge to the real physical value of moving mass. On the other hand, since M appears in the denominators of the adaptation law of other parameters, there is no way for other parameters to converge to their proper estimates when their adaptation law is also changing dramatically. Another important lesson learned from the initial research is using one Coulomb friction parameter to represent a symmetric Coulomb friction model will not successfully minimize the position tracking error. The Coulomb friction of our pneumatic system is asymmetric. Therefore, if the position errors in positive direction and negative direction are mixed together as the error information to feed one Coulomb friction adaptive law, this parameter will not converge but just roams around the initial value. Based on the initial approach and experimental results, the mass estimation is dropped out of the adaptation law and Coulomb friction is decoupled into two directions using two different parameters. So three friction parameters: F_v, F_{cpos} and F_{cneg} will be estimated. The experimental results will show that although mass adaptation is not included in the adaptation law, the system can still accommodate the payload disturbance through the adaptation of the three friction parameters.

The open loop dynamics of the pneumatic cylinder can be represented as:

$$F = M\ddot{x} + F_v\dot{x} + F_{cpos}sat1[\mathrm{sgn}(\dot{x})] + F_{cneg}sat2[\mathrm{sgn}(\dot{x})] \tag{17}$$

The control law is arbitrarily chosen as,

$$\hat{F} = M(\ddot{x}_d + k_v\dot{e} + k_p e) + \hat{F}_v\dot{x} + \hat{F}_{cpos}sat1[\text{sgn}(\dot{x})] + \hat{F}_{cneg}sat2[\text{sgn}(\dot{x})] \quad (18)$$

where $e = x_d - x$. k_v and k_p are positive constants chosen to reflect the performance specifications of the reference model. $\hat{F}_v$, $\hat{F}_{cpos}$ and $\hat{F}_{cneg}$ are three parameter estimates. Combining Equation (17) and (18) gives:

$$\begin{aligned} &M\ddot{x} + F_v\dot{x} + F_{cpos}sat1[\text{sgn}(\dot{x})] + F_{cneg}sat2[\text{sgn}(\dot{x})] \\ &\quad = M(\ddot{x}_d + k_v\dot{e} + k_p e) + \hat{F}_v\dot{x} + \hat{F}_{cpos}sat1[\text{sgn}(\dot{x})] + \hat{F}_{cneg}sat2[\text{sgn}(\dot{x})] \end{aligned} \quad (19)$$

Subtracting $M\ddot{x}$ from both sides of Equation (19) yields:

$$\begin{aligned} &F_v\dot{x} + F_{cpos}sat1[\text{sgn}(\dot{x})] + F_{cneg}sat2[\text{sgn}(\dot{x})] \\ &\quad = M[(\ddot{x}_d - \ddot{x}) + k_v\dot{e} + k_p e] + \hat{F}_v\dot{x} + \hat{F}_{cpos}sat1[\text{sgn}(\dot{x})] + \hat{F}_{cneg}sat2[\text{sgn}(\dot{x})] \end{aligned} \quad (20)$$

Since $\ddot{x}_d - \ddot{x} = \ddot{e}$, Equation (20) can be rearranged as:

$$\begin{aligned} &\ddot{e} + k_v\dot{e} + k_p e \\ &\quad = M^{-1}[(F_v - \hat{F}_v)\dot{x} + (F_{cpos} - \hat{F}_{cpos})sat1[\text{sgn}(\dot{x})] + (F_{cneg} - \hat{F}_{cneg})sat2[\text{sgn}(\dot{x})]] \end{aligned} \quad (21)$$

The proportional plus derivative filtered error is defined as: $e_1(s) = (s + \eta)e(s)$ (expressed in Laplace domain), where η is a positive constant. Equation (21) can be rewritten in matrix form as:

$$\ddot{e} + k_v\dot{e} + k_p e = M^{-1}\underbrace{\begin{bmatrix}\dot{x} & sat1[\text{sgn}(\dot{x})] & sat2[\text{sgn}(\dot{x})]\end{bmatrix}}_{H}\underbrace{\begin{bmatrix}F_v - \hat{F}_v \\ F_{cpos} - \hat{F}_{cpos} \\ F_{cneg} - \hat{F}_{cneg}\end{bmatrix}}_{\tilde{a}} \quad (22)$$

Equation (22) can be simply written as:

$$\ddot{e} + k_v\dot{e} + k_p e = M^{-1}H\tilde{a} \quad (23)$$

Equation (23) can be transformed into Laplace domain as:

$$e(s) = \frac{1}{s^2 + k_v s + k_p} M^{-1} H\tilde{a} \tag{24}$$

Substituting Equation (24) into $e_1(s)$ gives

$$e_1(s) = \frac{s + \eta}{s^2 + k_v s + k_p} M^{-1} H\tilde{a} \tag{25}$$

Equation (25) can be rewritten in state space form (with e_1 as the output):

$$\dot{X} = AX + BM^{-1} H\tilde{a} \tag{26}$$

$$e_1 = CX \tag{27}$$

where $X = \begin{bmatrix} e \\ \dot{e} \end{bmatrix}$, $A = \begin{bmatrix} 0 & 1 \\ -k_p & -k_v \end{bmatrix}$, $B = \begin{bmatrix} 0 \\ 1 \end{bmatrix}$ and $C = [\eta \quad 1]$.

Based on the Kalman-Yakubovich lemma [11], since the transfer function $h(s) = C[sI - A]^{-1} B = (\eta + 1)/(1 + k_p + k_v) > 0$ is strictly positive real, there exists two symmetric positive definite constant matrices P and Q for the system shown in Equations (26) and (27), such that $A^T P + PA = -Q$ and $PB = C^T$. The Lyapunov function candidate can be chosen as the following equation according to a standard form to stabilize the system[11]:

$$V(X, \tilde{a}) = X^T PX + \tilde{a}^T \Gamma^{-1} \tilde{a} \tag{28}$$

where $\Gamma = diag(\gamma_1, \gamma_2, \gamma_3)$, $\gamma_i \geq 0$ $(i = 1,2,3)$, which is also a symmetric positive definite constant matrix. Taking the derivative of V gives:

$$\dot{V}(X, \tilde{a}) = \dot{X}^T PX + X^T P\dot{X} + \dot{\tilde{a}}^T \Gamma^{-1} \tilde{a} + \tilde{a}^T \Gamma^{-1} \dot{\tilde{a}} \tag{29}$$

Since both $X^T P\dot{X}$ and $\tilde{a}^T \Gamma^{-1} \dot{\tilde{a}}$ are 1×1 matrices, $\dot{X}^T PX = X^T P\dot{X}$ and $\dot{\tilde{a}}^T \Gamma^{-1} \tilde{a} = \tilde{a}^T \Gamma^{-1} \dot{\tilde{a}}$, Equation (29) can be simplified as:

$$\dot{V}(X,\tilde{a}) = 2\dot{X}^T PX + 2\tilde{a}^T \Gamma^{-1}\dot{\tilde{a}} \tag{30}$$

Since PA is symmetric, $A^T P = PA$ and $B^T P = C$. Substituting Equation (26) into Equation (30) gives,

$$\dot{V}(X,\tilde{a}) = -X^T QX + 2\tilde{a}^T (H^T M^{-1} e_1 + \Gamma^{-1}\dot{\tilde{a}}) \tag{31}$$

If we choose $\dot{\tilde{a}} = -\Gamma H^T M^{-1} e_1$, then $\dot{V}(X,\tilde{a}) = -X^T QX \geq 0$, because Q is positive definite. Since

$$\tilde{a} = \begin{bmatrix} F_v - \hat{F}_v \\ F_{cpos} - \hat{F}_{cpos} \\ F_{cneg} - \hat{F}_{cneg} \end{bmatrix} = \underbrace{\begin{bmatrix} F_v \\ F_{cpos} \\ F_{cneg} \end{bmatrix}}_{p} - \underbrace{\begin{bmatrix} \hat{F}_v \\ \hat{F}_{cpos} \\ \hat{F}_{cneg} \end{bmatrix}}_{\hat{p}} = p - \hat{p} \tag{32}$$

Taking derivative of Equation (32) yields $\dot{\tilde{a}} = -\dot{\hat{p}}$, therefore

$$\dot{\hat{p}} = \Gamma H^T M^{-1} e_1 = diag(\gamma_1, \gamma_2, \gamma_3) \begin{bmatrix} \dot{x} \\ sat1[\text{sgn}(\dot{x})] \\ sat2[\text{sgn}(\dot{x})] \end{bmatrix} M^{-1} e_1 \tag{33}$$

Equation (33) can be simplified as

$$\begin{bmatrix} \dot{\hat{F}}_v \\ \dot{\hat{F}}_{cpos} \\ \dot{\hat{F}}_{cneg} \end{bmatrix} = \begin{bmatrix} \gamma_1 \dot{x} \\ \gamma_2 sat1[\text{sgn}(\dot{x})] \\ \gamma_3 sat2[\text{sgn}(\dot{x})] \end{bmatrix} M^{-1} e_1 \tag{34}$$

which is the update law for the estimation of parameters. The derivation is based on Lyapunov stability theory.

5. Experimental Results

Experiments were conducted to show accurate step and sinusoidal position tracking with adaptive friction compensation. A photograph of the experimental setup is shown in Figure 2-4.

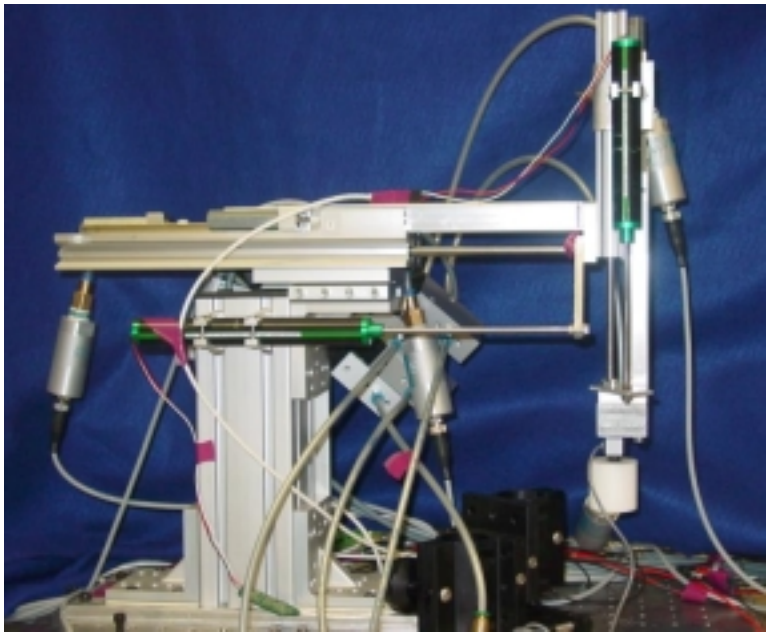

Figure 2-4. The experimental setup of the pneumatic actuation servo system.

The pneumatic manipulator is based on a Festo two degree-of-freedom pick and place pneumatic system. The position tracking experiments are carried out using the vertical direction double acting pneumatic cylinder (SLT-16-100-P-A), which has a stroke length of 100 mm, inner diameter of 16mm and piston rod diameter of 6 mm. A linear potentiometer (Midori LP-100F) with 100 mm maximum travel is used to measure the linear position of the vertical cylinder. The velocity was obtained from position by utilizing an analog differentiating filter with a 20 dB roll-off at 33 Hz. The acceleration

signal was obtained from the velocity signal with a digital differentiating filter with a 20 dB roll-off at 30 Hz. One four-way proportional valve (Festo MPYE-5-M5-010-B) is attached to the two chambers of the vertical cylinder. Two pressure transducers (Festo SDE-16-10V/20mA) are attached to each cylinder chamber, respectively. Control is provided by a Pentium 4 computer with one A/D board (National Instruments PCI-6031E) for analog input channels for sensors and another A/D board (Measurement Computing PCIM-DDA06/16) for analog output channels to control the proportional valves. The middle point of the cylinder stroke is defined as the zero position.

The moving mass of the vertical cylinder is 0.67 kg, a 0.38 kg mass is attached to it as a payload. 20 mm and 60 mm step response are presented in Figure 2-5 and 2-6. It can be seen that the adaptive friction compensation can effectively compensate the friction change generated by the amplitude change. The parameters all converge quickly. The steady state error of step response is within 0.1 mm. The rise time (10% to 90%) is about 200 ms for step inputs from -30mm to 30 mm.

0.5 Hz and 1 Hz sinusoidal inputs with 60 mm amplitude are presented in Figure 2-7 and 2-8. It can be seen that the adaptive friction compensation can effectively compensate the friction change generated by velocity change. For the 0.5 Hz sinusoidal input, the tracking error is within 0.7 mm. For the 1 Hz sinusoidal input, the tracking error is within 1 mm.

Figure 2-9 and Figure 2-10 show that the system can well accommodate the payload disturbance and still maintain accurate position control for both step input and sinusoidal input. The moving mass is changed from 1.05kg to 1.78kg by assuming that the end effector grasps a 0.73 kg part (the gravity is 7.15 N), but the gravity compensation

is still using 1.05 kg to see if the adaptive compensation can compensate this gravity compensation error. Comparing Figure 2-6g with Figure 2-9f, it can be seen that the positive direction Coulomb friction has changed from 4.2 N to –2.9 N. The difference is 7.1 N, which is exactly the gravity compensation error. Comparing Figure 2-6h with Figure 2-9g, it can be seen that the negative direction Coulomb friction has changed from 4.1 N to 11.2 N. The difference is also 7.1 N, the gravity compensation error again. It is obvious that the adaptive Coulomb compensation accurately compensates the gravity compensation estimation error and maintains good position tracking performance. The steady state error with payload disturbance is still within 0.1 mm.

(a) 0.3 Hz 20mm step tracking

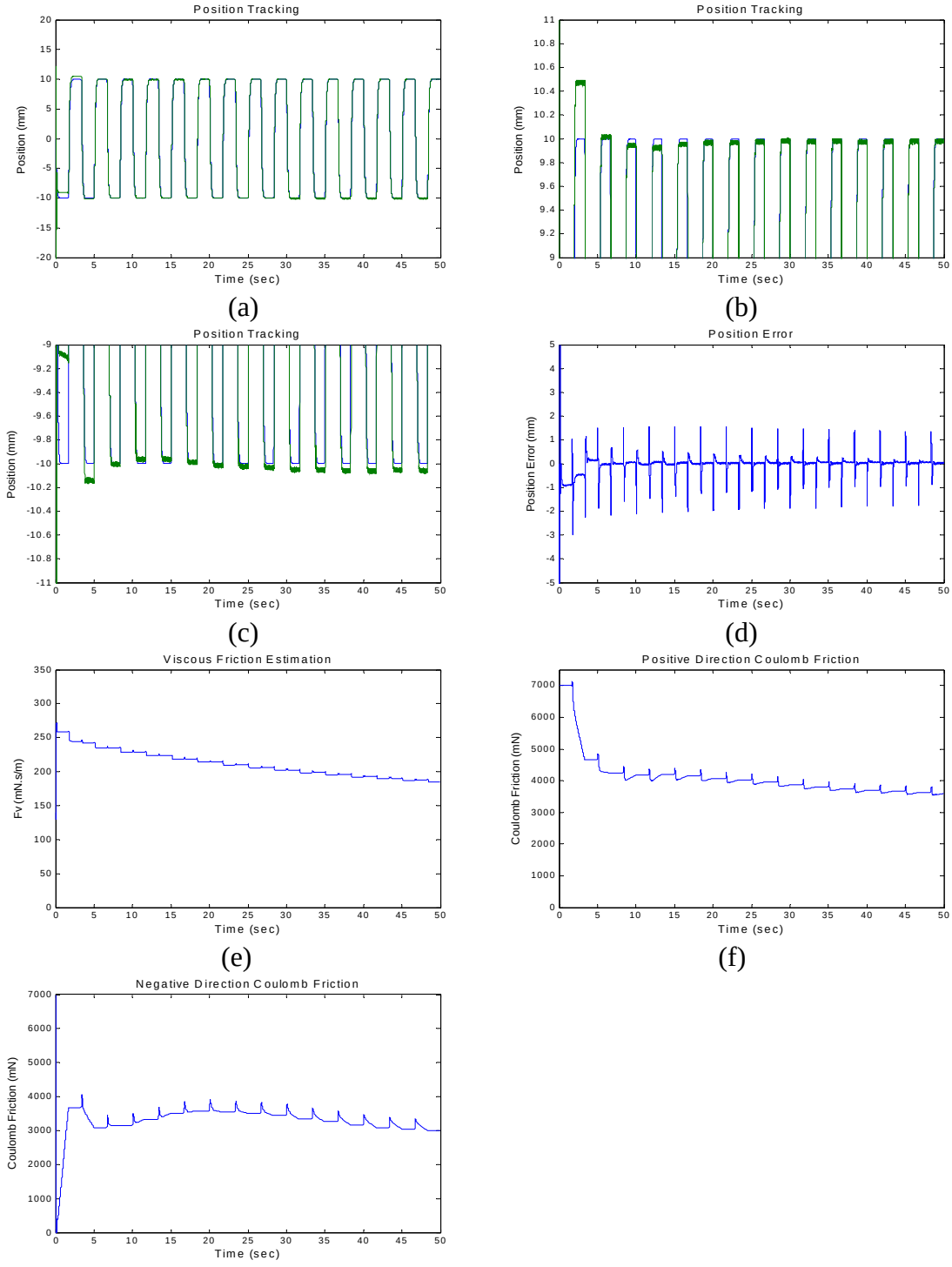

Figure 2-5. 0.3 Hz 20mm step response. (a) position tracking, (b) upper side steady state error, (c) lower side steady state error, (d) position error, (e) viscous friction estimation, (f) positive direction Coulomb friction estimation and (g) negative direction Coulomb friction estimation.

(b) 0.3 Hz 60mm step tracking

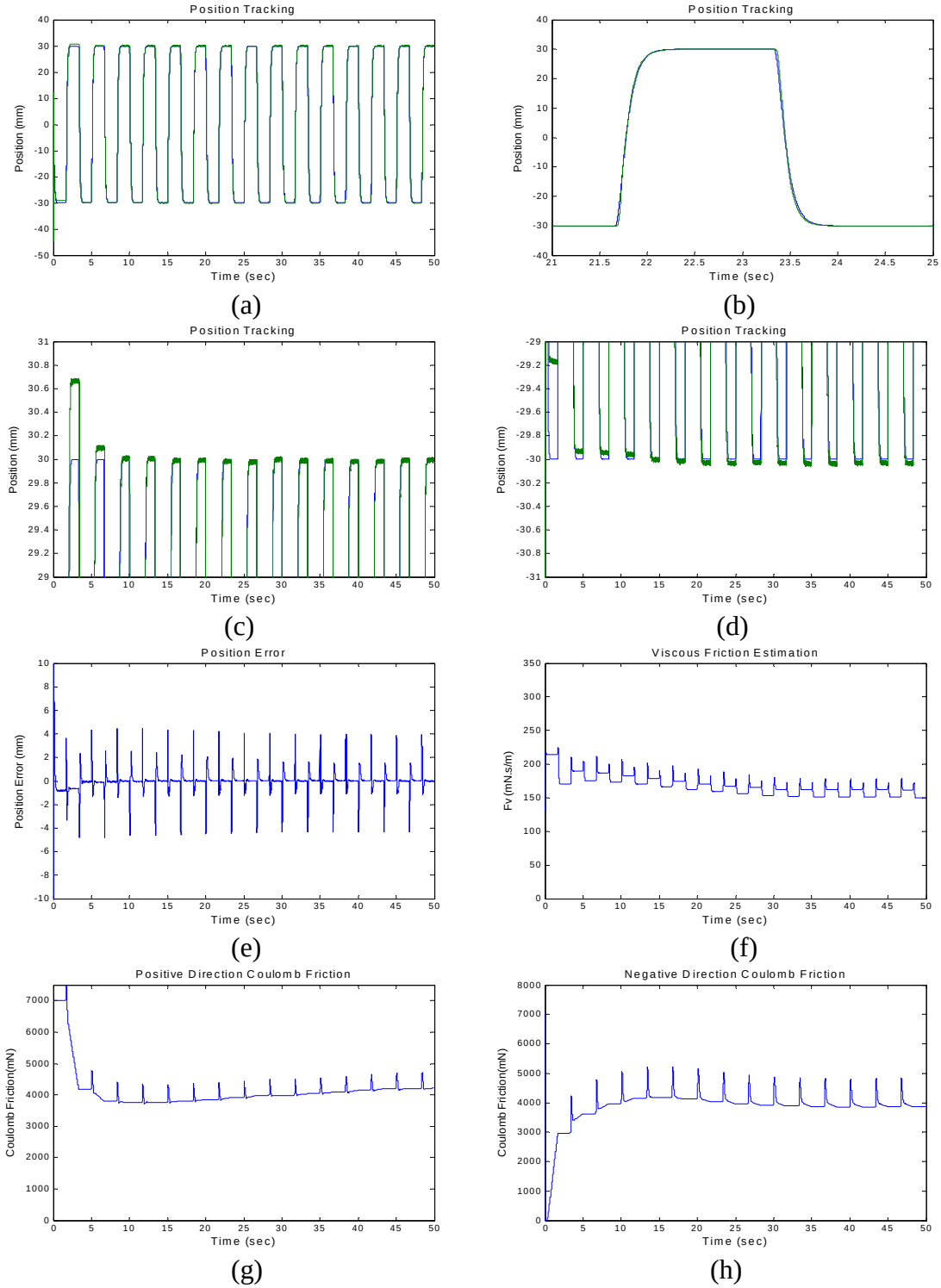

Figure 2-6. 0.3 Hz 60mm step response. (a) position tracking, (b) zoom out of one cycle, (c) upper side steady state error, (d) lower side steady state error, (e) position error, (f) viscous friction estimation, (g) positive direction Coulomb friction estimation and (h) negative direction Coulomb friction estimation.

(c) 0.5 Hz 60mm sinusoidal tracking

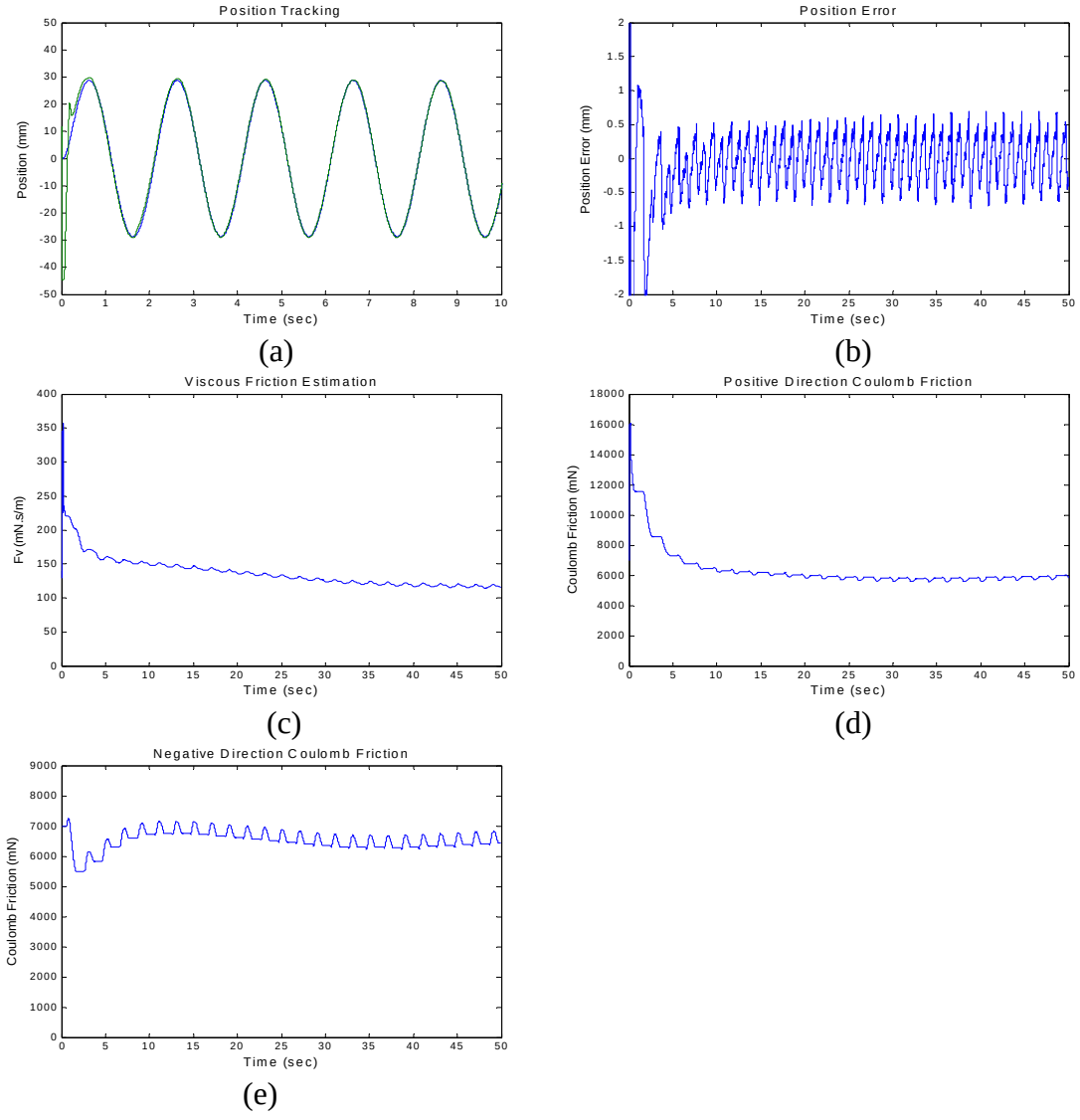

Figure 2-7. 0.5 Hz 60mm sinusoidal tracking. (a) position tracking, (b) position error, (c) viscous friction estimation, (d) positive direction Coulomb friction estimation and (e) negative direction Coulomb friction estimation.

(d) 1 Hz 60mm sinusoidal tracking

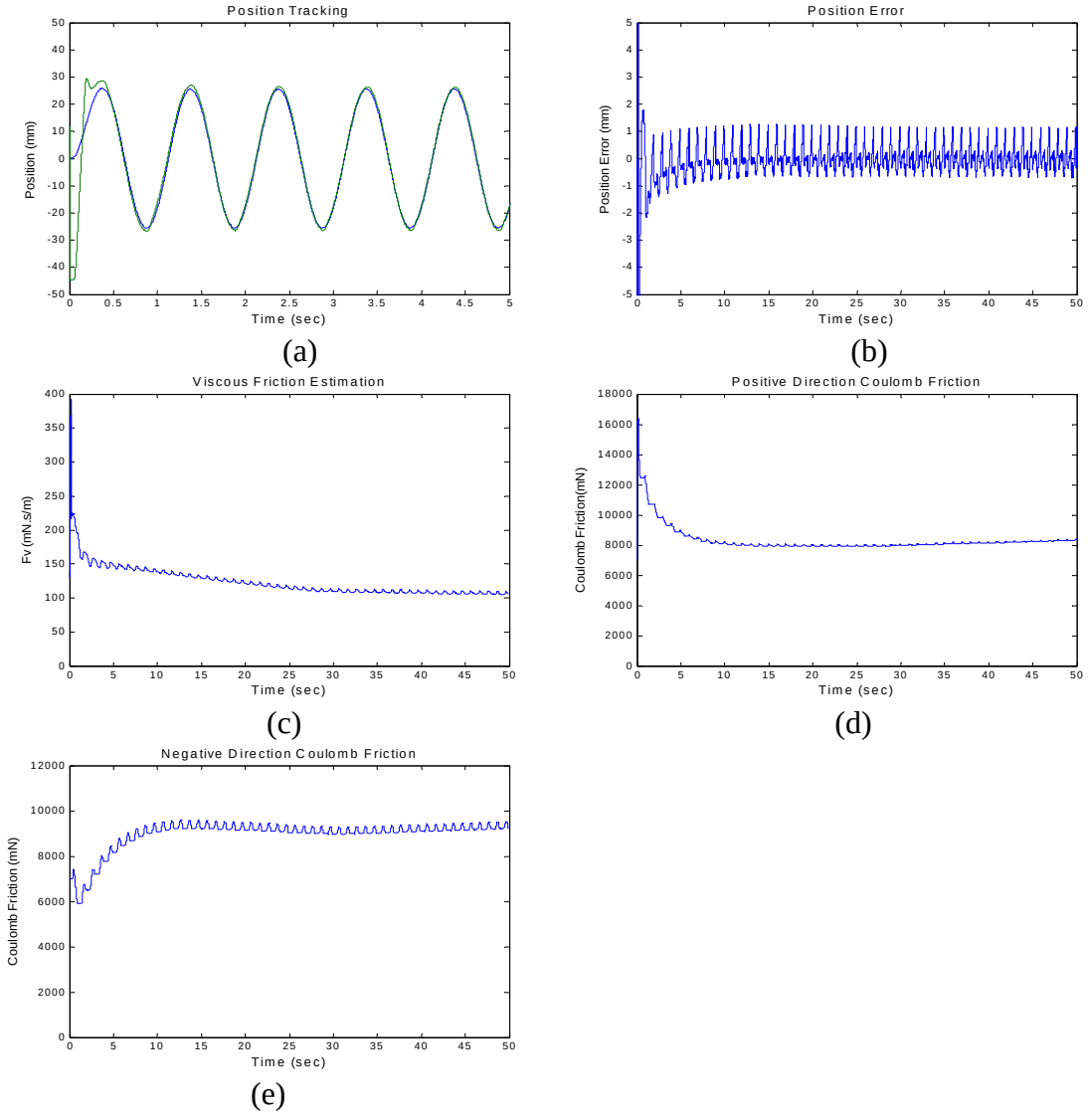

Figure 2-8. 1 Hz 60mm sinusoidal tracking. (a) position tracking, (b) position error, (c) viscous friction estimation, (d) positive direction Coulomb friction estimation and (e) negative direction Coulomb friction estimation.

(e) 0.3 Hz 60mm step tracking with payload disturbance

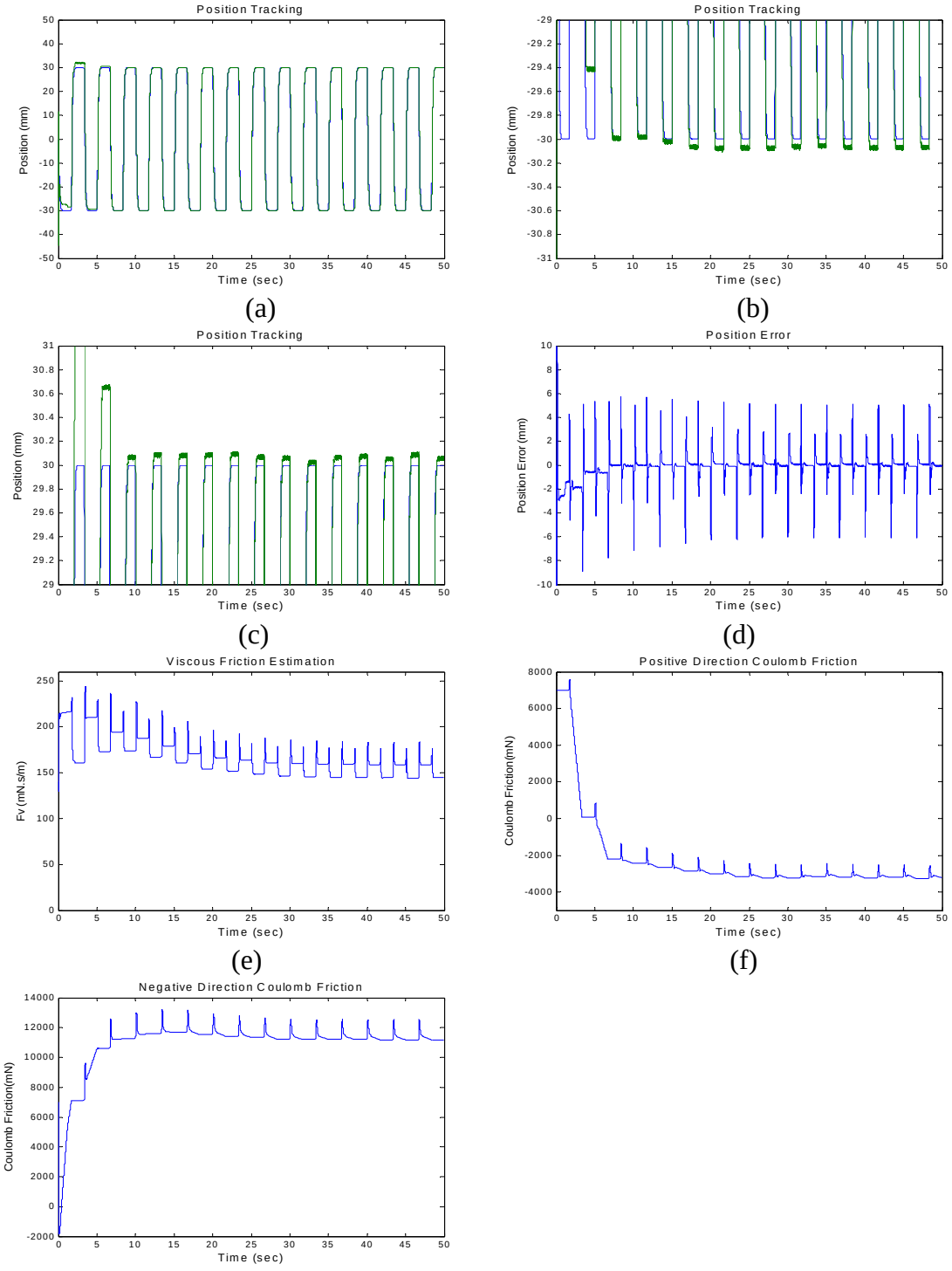

Figure 2-9. 0.3 Hz 60mm step tracking with mass error. (a) position tracking, (b) upper side steady state error, (c) lower side steady state error, (d) position error (e) viscous friction estimation, (f) positive direction Coulomb friction estimation and (g) negative direction Coulomb friction estimation.

(f) 0.5 Hz 60mm sinusoidal tracking with payload disturbance

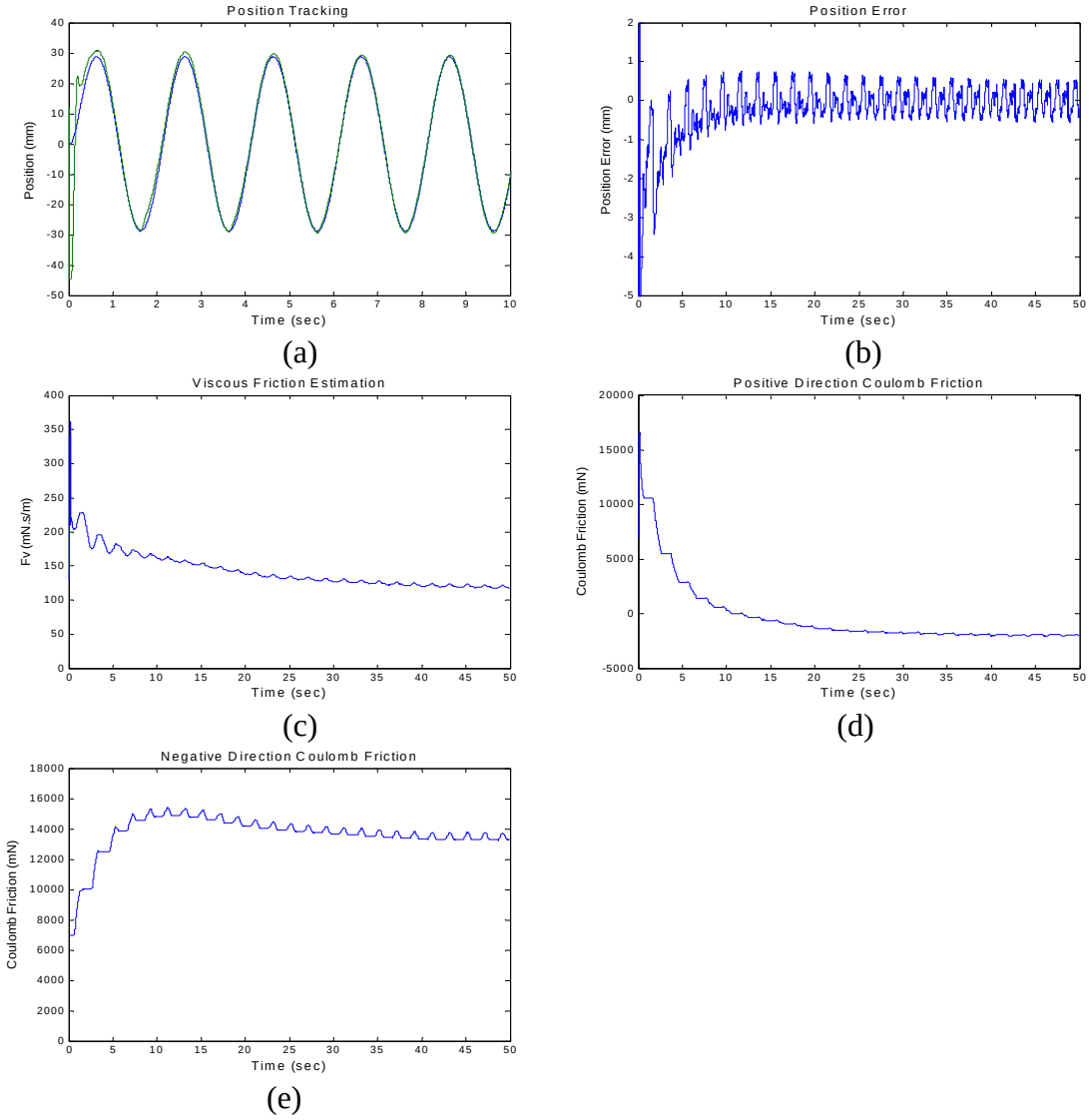

Figure 2-10. 1 Hz 60mm sinusoidal tracking with mass error. (a) position tracking, (b) position error, (c) viscous friction estimation, (d) positive direction Coulomb friction estimation and (e) negative direction Coulomb friction estimation.

6. Conclusions

Accurate position control in free space for pneumatic actuators is achieved using a MRAC. The position control performance and adaptive parameter convergence are comparable to electric motor systems. The system can well adapt to inputs with different magnitude and frequency and maintain fine position tracking. The adaptive friction compensation can also compensate the error generated by payload uncertainty.

References

[1] Zhu, Y. and Barth, E. J., "Planar Peg-in-hole Insertion Using a Stiffness Controllable Pneumatic Manipulator," *Proceedings of the 2005 International Mechanical Engineering Congress and Exposition*, 2005.

[2] Armstrong, B. and Canudas de Wit, C., "Friction Modeling and Compensation," *The Control Handbook* (by William S. Levine), CRC Press, pp. 1369-1382, 1996.

[3] Liu, T., Lee, Y. and Chang, Y., "Adaptive Controller Design for a Linear Motor Control System," *IEEE transactions on Aerospace and Electronic Systems*, vol. 40, no. 2, pp. 601-616, 2004.

[4] Koseeyaporn, P., Cook, G. E. and Strauss, A. M., "Adaptive Voltage Control in Fusion Arc Welding," *IEEE Transactions on Industry Applications*, vol. 36, no. 5, 2000.

[5] Wang, J, Pu, J. and Moore, P., "Accurate Position Control of Servo Pneumatic Actuator Systems: an Application for Food Packaging," *Control Engineering Practice*, vol. 7, pp. 699-706, 1999.

[6] Chillari, S., Guccione, S. and Muscato, G., "An Experimental Comparison between Several Pneumatic Position Control Methods," *Proceedings of the 2001 IEEE Conference on Decision and Control*, pp. 1168-1173, 2001.

[7] Aziz, S. and Bone, G. M., "Automatic Tuning of an Accurate Position Controller for Pneumatic Actuators," *Proceedings of the 1998 IEEE/RSJ International Conference on Intelligent Robots and Systems*, pp.1782-1788, 1998.

[8] Ning, S. and Bone, G. M., "High Steady-state Accuracy Pneumatic Servo Positioning System with PVA/PV Control and Friction Compensation," *Proceedings of the 2002 IEEE International Conference on Robotics and Automation*, pp. 2824-2829, 2002.

[9] Karpenko, M. and Sepehri, N., "Design and Experimental Evaluation of a Nonlinear Position Controller for a Pneumatic Actuator with Friction," *Proceedings of the 2004 American Control Conference*, Bonston, MA, pp. 5078-5083, 2004.

[10] Van Varseveld, R. B. and Bone, G. M., "Accurate Position Control of a Pneumatic Actuator Using On/Off Solenoid Valves," *IEEE/ASME Transactions on Mechatronics*, vol. 2, no. 3, pp. 195-204, 1997.

[11] Slotin, J. E. and Li, W., *Applied Nonlinear Control*, pp. 338, Prentice Hall, 1991.

ADDENDUM TO MANUSCRIPT I

A1. Characterization of a Proportional Valve

The standard nominal flow rate or the coefficient of velocity (CV factor) is generally the technical data used by industrial pneumatic valves manufacturer to compare the capability of different valves. To design a nonlinear controller using pneumatic proportional valves, the discharging coefficient is the most important unknown parameter of a valve, which needs to be determined firstly.

The Festo proportional directional control valve MPYE-5-M5-010-B features a unique internal control loop for accurate spool displacement. The nominal bore size is 2mm (diameter) featuring two holes for charging and discharging. The flow rate curve from Festo catalog is shown in Figure 2-11. This curve is generated under typical nominal condition: the upstream pressure is 6 bar and the downstream pressure is 5 bar.

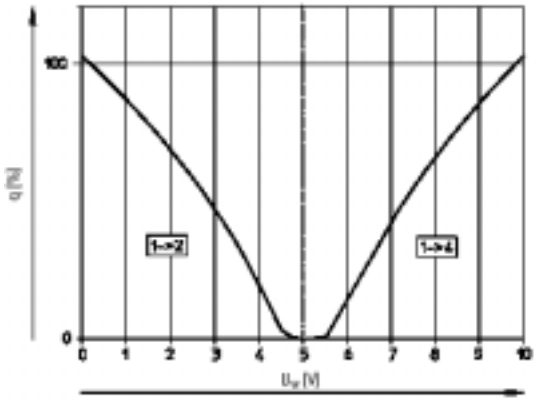

Figure 2-11. Voltage type Festo MPYE-5-*-010-B flow rate curve. ($\pm 10\%$).

For MPYE-5-M5-010-B, the maximum flow rate is about 100 litre/min. According to Equation (9), the compressible mass flow rate though a valve orifice with effective area A_v can be described as:

$$\dot{m}_{in/out(a,b)} = \frac{C_f A_v P_u}{\sqrt{T}} C_m \tag{35}$$

where $C_m = C_2 (\frac{P_d}{P_u})^{(1/k)} \sqrt{1 - (\frac{P_d}{P_u})^{(k-1)/k}}$ for choked flow, because $\frac{P_d}{P_u} > C_r$ (under nominal condition). Therefore, C_m can be calculated using the expression for unchoked flow in Equation (36), $C_m = 0.0309$. From Equation (35), we know,

$$C_f = \frac{\dot{m}\sqrt{T}}{A_v P_u C_m} \tag{36}$$

The nominal bore size is 2 mm, there are two holes in the valve. So total maximum orifice area is $A_{v\_\max} = 6.28\, mm^2$, and the maximum volume flow rate is 100 litre/min, the density of air at standard atmospheric pressure (20 degree) is 1.204 kg/m^3, So the maximum mass flow rate can be calculated as $\dot{m} = 0.002 kg/s$. Using Equation (36), the discharging coefficient can be calculated as: $C_f = 0.2939$. All the parameters are summarized in Table 2-1.

Table 2-1. Parameters for valve characterization.

R	universal gas constant	287 m^2/s^2K
k	ratio of specific heats of standard air	1.4
C_1	constant	0.040418
C_2	constant	0.156174
T	air temperature	293 K
C_r	pressure ratio that divides the flow regimes into unchoked and choked flow	0.528
P_u	upstream pressures	600000 Pa
P_d	downstream pressures	500000 Pa
C_f	discharge coefficient of the valve	0.2939

Table 2-2. Valve characterization values.

Voltage (volt)	Spool Pos. (mm)	Orifice Area (mm^2)	Mass flow rate (g/sec)	Cal. Vol. flow rate (l/min)	Exp. Vol. flow rate (l/min)
5	0	0	0	0	0
5.125	0.05	0.0418	0.0133	0.6638	0.11
5.25	0.1	0.1175	0.0374	1.8632	0.23
5.375	0.15	0.2141	0.0682	3.3963	0.44
5.5	0.2	0.3270	0.1041	5.1875	1.75
5.625	0.25	0.4533	0.1443	7.1912	3.51
5.75	0.3	0.5909	0.1881	9.3754	7.89
5.875	0.35	0.7385	0.2350	11.716	10.09
6	0.4	0.8946	0.2848	14.192	14.04
6.125	0.45	1.0582	0.3369	16.787	17.54
6.25	0.5	1.2284	0.3910	19.487	21.05
6.375	0.55	1.4043	0.4470	22.278	23.68
6.5	0.6	1.5853	0.5047	25.150	27.63
6.625	0.65	1.7707	0.5637	28.091	30.7
6.75	0.7	1.9598	0.6239	31.090	34.21
6.875	0.75	2.1521	0.6851	34.141	39.04
7	0.8	2.3470	0.7471	37.232	42.98
7.125	0.85	2.5439	0.8098	40.355	45.61
7.25	0.9	2.7423	0.8730	43.503	50
7.375	0.95	2.9417	0.9364	46.666	53.07
7.5	1	3.1416	1.0000	49.837	54.82
7.625	1.05	3.3415	1.0637	53.009	57.01
7.75	1.1	3.5409	1.1272	56.172	60.96
7.875	1.15	3.7393	1.1903	59.322	63.6
8	1.2	3.9362	1.2530	62.443	65.79
8.125	1.25	4.1310	1.3151	65.534	67.54
8.25	1.3	4.3233	1.3763	68.584	69.74
8.375	1.35	4.5125	1.4365	71.585	72.81
8.5	1.4	4.6978	1.4955	74.525	75.88
8.625	1.45	4.8788	1.5531	77.397	78.07
8.75	1.5	5.0548	1.6091	80.189	80.26
8.875	1.55	5.2250	1.6633	82.888	82.46
9	1.6	5.3886	1.7154	85.483	85.09
9.125	1.65	5.5447	1.7651	87.959	86.84
9.25	1.7	5.6922	1.8120	90.299	89.47
9.375	1.75	5.8299	1.8558	92.484	92.1
9.5	1.8	5.9562	1.8960	94.487	94.74
9.625	1.85	6.0691	1.9320	96.279	96.49
9.75	1.9	6.1657	1.96276	97.812	98.25
9.875	1.95	6.2413	1.9868	99.011	100

Based on the calculated C_f, the dynamics of the valve is completely characterized. Since the nominal bore size is 2mm, so the voltage from 5 volts (fully closed) to 10 volts (fully open) should correspond to spool position from 0 to 2 mm. This is shown in column 1 and 2 of Table 2-2. Then based on the spool position, the orifice area can be calculated in column 3, so that the mass flow rate can be calculated in column 4 using Equation (34). Then the mass flow rate is transformed into volume flow rate in Column 5 and compared with Column 6.Then the data in column 5 and 6 are plotted in Figure 2-12.

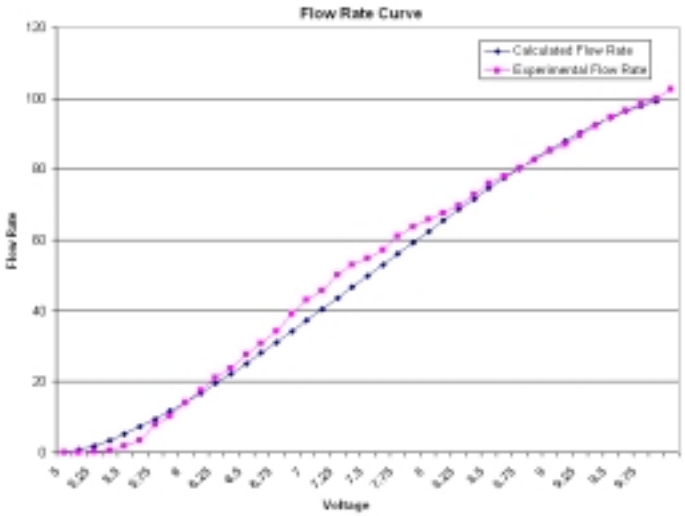

Figure 2-12. Calculated and experimental flow rate curves.

It can be seen from Figure 2-12 that based on the calculated C_f, the calculated valve flow rate curve is very close to the experimental data. So C_f can be used for sliding mode force controller design. In the simulation and experiments, a lookup table will be used to implement the nonlinear relationship between voltage and mass flow rate without considering the valve dynamics.

A2. Contact Tasks Without Force Feedback

Considering the procedure when one's hand approaches an object, the fingers are soft and faster speed is used when the hand is further from the estimated contact point, as the hand gets closer, the speed would slow down and minimize the contact force to minimize the likelihood that the contact point would be disturbed or that the hand will be injured. The pneumatic system has the intrinsic compliance like a soft hand, which is something we do not have to control. This biological response will be mimicked through the unique feature of pneumatic actuator. The idea is to use a sigmoid velocity function as input to generate the desired actuator force, plus friction compensation and gravity compensation. The desired contact force can be controlled proportionally by the final velocity immediately before contact happens. Because of the flatness of the sigmoid function when the end effecter gets close to the estimated contact position, the contact force is almost independent of the position uncertainty and contact surface stiffness. Let the distance between current position and the estimated contact position be $|x - x_d|$, which is the input of the sigmoid function, and the output of the sigmoid function is the desired velocity. So the relationship can be represented as,

$$\dot{x}_d = \frac{C_1}{1 + e^{-(|x - x_d| - C_2)/C_3}} + C_4 \tag{37}$$

For example, if $C_1 = 150$, $C_2 = 35$, $C_3 = 7$ and $C_4 = 50$, the sigmoid function is plotted as in Figure 2-13 By adjusting these four parameters, the desired velocity trajectory can

be easily generated. The most important parameter is C_4, which determines the final velocity before contact, so it also determines the final contact force.

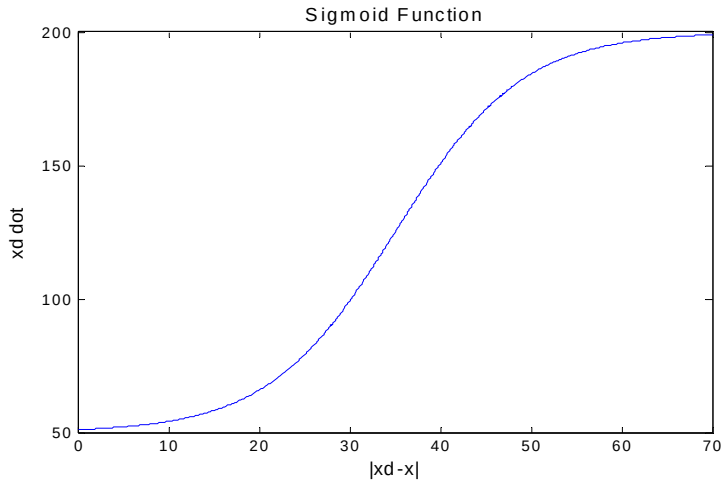

Figure 2-13. Sigmoid function relationship between distance to desired position and desired velocity.

The desired actuator force is chosen as,

$$F_d = M\ddot{x} + B\dot{x} + F_f - b(\dot{x} - \dot{x}_d) \tag{38}$$

where B is the viscous friction parameter and F_f is the Coulomb friction. Equation (38) is similar to a standard impedance control relationship. The position error portion is not included because our input is going to be a velocity trajectory. For contact tasks, generally position tracking is not important along the force control degree-of-freedom. More important thing is that the actuator is going to behave like a passive and dissipative air damper, impact energy is going to be transformed and released quickly, which eliminates big overshoot and bouncing.

It can be seen that when the contact happens, both $\dot{x}$ and $\ddot{x}$ become zero. The desired force becomes $F_d = F_f + b\dot{x}_d$, since the actuator force tracking has very high bandwidth, we assume $F_a = F_d$, Substituting this into the system dynamic equation ($M\ddot{x} = F_a - B\dot{x} - F_f - F_e$) gives $F_e = b\dot{x}_d$, so by controlling the final flat region velocity of the actuator, the contact force can be closely controlled without knowing the stiffness and the accurate position of the contact surface.

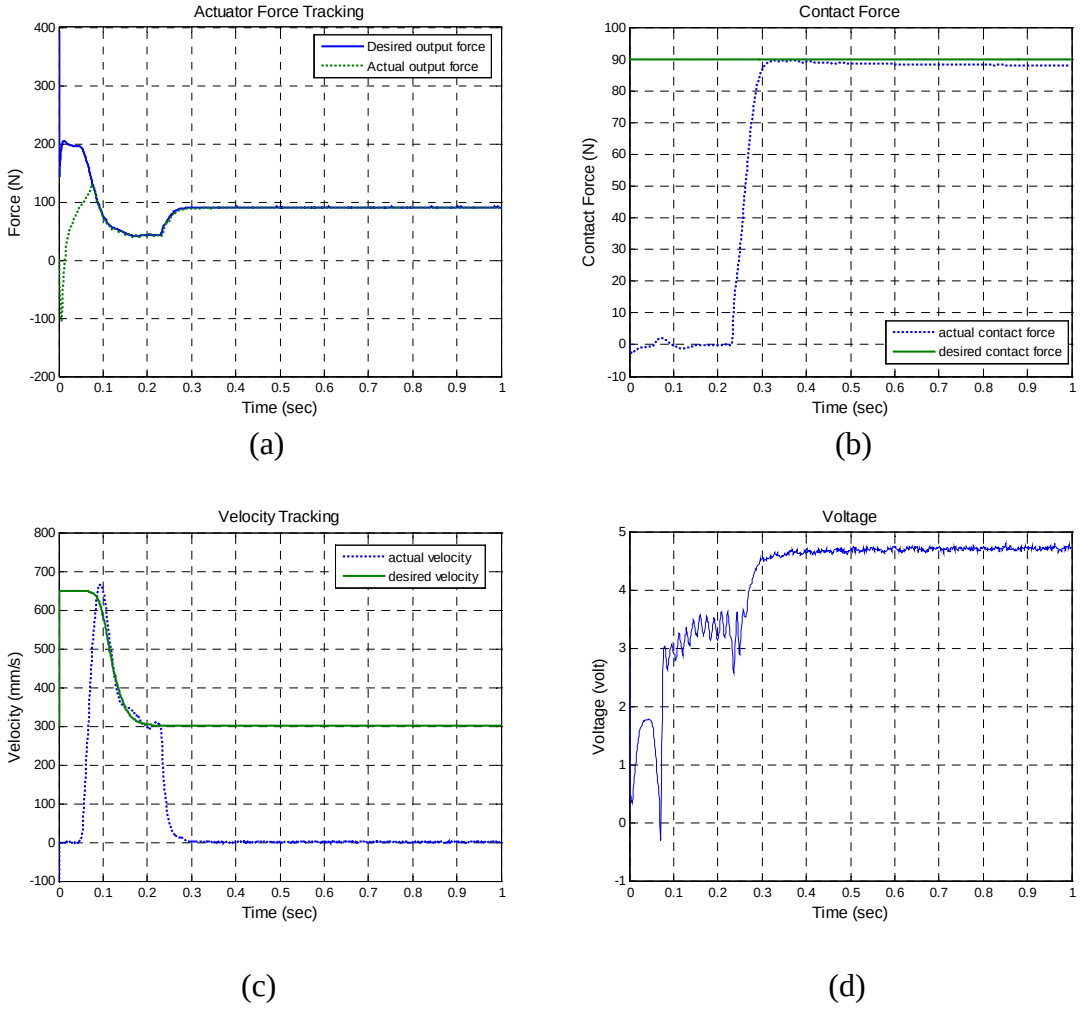

Figure 2-14. Contact task with 90 N desired contact force. (a) actuator force tracking, (b) contact force, (c) velocity tracking and (d) voltage input of the proportional valve.

It can be seen from the velocity tracking in Figure 2-14 that the velocity tracking is not very accurate sometimes, but the pneumatic actuator can well accommodate the velocity error, and velocity error immediately before the contact shows very little influence on the open loop contact force.

A3. Intuitive Teaching and Playback of Contact Tasks

Today, industrial automation with robots is efficient and fast only for large lot size applications in free space. The use of robots to automate some tasks involving contact with a constrained environment and complex motion planning has not been widespread because they are difficult to program. The general objective of this work is to design an efficient and intuitive robot programming methodology by directly guiding the robot in the most natural way for force-controlled contact tasks like polishing and applications of small lot sizes with a very high number of part variants like painting.

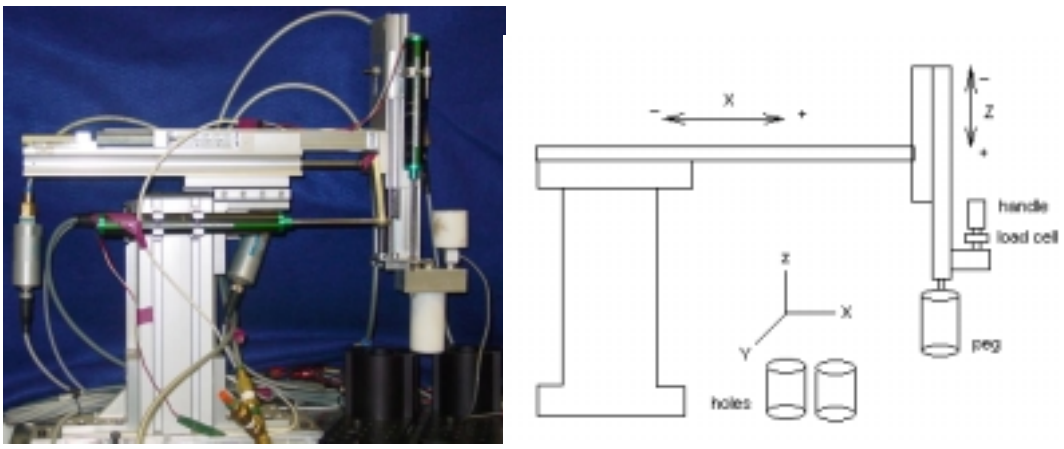

(a) (b)

Figure 2-15. (a) Experimental setup and (b) schematic of the 2-DOF pneumatic manipulator for intuitive teaching and playback.

The basic schematic for the manipulator is shown in Figure 2-15. Position control is used for X direction and force control is used for Z direction. In the teaching mode, the load cell information is recorded and amplified (x2) so that it can be used as the input to the actuator force controller along Z direction. Simultaneously, the X direction works in friction cancellation mode, so that it can freely slide without adding obvious disturbance to the Z direction load cell from the human operator. The X direction position is also recorded. In the playback mode, the X direction position and Z direction force are carried out simultaneously to replay the constrained motion recorded in the teaching mode.

As an illustration, the peg is taught to move in and out of the two holes in a series of random interaction tasks. The operation taught by operator is an arbitrary combination of free space motion and constrained motion with hard surface unpredicted contact. The recorded position trajectory along X direction and force profile along Z direction are accurately repeated as shown in Figure 2-16. And the series of constrained interaction tasks are accurately replayed.

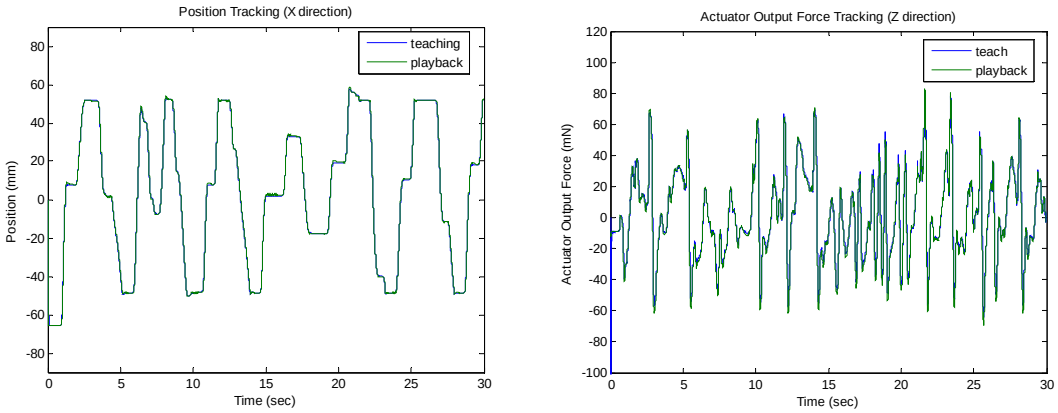

(a) (b)

Figure 2-16. Playback results of a series of randomly taught tasks. (a) X direction position playback and (b) Z direction force playback.

CHAPTER III

MANUSCRIPT II

PASSIVITY-BASED IMPACT AND FORCE CONTROL OF A PNEUMATIC ACTUATOR

Yong Zhu and Eric J. Barth

Department of Mechanical Engineering
Vanderbilt University
Nashville, TN 37235

Submitted as a Full Paper to the
ASME Journal of Dynamic Systems, Measurement and Control

Abstract

To carry out stable and dissipative contact tasks with an arbitrary environment, it is critical for a pneumatic actuator to be passive with respect to a supply rate consisting of the spool valve position input and the actuation force output. A pseudo-bond graph model with the inner product between spool valve position input and actuation force output as a pseudo supply rate is developed. Using this pseudo-bond graph model, an open-loop pneumatic actuator controlled by a four-way proportional valve can be proven to be not passive with respect to the pseudo supply rate. And it can also be proven to be passive with respect to the pseudo supply rate under a closed-loop feedback control law. The passivity of the closed-loop pneumatic actuator is verified in impact and force control experiments. The experimental results also validate the pseudo-bond graph model. The pseudo-bond graph model can be used in other passivity analysis and controller designs for pneumatic actuation systems.

1. Introduction

Control of the interaction force between a robot manipulator and its environment is critical for the successful execution of many industrial tasks such as polishing, assembly and deburring, etc. Additionally, newfound interest and research is being conducted regarding interactions and co-existence of robots and humans not only on the shop floor, but also for applications at home and in the medical industry (i.e. entertainment, service robotics, and rehabilitation). Maintaining a stable and safe interaction force is the key aspect among these applications.

Tasks that require a high degree of interaction with the environment require the actuator to be an impedance as opposed to an admittance [1]. Many approaches have been taken to have an actuator contact with an environment and maintain a certain contact force for electrical systems [2], hydraulic systems [3] [4] and pneumatic systems as well [5]. Most of these approaches divide the task into three modes: free space mode, constrained mode and transition mode. Different switching control strategies are used to guarantee stability and minimize bouncing.

Another widely used approach for contact task control is impedance control [6] [7]. The key point of the impedance control method is that one controller deals with all stages of the contact task. Hogan [6] proposed stable contact tasks using impedance control. Hogan [7] also showed that if an actuation system has the behavior of a simple impedance, then the stability of the system is preserved when it is coupled to a stable environment. The limitation of the impedance control approach is that it requires accurate environment and stiffness information for good force control.

An actuator can be stable in free space but can become unstable when it is coupled to a not well-characterized environment. Stable interaction can be achieved either in a passive way, by using a suitable compliant mechanical device, or in an active way, by designing an interaction control strategy. A passive system can interact stably with any strictly passive environment [8]. Safe and stable interaction can be achieved if the actuation system is passive with respect to the environment and/or a human operator. A system is said to be passive if the energy absorbed over any period of time is greater than or equal to the increase in the energy stored over the same period [9]. Consider a system with a general form [10]:

$$\dot{V}(t) = y^T u - g(t) \tag{1}$$

Where $V(t)$ and $g(t)$ are scalar functions of time. Generally $V(t)$ is called a storage function and $g(t)$ is the dissipative term, u is the system input and y is the system output. A supply rate can be represented as the scalar $s(u, y) = y^T u$. If V is lower bounded and $g(t) \geq 0$, the system is said to be passive, or a passive mapping between u and y. Furthermore, a passive system is said to be dissipative if

$$\int_o^\infty g(t)dt > 0 \tag{2}$$

Integrating Equation (1) gives,

$$V(t) - V(0) = \int_0^t s(u, y)d\tau - \int_0^t g(t)d\tau \leq \int_0^t s(u, y)d\tau \tag{3}$$

Since $V(t)$ is lower bounded and $V(0)$ is the lower bounded initial valve of the storage function, $\int_0^t s(u, y)d\tau$ is lower bounded. Thus, passivity is generally defined as: a system is said to be passive with respect to the supply rate $s(u, y)$ if, for a given initial condition, there exists a c ($|c| < \infty$) so that for all time t and for all input u

$$\int_0^t s(u, y)d\tau \geq -c^2 \tag{4}$$

The directional control valve is the only non-passive device in a hydraulic actuation system. Li [11] has proven that if appropriate first order or second order spool dynamics can be implemented, the spool valve can become passive. The same dynamic passive valve method has been used in bilateral teleoperation of a hydraulic actuator [12]. The passivity concept is also used to design a hydraulic backhoe/force feedback joystick

system [13]. Other than hydraulic systems, some other passive systems, such as Cobots [14] and smart exercise machines [15], have also been designed for different human-robot interaction tasks. As will be shown, the fundamental energetic properties of pneumatic actuation can be exploited to provide stable interaction forces with any passive environment. Another convenient property of a pneumatically actuated system that will be exploited is the ability to measure actuation forces using pressure sensor feedback.

The passivity properties of a pneumatic system have not previously been investigated explicitly. The objective of this paper is to investigate the passivity properties of a pneumatic actuator using closed-loop feedback control and apply the passivity properties to impact and force control. The paper is organized as follows. First in section 2, a pseudo-bond graph model of a pneumatic actuator is proposed. Then a closed-loop feedback control system is proven to be passive in section 3. Section 4 shows the experimental results of impact and force control utilizing the methods and tools developed. Finally, section 5 contains concluding remarks.

2. Pseudo-bond Graph Model for a Pneumatic Actuator

A bond graph model for hydraulic systems with incompressible fluid [11] is shown in Figure 3-1a. The pressure difference (P) and volumetric flow rate (Q) are directly associated with the actuator work output ($F\dot{x}$) through a transformer. The inner product between the effort and flow, generally called the supply rate, represents the true hydraulic power input to the hydraulic system. Since pressure difference is directly associated with the output actuation force and volumetric flow rate can be directly

specified by the spool valve position input, the bond graph representation of a hydraulic system lends good insight into its passivity analysis.

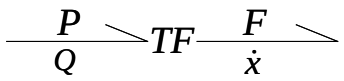

(a)

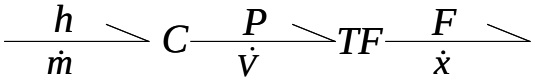

(b)

Figure 3-1 Bond graph models for (a) a hydraulic actuator and (b) a pneumatic actuator.

In a pneumatic actuator, specific enthalpy (h) is the effort variable and mass flow rate ($\dot{m}$) is the flow variable for the bond graph as shown in Figure 3-1 (b). Because of the capacitance associated with the compressibility of a gas, the behavior of a pneumatic actuator is fundamentally different than the behavior of a strictly incompressible hydraulic system. The supply rate $s(h,\dot{m}) = h\dot{m}$ is no longer directly related to the actuator work output ($F\dot{x}$). This makes the passivity analysis of a pneumatic actuator less straightforward than for a hydraulic actuator. To design a passive pneumatic actuation system, it is useful to first establish a pseudo-bond graph model to directly associate the spool valve position input with the actuation force output. A simple passivity analysis of a spring-mass system is first given to help elucidate this idea through analogy.

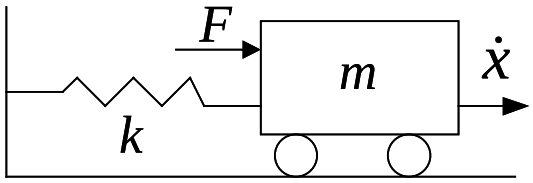

Figure 3-2. A spring-mass system.

The dynamic equation of the spring-mass system as shown in Figure 3-2 is,

$$m\ddot{x} + kx = F \tag{5}$$

The total energy of the system is,

$$V = \frac{1}{2}m\dot{x}^2 + \frac{1}{2}kx^2 \tag{6}$$

Taking the time derivative of Equation (6) yields,

$$\dot{V} = m\dot{x}\ddot{x} + kx\dot{x} = \dot{x}(m\ddot{x} + kx) = F\dot{x} \tag{7}$$

This spring-mass system is passive with respect to the supply rate $s(F, \dot{x}) = F\dot{x}$ according to Equation (1), where $g(t) = 0$. The same analysis can be done via a different approach by choosing the storage function as,

$$V = \frac{1}{2}m\dot{x}^2 \tag{8}$$

Taking the time derivative of Equation (8) gives,

$$\dot{V} = m\dot{x}\ddot{x} = \dot{x}(F - kx) = F\dot{x} - kx\dot{x} = F\dot{x} - g(t) \tag{9}$$

Since $\int_0^t kx\dot{x}d\tau = \frac{1}{2}kx^2 \geq 0$, the spring-mass system is still shown to be passive with respect to the same supply rate $s(F, \dot{x}) = F\dot{x}$. It will be shown that a pneumatic system

has a form more similar to Equation (9) than Equation (7) for a properly chosen storage function.

A mathematical model of a pneumatic actuator has been well described [16] [17]. Assuming that the gas is perfect, the temperature and pressure within the two chambers are homogeneous, and the kinetic and potential energy of the fluid are negligible, the rate of change of pressure within each pneumatic chamber a and b of the actuator can be expressed as,

$$\dot{P}_{a,b} = \frac{rRT}{V_{a,b}}\dot{m}_{a,b} - \frac{rP_{a,b}\dot{V}_{a,b}}{V_{a,b}} \tag{10}$$

where r is the thermal characteristic coefficient, with $r = 1$ for the isothermal case and $r = \gamma$ for the adiabatic case (γ is the specific heat ratio), R is the ideal gas constant, T is the temperature, $V_{a,b}$ is the volume of chamber a and b, respectively, and $P_{a,b}$ is the pressure in chamber a and b, respectively, $\dot{m}_{a,b}$ is the mass flow rate into chamber a and b, respectively. All analysis carried out in this paper is based on an isothermal assumption [17]. Strictly speaking, this assumption introduces a thermal bond to the pneumatic actuation system not shown in Fig. 1b. Since this thermal bond is always dissipative, it can be neglected from the sufficient passivity conditions that will follow.

The actuation force of a pneumatic actuator can be expressed as Eq. (11) using absolute pressures,

$$F_a = P_a A_a - P_b A_b - P_{atm} A_r \tag{11}$$

where P_{atm} is the atmospheric pressure and $A_r = A_a - A_b$. Since the bandwidth of the valve is typically much higher than the bandwidth of the closed-loop system, it will be assumed that the spool valve position x_v is proportional to the control voltage. Therefore,

in all the analysis, the spool valve position is considered as the control input, and $x_v = 0$ corresponds to the center spool position and is defined as zero mass flow rate.

To model a pneumatic actuator as a one-port device, the storage function is chosen as:

$$V_1 = \frac{1}{2}(P_a A_a - P_b A_b - P_{atm} A_r)^2 \tag{12}$$

Taking the time derivative of Equation (12) yields:

$$\dot{V}_1 = F_a(\dot{P}_a A_a - \dot{P}_b A_b) \tag{13}$$

Substituting Equation (10) into Equation (13) yields:

$$\dot{V}_1 = F_a(\frac{rRTA_a}{V_a}\dot{m}_a - \frac{rRTA_b}{V_b}\dot{m}_b) + F_a(-\frac{r\dot{V}_a A_a}{V_a}P_a + \frac{r\dot{V}_b A_b}{V_b}P_b) \tag{14}$$

Refering to Liu and Bobrow's work [18] on the linearized characteristics of a 4-way spool valve, if the valve operates within its mechanical operating range, it can be accurately characterized in a linear form as,

$$\dot{m}_a = C_1 x_v - C_2 P_a \tag{15}$$

$$\dot{m}_b = -C_1 x_v - C_2 P_b \tag{16}$$

where C_1 and C_2 are two positive constants depending on the valve design. For a given positive valve opening, there is a maximum mass flow rate as the downstream and upstream pressure ratio reaches a critical value ($\frac{P_d}{P_u} < 0.528$), called choked flow. The coefficient C_2 is typically very small compared to other terms of the system and has a very small effect on the system performance. In particular, when under choked flow conditions, $C_2 = 0$. The maximum mass flow rate occurs under choked flow conditions,

and the unchoked flow rate is bounded by the choked flow rate. Therefore, if passivity can be shown for the choked flow rate condition, it will also hold for unchoked flow. Additionally from a practical standpoint, most pneumatic actuation systems operate in the choked flow regime most of the time. Therefore, the mass flow rate is modeled as proportional to the orifice area of the valve, which is approximately proportional to the valve spool position x_v:

$$\dot{m}_a = C_1 x_v \tag{17}$$

$$\dot{m}_b = -C_1 x_v \tag{18}$$

The volume of each chamber of a pneumatic actuator is related to the actuator position *x* by:

$$\dot{V}_a = A_a \dot{x} \tag{19}$$

$$\dot{V}_b = -A_b \dot{x} \tag{20}$$

Substituting Equations (17)-(20) into Equation (14) yields:

$$\dot{V}_1 = (\frac{rRTA_a}{V_a} + \frac{rRTA_b}{V_b}) C_1 x_v F_a - F_a \dot{x} (\frac{rA_a^{\ 2}}{V_a} P_a + \frac{rA_b^{\ 2}}{V_b} P_b) \tag{21}$$

Let $k_1 = (\frac{RTA_a}{V_a} + \frac{RTA_b}{V_b}) r C_1$, and $k_2 = \frac{rA_a^{\ 2}}{V_a} P_a + \frac{rA_b^{\ 2}}{V_b} P_b$, where $k_1 > 0$ and $k_2 > 0$.

Equation (21) can be rewritten as:

$$\dot{V}_1 = k_1 x_v F_a - k_2 F_a \dot{x} \tag{22}$$

Comparing Equation (22) with Equation (9), we can see that although a pneumatic system has very nonlinear dynamics, it can be closely modeled in a similar structure as a spring-mass linear system using the new storage function (pseudo energy). The pseudo-bond graph model based on Equation (12) can help us associate the spool valve position

input and the actuation force output for passivity analysis. Furthermore, in the pseudo-bond graph model, the supply rate is the inner product of input and output of the pneumatic actuator, and the active term x_v only appears in the supply rate. The term $-k_2 F_a \dot{x}$ will be shown to be a passive term associated with the actuator's kinetic energy. Its role is similar to $-kx\dot{x}$ in Equation (9) for the spring-mass system, which is also a passive term.

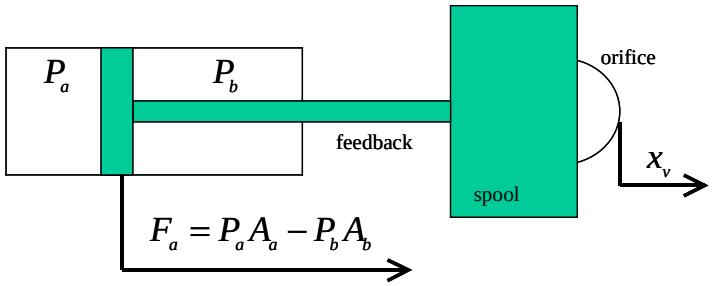

Figure 3-3. Passive valve-actuation schematic. Feedback is indicated as a virtual link between the actuator and valve spool position.

The power form of the storage function shown in Equation (22) is central to the idea of this paper. Since $V_1 = \frac{1}{2}(P_a A_a - P_b A_b - P_{atm} A_r)^2 \geq 0$ and therefore lower bounded, we can consider V_1 as the pseudo-energy of a pneumatic actuator. Defining F_a and x_v in the same sense (see Figure 3-3), positive power is delivered to the system when $F_a x_v < 0$. Therefore the supply rate is defined as $s(x_v, F_a) \coloneqq -x_v F_a$. This is similar to the approach taken in [10] in defining the supply rate as $s(P_L, Q) \coloneqq -P_L Q$ for a hydraulic actuation system. The perspective taken will be to find a control law that passifies this

system. The passified actuation system will then be capable of interacting with any passive environment in a stable manner.

A comparison of the spring-mass, pneumatic and hydraulic systems are summarized in Table 3-1 showing the analogous role of the pseudo-bond for a pneumatic actuator.

Table 3-1. The comparison of spring-mass, pneumatic and hydraulic systems.

	Spring-mass **(true bond)**	Pneumatic actuator **(pseudo-bond)**	Hydraulic actuator **(true bond)**
Effort	F	x_v	P_L
Flow	$\dot{x}$	F_a	Q
Supply rate	$F\dot{x}$	$-x_v F_a$	$-P_L Q$
Storage function	$V = \frac{1}{2} m\dot{x}^2$	$V = \frac{1}{2}(P_a A_a - P_b A_b - P_{atm} A_r)^2$	$V = \frac{1}{2} x_v{}^2$

This section can be concluded with the following two lemmas:

Lemma 1: A pneumatic actuator controlled by a four-way proportional valve can be considered using a pseudo-bond with a supply rate $s(x_v, F_a) := -x_v F_a$ ***for passivity analysis.***

Lemma 2: A pneumatic actuator controlled by a four-way proportional valve <u>in an open-loop manner</u> is not passive with respect to the supply rate $s(x_v, F_a) := -x_v F_a$**.**

Lemma 1 is based on the previous explanation in this section. The proof of Lemma 2 is shown here.

<u>Proof</u> [11]:

From Equation (22), we know that the supply rate to the open-loop pneumatic actuator is $x_v F_a$. For any $x_v \neq 0$, define the average supply rate as $s_0(F_a, x_v)$,

$$\int_0^t -F_a x_v d_\tau = -s_0 \cdot t$$

Thus, for any finite positive number c^2 ($|c| < \infty$), there exists a time $t > \frac{c^2}{s_0}$ to make,

$$\int_0^t -F_a x_v d_\tau < -c^2$$

Therefore, the open-loop pneumatic actuator controlled by a proportional valve is not passive with respect to the supply rate $s(x_v, F_a) := -x_v F_a$.

3. Passive Pneumatic Actuator

To passify the pneumatic actuator in free space, the actuation force is fed back using pressure sensor measurements. If a pneumatic system can be proven to be passive in free space, it will be able to interact in a stable manner with any passive environment. This will enable stable and well-behaved impact and force control. Therefore, we can assume $F_a = M\ddot{x}$ (free space case) in the passivity analysis, where F_a is the actuation force, M is the actuator moving mass, and x is the actuator position. This is summarized by the following lemma.

Lemma 3: A pneumatic actuator controlled by a four-way proportional valve is passive with respect to the supply rate $s(x_v, F_a) := -x_v F_a$ ***under the closed-loop feedback control law:*** $\dot{x}_v = -k_0 F_a$***, where*** k_0 ***is a positive feedback gain.***

Proof:

The same storage function is chosen as Equation (12) for the pneumatic actuator, with the associated power form given by Equation (22). The feedback system is constructed as shown in Figure 3-4,

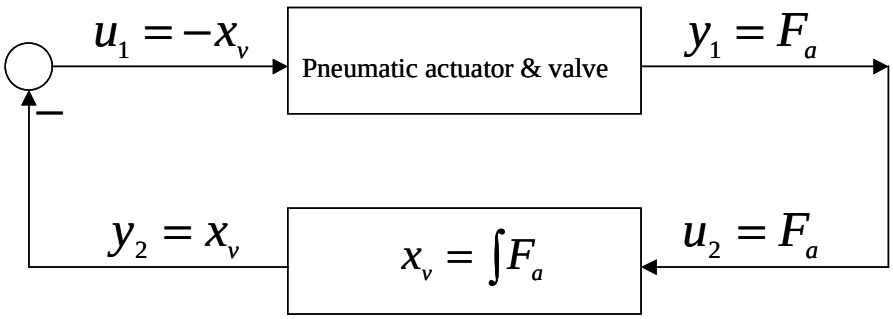

Figure 3-4. Closed-loop feedback control structure.

The feedback control law is,

$$\dot{x}_v = -k_0 F_a \tag{23}$$

A storage function is chosen for the feedback control law dynamics given by:

$$V_2 = \frac{1}{2} x_v^{\,2} \tag{24}$$

Taking the time derivative gives:

$$\dot{V}_2 = x_v \dot{x}_v = -k_0 F_a x_v \tag{25}$$

The total storage function for the closed-loop system is then given as:

$$V = V_1 + V_2 \tag{26}$$

Taking the time derivative of Equation (26) gives,

$$\dot{V} = \dot{V}_1 + \dot{V}_2 \tag{27}$$

Substituting Equations (22) and (25) into (27) gives,

$$\dot{V} = (k_1 - k_0) F_a x_v - k_2 F_a \dot{x} \tag{28}$$

Since k_1 is upper bounded, there ***always*** exists a positive feedback gain $k_0 > k_1$ to make,

$$\dot{V} = -\delta \cdot F_a x_v - k_2 F_a \dot{x} \tag{29}$$

where, δ is a positive constant. The supply rate to the pneumatic system is $s(x_v, F_a) := -x_v F_a$, resulting in:

$$\dot{V} = \delta \cdot s(x_v, F_a) - k_2 F_a \dot{x} \tag{30}$$

To analyze the passivity of the closed-loop system, two cases must be considered regarding the dissipation term $k_2 F_a \dot{x}$.

<u>*Case 1*</u>: $F_a \dot{x} \geq 0$

This implies that the kinetic energy of the actuator does not decay. From Equation (30), $F_a \dot{x} \geq 0$ and $k_2 > 0$ we get,

$$\dot{V} = \delta \cdot s(x_v, F_a) - k_2 F_a \dot{x} \leq \delta \cdot s(x_v, F_a) \tag{31}$$

Integrating Equation (31) gives,

$$V(t) - V(0) \leq \delta \cdot \int_0^t s(x_v, F_a) d_\tau \tag{32}$$

Since $V(t)$ is lower bounded by $V(t) \geq 0$, we get

$$\int_0^t s(x_v, F_a) d_\tau \geq -\frac{V(0)}{\delta} \tag{33}$$

Therefore, the closed-loop system is passive for $F_a \dot{x} \geq 0$. Furthermore, since $g(t) = k_2 F_a \dot{x}$ is non-negative and uniformly continuous, $g(t)$ tends to zero as $t \to \infty$ [10]. This implies that the power input to $F_a \dot{x}$ tends to zero as $t \to \infty$ for $F_a \dot{x} \geq 0$.

Case 2: $F_a \dot{x} < 0$

This implies that the kinetic energy of the actuator is being dissipated. It is intuitive that since the system is dissipative, it is passive. To prove it strictly, the storage function is chosen as,

$$V = V_1 + V_2 + C \cdot \frac{1}{2} M \dot{x}^2 \tag{34}$$

where C is the upper bound of k_2:

$$C \geq k_2 \geq 0 \tag{35}$$

Taking the time derivative of Equation (34) gives,

$$\dot{V} = \dot{V}_1 + \dot{V}_2 + C \cdot F_a \dot{x} \tag{36}$$

Substituting Equation (30) for $\dot{V}_1 + \dot{V}_2$ into Equation (36) gives,

$$\dot{V} = \delta \cdot s(x_v, F_a) - F_a \dot{x}(k_2 - C) \tag{37}$$

Since $F_a \dot{x}(k_2 - C) \geq 0$, Equation (37) yields,

$$\dot{V} \leq \delta \cdot s(x_v, F_a) \tag{38}$$

Integrating Equation (38) proves that the closed-loop system is passive for the case $F_a \dot{x} < 0$. Furthermore, since $g(t) = (k_2 - C) F_a \dot{x}$ is non-negative and uniformly continuous, $g(t)$ tends to zero as $t \to \infty$ [10]. This implies that the power input $F_a \dot{x}$ tends to zero as $t \to \infty$ for $F_a \dot{x} < 0$.

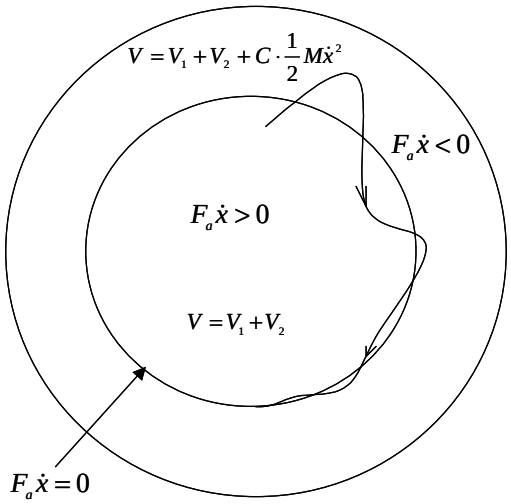

Figure 3-5. Passivity illustration for the pneumatic system with multiple storage functions.

Combining the two cases, we can conclude that the pneumatic actuator controlled by a four way proportional valve is passive with respect to the supply rate given by $s(x_v, F_a) = -x_v F_a$ under the feedback control law $\dot{x}_v = -k_0 F_a$. Furthermore, the actuation power output $F_a\dot{x}$ always tends to zero as $t \to \infty$. The two cases with their associated storage functions are shown in Figure 3-5. This passivity has been verified experimentally (not shown here).

4. Passive Impact and Force Control

The pneumatic actuator and valve closed-loop system has been shown to be passive using pressure feedback to obtain the actuation force and using the control law of Equation (23). This is not particularly useful if the valve can only passively dissipate to zero mass flow rate. Another input and output port should be added to the passive control

structure so that the actuator can output a desired nonzero actuation force. The control law is modified to the following,

$$\dot{x}_v = -k_0 (F_a - F_d) \tag{39}$$

where F_d is the desired actuation force, and F_a is the actuation force as determined by pressure feedback measurements and Equation (11). The new control law is illustrated in Figure 3-6 and will be proven to be passive. It can be seen from Figure 3-6 that the input does not change the passive structure of the closed-loop system given that F_d is an exogenous input.

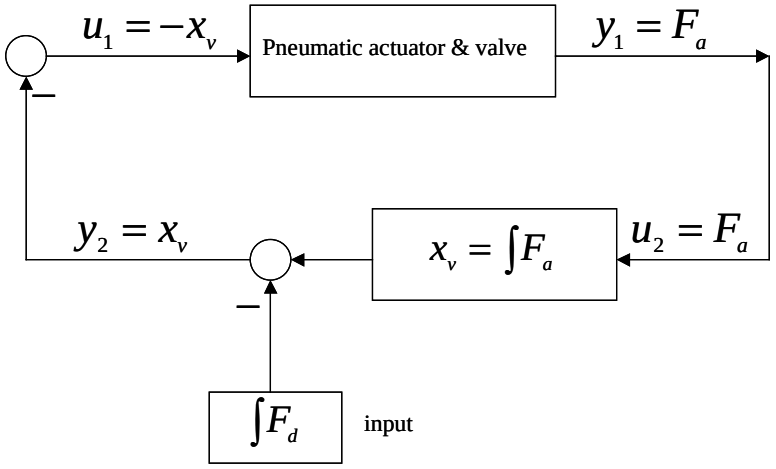

Figure 3-6. Illustration of passive force control.

Proof:

The same storage function is chosen as Equation (12). Substituting Equation (39) into Equation (25) gives,

$$\dot{V}_2 = x_v \dot{x}_v = -k_0 F_a x_v + k_0 F_d x_v \tag{40}$$

Substituting Equation (40) and Equation (22) into Equation (27) gives,

$$\dot{V} = -\delta \cdot F_a x_v + k_0 F_d x_v - k_2 F_a \dot{x} = s((x_v, x_v),(F_a, F_d)) - k_2 F_a \dot{x} \tag{41}$$

Now the pneumatic actuator closed-loop control system can be seen as a two-port system with supply rate $s((x_v, x_v),(F_a, F_d)) = -\delta \cdot F_a x_v + k_0 F_d x_v$. The closed-loop system is still passive based on the previous proof of lemma 3.

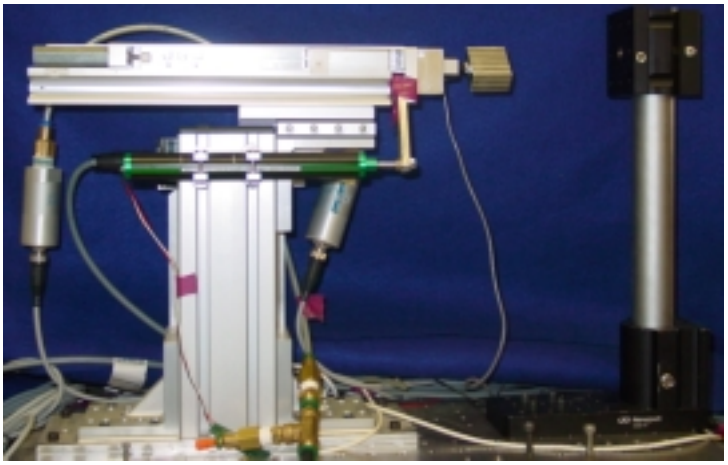

Figure 3-7. Experimental setup for impact and force control.

Experiments were carried out using the experimental setup shown in Figure 3-7. The experimental results will verify the passivity of the closed-loop system and show the application of the passivity properties to impact and force control of a pneumatic actuator. The setup consists of the horizontal actuator of a Festo two degree-of-freedom pick and place pneumatic system (the vertical degree-of-freedom has been removed). The double acting pneumatic actuator (Festo SLT-20-150-A-CC-B) has a stroke length of 150 mm, inner diameter of 20mm and piston rod diameter of 8mm. A linear potentiometer (Midori LP-150F) with 150 mm maximum travel is used to measure the linear position of the actuator. One four-way proportional valves (Festo MPYE-5-M5-010-B) is attached to

the chambers of the actuator. Two pressure transducers (Festo SDE-16-10V/20mA) are attached to each actuator chamber, respectively. Control is provided by a Pentium 4 computer with an A/D card (National Instruments PCI-6031E), which controls the proportional valve through an analog output channel. A load cell (Transducer Techniques MLP-25) is mounted at the end of the actuator to measure the impact and contact force when it hits a rigid environment (also shown in Figure 3-7), but is not used for control purposes.

For a desired interaction force $F_d = 40N$, the passified actuation system is driven by an input of F_d plus a constant coulomb friction compensation (assumed to be a constant) towards an unknown environment, which is a stiff wall. Experimental results are shown below in Figure 3-8. Although the velocity in free space is not explicitly controlled, it is typical of impact experiments, such as those of [19], in terms of approach velocity and the magnitude of the desired contact force.

As can be seen in Figure 3-8, the unexpected impact is stable and dissipative. The velocity of the actuator suddenly drops to zero right after the impact because of the passivity properties of the closed-loop system. The problem with the experimental results shown in Figure 3-8 is that the valve control voltage (proportional to the valve spool position) oscillates for quite a long period of time after the impact because there is no dissipative term in the control law. The valve response finally damps out because of the natural damping of the valve, which is not enough to absorb the energy quickly after the impact occurs. A dissipative term is therefore added to the valve dynamics to cure this problem, and the desired valve dynamics (control law) can be modified as

$$\dot{x}_v = -k_0(F_a - F_d) - k_d x_v \tag{42}$$

where, k_d is a positive constant dissipative term.

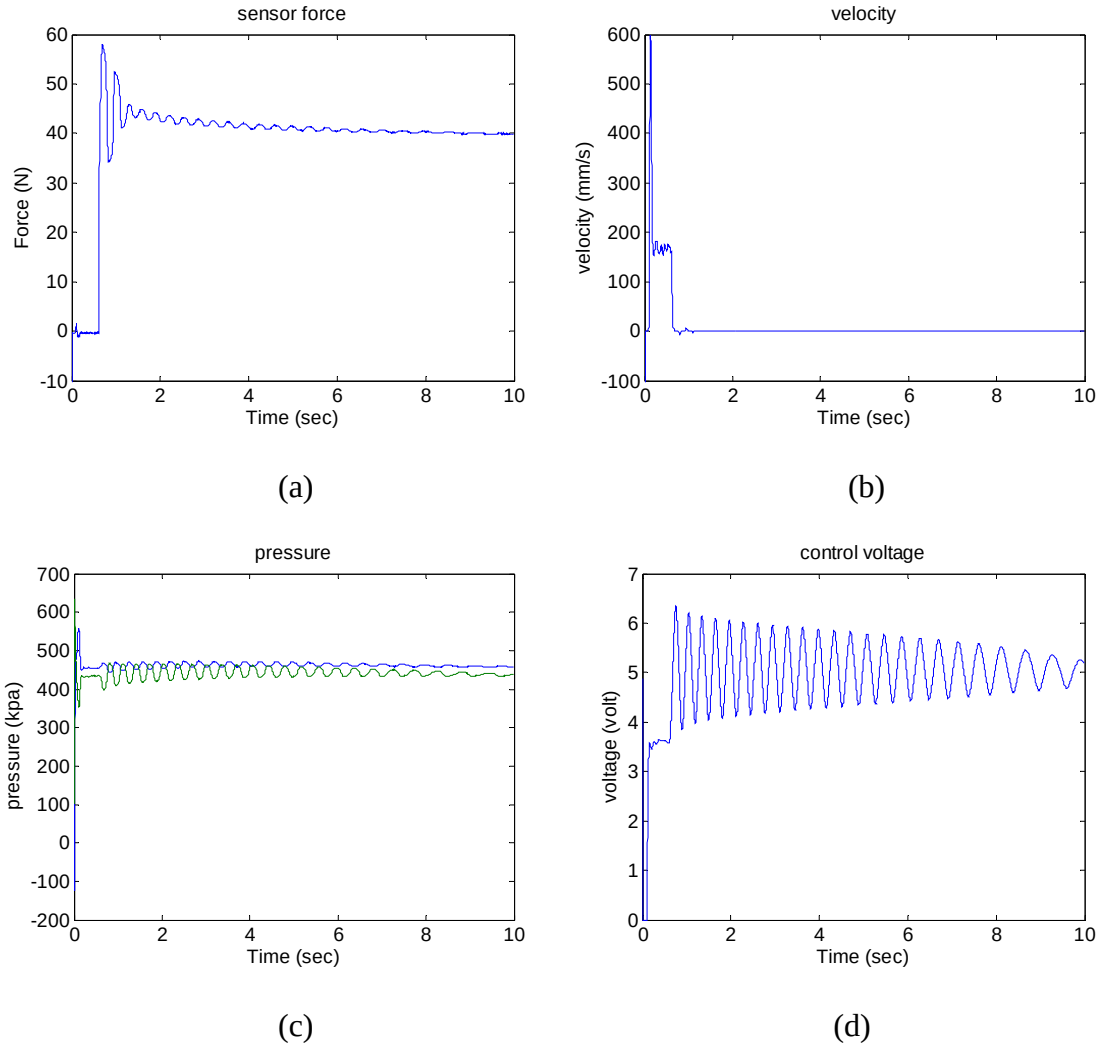

Figure 3-8. Impact and force control without the dissipative term. (a) sensor force, (b) velocity, (c) pressure and (d) control voltage.

Since a purely dissipative term is added, it is like adding a damper to the analogous spring-mass system of section 2, and the closed-loop pneumatic actuator can be easily proven to be still passive. It is shown in Figure 3-9 that the dissipative term can almost eliminate the valve oscillations after contact. Although the approach velocity is

appreciable at 0.15 m/s and the desired contact force is 40 N, the passive system can suppress the impact force and dissipate the kinetic energy effectively. For all the experimental results, note that a five volt input to the valve corresponds to zero mass flow rate.

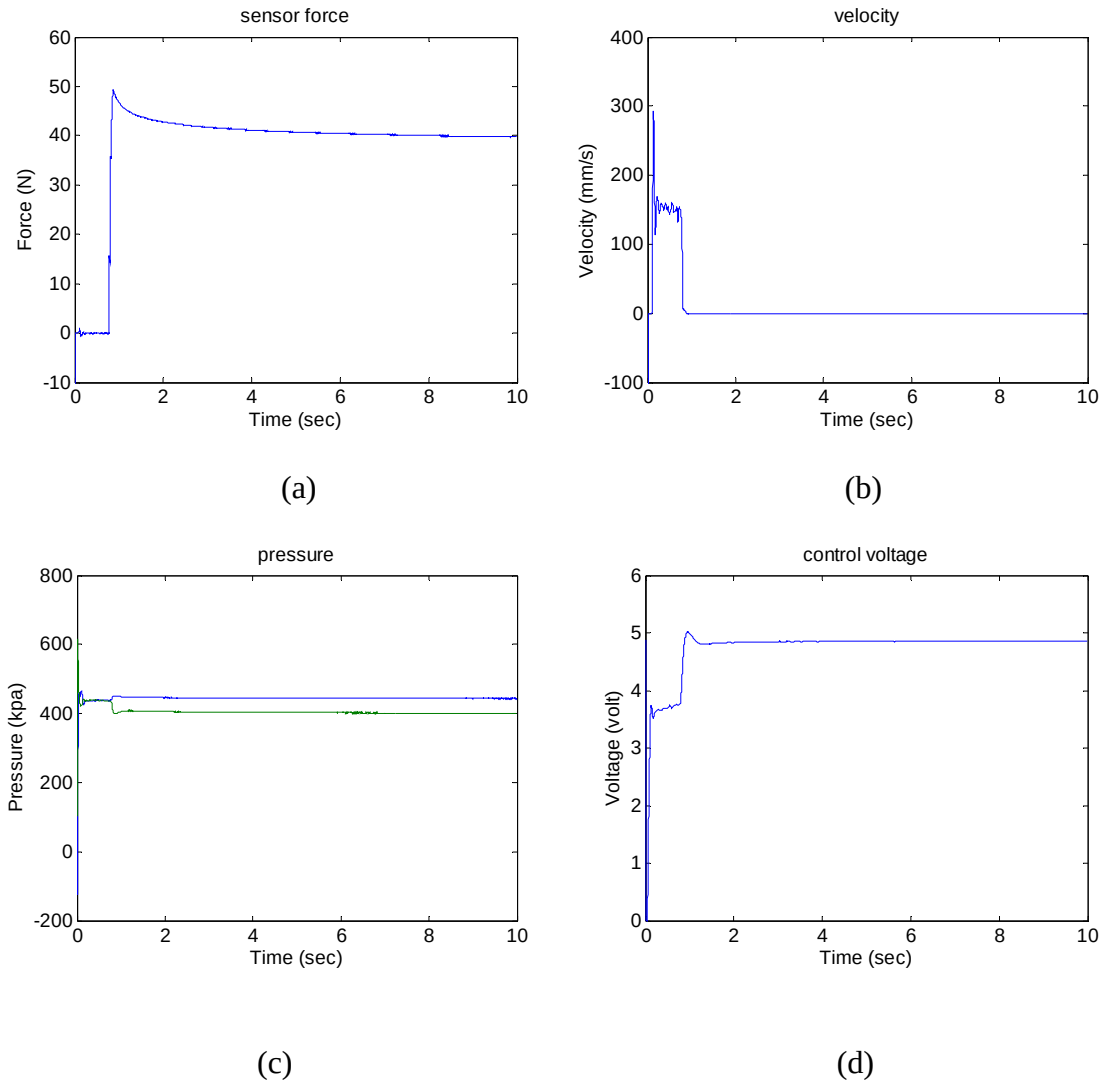

Figure 3-9. Impact and force control with the dissipative term. (a) sensor force, (b) velocity, (c) pressure and (d) control voltage.

5. Conclusions

Passivity analysis and control design of a pneumatic actuator controlled by a four-way proportional valve is presented in this paper. A pseudo-bond graph model is presented and used to prove the closed-loop passivity of a pneumatic actuator. The resulting passive closed-loop pneumatic system is able to interact with any passive environment in a safe and stable manner. Additionally, the formulation is able to produce a desired interaction force by using pressure sensors in the actuator chambers instead of external force sensing. It should be emphasized that this control approach for pneumatic systems reduces what is typically a complicated nonlinear control problem into one which is nearly trivial. The passivity properties allow strict guarantees for extremely simple but effective control laws. However, this general passivity analysis and control design can also be applied to more sophisticated nonlinear model-based control laws for interacting with not well characterized environments. With respect to application, the passivity properties of the closed-loop pneumatic feedback control system are advantageous for impact and force control by providing non-oscillatory contact forces with little overshoot. This passivity methodology is appropriate for application to many human-robot interaction tasks given that the human is typically considered passive.

References

[1] Hogan, N., "Impedance Control: An Approach to Manipulation: Part I - Theory," *Transactions of the ASME in the Journal of Dynamic Systems, Measurement, and Control*, vol. 107, pp. 1-7, 1985.

[2] Wu, Y., Tarn, T., Xi, N. and Isidori, N., "On Robust Impact Control via Positive Acceleration Feedback for Robot Manipulators," *Proceedings of the 1996 IEEE International Conference on Robotics and Automation*, pp. 1891-1896, 1996.

[3] Niksefat, N., Wu, C. Q. and Sepehri, N., "Design of a Lyapunov Controller for an Electro-hydraulic Actuator During Contact Tasks," *Transactions of the ASME in the Journal of Dynamic Systems, Measurement and Control*, vol. 123, pp. 299-307, 2001.

[4] Sekhavat, P., Wu, Q. and Sepehri, N., "Impact Control in Hydraulic Actuators," *Transactions of the ASME in the Journal of Dynamic Systems, Measurement and Control*, vol. 127, pp. 197-205, 2005.

[5] Bobrow, J. E. and McDonell, B. W., "Modeling, Identification, and Control of a Pneumatically Actuated, Force Controllable Robot," *IEEE Transactions on Robotics and Automation*, vol. 14, pp. 732-742, 1998.

[6] Hogan, N., "Stable Execution of Contact Tasks Using Impedance Control," *Proceedings of the 1987 IEEE international Conference on Robotics and Automation*, pp. 1047-1054, 1987.

[7] Hogan, N., "On the Stability of Manipulators Performing Contact Tasks," *IEEE Journal of Robotics and Automation*, vol. 4, pp. 677-686, 1988.

[8] Vidyasagar, M., *Analysis of Nonlinear Dynamic Systems*, 2nd Edition, Prentice Hall, 1993.

[9] Khalil, H. K., *Nonlinear Systems*, 3rd Edition, Prentice Hall, 2001.

[10] Slotine, J. and Li, W., *Applied Nonlinear Control*, Prentice Hall, 1991.

[11] Li, P., "Toward Safe and Human Friendly Hydraulics: The Passive Valve," *Transactions of the ASME in the Journal of Dynamics, Measurement and Control*, vol. 122, pp. 402-409, 2000.

[12] Krishnaswamy, K. and Li, P., "Passive Teleoperation of a Multi Degree of Freedom Hydraulic Backhoe Using Dynamic Passive Valve," *Proceedings of the 2003 International Mechanical Engineering Congress and Exposition*, Washington D.C., pp. 149-156, 2003.

[13] Krishnaswamy, K. and Li, P., "Bond Graph Based Approach to Passive Teleoperation of a Hydraulic Backhoe," *Transactions of the ASME in the Journal of Dynamics, Measurement and Control*, vol. 128, pp. 176-185, 2006.

[14] Colgate, J. E., Wannasuphoprasit, W. and Peshkin, M. A., "Cobots: Robots for Collaboration with Human Operators," *Proceedings of the 1996 International Mechanical Engineering Congress and Exposition*, vol. 58, New York, NY, pp. 433-439, 1996.

[15] Li, P. Y. and Horowitz, R., "Control of Smart Exercise Machines: Part I. Problem Formulation and Non-adaptive Control," *IEEE/ASME Transactions on Mechatronics*, vol. 2, no. 4, pp. 237-247, 1996.

[16] McCloy, D., and Martin, H.R., *Control of Fluid Power: Analysis and Design*, 2nd (revised) edition, John Wiley & Sons, 1980.

[17] Richer, E. and Hurmuzlu, Y., "A High Performance Pneumatic Force Actuator System: Part I - Nonlinear Mathematical Model," *Transactions of the ASME in the Journal of Dynamic Systems, Measurement and Control*, vol. 122, no. 3, pp. 416-425, 2000.

[18] Liu, S. and Bobrow, J. E., "An Analysis of a Pneumatic Servo System and Its Application to a Computer-Controlled Robot," *Transactions of the ASME in the Journal of Dynamics, Measurement and Control*, vol. 110, pp. 228-235, 1988.

[19] Youcef-Toumi, K. and Gutz, D.A., "Imapct and Force Control: Modeling and Experiments," *Transactions of the ASME in the Journal of Dynamics, Measurement and Control*, vol. 116, pp. 89-98, 1994.

ADDENDUM TO MANUSCRIPT II

A1. Pressure Control

The basic control schematic diagram of the pneumatic impedance controller is shown in Figure 3-10.

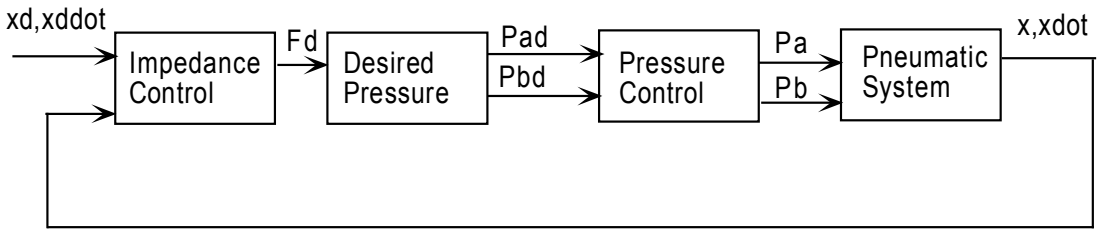

Figure 3-10. Diagram of the pneumatic impedance controller.

As a prerequisite to specifying the force necessary to uphold a desired impedance relationship between the interaction force and the motion errors of the actuator, it is necessary to be able to specify the actuation force at a high bandwidth. In a pneumatic system, this amount to being able to control the pressure in each side of the actuator. Figure 3-11 shows a schematic of the pneumatic actuation system. In order to control both the difference in pressure between the two sides of the actuator (in order to specify the actuation force), and to control the sum of the pressures of the two sides (in order to specify the compliance of the actuator), two three-way proportional spool valves are used to control the pressures in the two sides of the actuator separately. This section will consider the control of pressure in one side of the actuator using its respective three-way proportional valve.

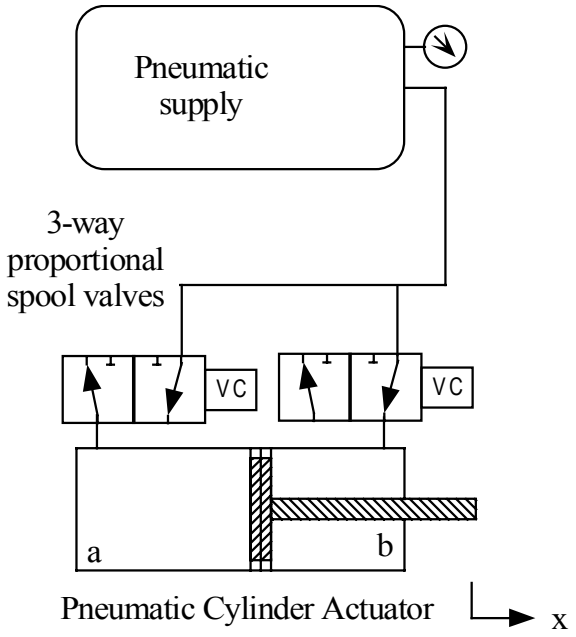

Figure 3-11. Schematic of the pneumatic actuation system. The pressure in each side of the actuator is separately controlled with a three-way proportional valve.

A mathematical model of a pneumatic actuator has been well studied. Assuming that the gas is perfect, the temperature and pressure within the two chambers are homogeneous, and the kinetic and potential energy of fluid are negligible, the rate of change of pressure within each pneumatic chamber can be expressed as,

$$\dot{P} = \frac{rRT}{V}\dot{m} - \frac{rP\dot{V}}{V} \tag{43}$$

where r is the thermal characteristic coefficient, with $r = 1$ for isothermal case, R is the ideal gas constant, T is the temperature, V is the control volume, and P is the pressure. Given the highly non-linear nature of the pressure dynamics, a model-based nonlinear controller is required to achieve adequate tracking. Treating the mass flow rate $\dot{m}$ as the

control variable u, and defining $f(\mathbf{x}) = -\frac{rP\dot{V}}{V}$, $b(\mathbf{x}) = \frac{rRT}{V}$, and $\mathbf{x}^T = [V \quad \dot{V} \quad P]$, the pressure dynamics can be stated more conveniently as:

$$\dot{P} = f(\mathbf{x}) + b(\mathbf{x})u \tag{44}$$

Using this standard notation, sliding mode control can be utilized to establish pressure tracking control. The sliding surface is selected as:

$$s = e + 2\lambda \int e + \lambda^2 \iint e \tag{45}$$

where $e = P - P_d$ is the pressure tracking error and P_d is the desired pressure. The forcing term, s, of this desired error dynamic can be driven to zero by defining the standard positive-definite Lyapunov function $\mathbf{V} = \frac{1}{2}s^2$, and ensuring that the derivative of this function is negative semi-definite. Given that $b(\mathbf{x}) = \frac{rRT}{V} > 0$, where the volume of the chamber V is physically always greater than zero, the derivative of the Lyapunov function is enforced to be the following,

$$\dot{\mathbf{V}} = s\dot{s} = -K|s|b(\mathbf{x}) \leq 0 \tag{46}$$

where $K > 0$. Solving for $\dot{s}$, this requires:

$$\dot{s} = -K\,\mathrm{sgn}(s)b(x) \tag{47}$$

Taking the derivative of Equation (45) and substituting $\dot{e} = \dot{P} - \dot{P}_d$ and $\dot{P}$ from Equation (44), this gives:

$$\dot{s} = b(\mathbf{x})u + f(\mathbf{x}) - \dot{P}_d + 2\lambda e + \lambda^2 \int e \tag{48}$$

Combining Equations (47) and (48) results in the following typical sliding mode control law:

$$u = \frac{1}{b(\mathbf{x})}\left[\dot{P}_d - f(\mathbf{x}) - 2\lambda e - \lambda^2 \int e\right] - K\,\mathrm{sgn}(s) \tag{49}$$

Equation (49) indicates the required mass flow rate for robust pressure tracking. To achieve this mass flow rate by controlling the flow orifice area of the valve, the mass flow rate equation relating the upstream and downstream pressures across the valve needs to be utilized. This is exactly the same as the description from Equation (6) to Equation (10) in Chapter II. In the interests of brevity, this portion is not shown here. Finally, the required valve area is found by the following relationship:

$$A = \begin{cases} u / \Psi(P_s, P) & \text{for } u \geq 0 \\ u / \Psi(P, P_{atm}) & \text{for } u < 0 \end{cases} \tag{50}$$

The control law specified by Equations (49-50) applied to each valve separately will enable the independent pressure tracking of each side of the pneumatic actuator. It should be noted that Equation (45) is an unconventional choice for the sliding surface. Given that the control influence appears in the first derivative of pressure as indicated in Equation (43), more conventional choices for the sliding surface are $s = e$ or $s = e + \lambda \int e$. However, these choices provided inferior pressure tracking experimentally.

A2. Impedance Control

The equation of motion for the pneumatic cylinder can be expressed as:

$$M\ddot{x} + B\dot{x} + F_f = F + F_e \tag{51}$$

where $F = P_a A_a - P_b A_b - P_{atm} A_r$ is the force provided by the pneumatic actuator with the pressures in each side of the cylinder P_a and P_b acting on their respective areas A_a and

A_b along with atmospheric pressure P_{atm} acting on the area of the rod A_r. Other forcing terms include Coulomb friction F_f, viscous friction $B\dot{x}$, and the force of the environment acting on the actuator F_e. As a matter of control philosophy, this control problem is atypical and interesting in that you want the control system to reject all disturbances *except* that coming from the environment F_e. The desired dynamic impedance behaviour relating the motion to external forces due to contact with the environment (or in free space when $F_e = 0$) can be expressed as

$$m(\ddot{x} - \ddot{x}_d) + b(\dot{x} - \dot{x}_d) + k(x - x_d) = F_e \tag{52}$$

where *m*, *b*, *k* are the target inertia, damping and spring constant, and x_d is the desired position. To enforce this impedance behaviour, it is necessary to specify the actuation force such that Equation (51) becomes Equation (52). As discussed, there are two ways of achieving this objective. The typical impedance control approach requires a measurement of the interaction force but avoids requiring a measurement of the acceleration. The approach taken here is to avoid using a load cell in favour of utilizing the acceleration. The desired actuation force is therefore required to be:

$$F_d = (\widetilde{M} - m)\ddot{x} + (\widetilde{B} - b)\dot{x} - k(x - x_d) + m\ddot{x}_d + b\dot{x}_d + \widetilde{F}_f \tag{53}$$

where $\widetilde{M}$, $\widetilde{B}$, and $\widetilde{F}_f$ are the estimated inertia, damping and coulomb friction of the pneumatic actuator. Assuming that the actual force *F* can be driven to the desired force F_d at a sufficiently high bandwidth through rapid and accurate pressure control of each side of the actuator, the dynamics become:

$$m(\ddot{x} - \ddot{x}_d) + b(\dot{x} - \dot{x}_d) + k(x - x_d) = F_e + (\widetilde{M} - M)\ddot{x} + (\widetilde{B} - B)\dot{x} + (\widetilde{F}_f - F_f) \tag{54}$$

Equation (54) relates the importance of adequately modelling the system such that the residual modelling error terms can be kept small so that Equation (54) is a close approximation of the desired impedance behaviour given by Equation (52).

To achieve the desired force profile specified in Equation (53), and to simultaneously specify the compliance of the actuator, the following constraint relationship can be established between the desired pressure in chamber *a* and *b*,

$$P_{ad} + P_{bd} = P_{sum} \tag{55}$$

where P_{ad} and P_{bd} are the desired pressure in chamber *a* and *b*, respectively, P_{sum} is a constant parameter. A linearized analysis reveals that the sum of the pressures specifies the compliance of the actuator. By maintaining a particular open-loop compliance, and specifying an appropriate target damping, low-bandwidth acceleration feedback may be utilized to enforce the desired impedance behaviour while maintaining stability.

The actuation force provided by the cylinder can be expressed as:

$$P_{ad} A_a - P_{bd} A_b - P_{atm} A_r = F_d \tag{56}$$

Combining Equation (55) and Equation (56) gives the desired pressure of chamber *a* and *b* to be feed to the pressure tracking controller:

$$P_{ad} = \frac{F_d + P_{sum} A_b + P_{atm} A_r}{A_a + A_b} \text{ and } P_{bd} = P_{sum} - P_{ad} \tag{57}$$

A3.Experimental Results of Impedance-based Contact Tasks

Experiments were conducted to show a) the pressure tracking performance, b) the motion control of the actuator in free-space and c) the force when transitioning from non-

contact to contact when hitting an unpredicted stiff wall. A photograph of the experimental setup is shown in Figure 3-12.

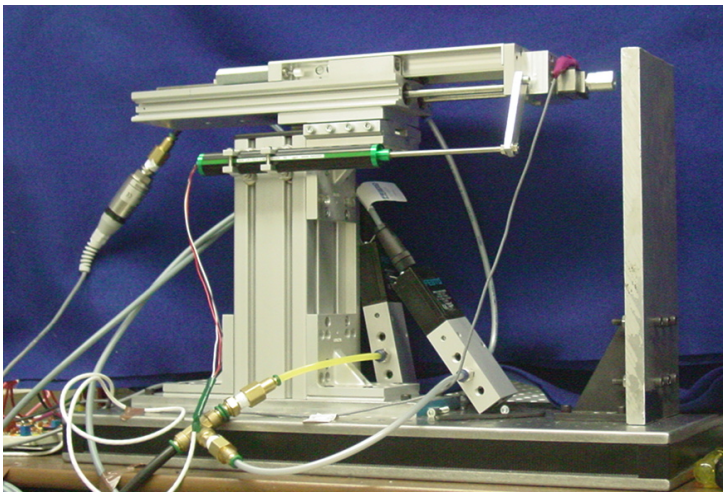

Figure 3-12. The experimental setup of the pneumatic actuation servo system.

A. Pressure Tracking

Figure 3-13 shows the closed-loop pressure tracking on one side of the actuator at 10 Hz utilizing the control law specified in section A1.

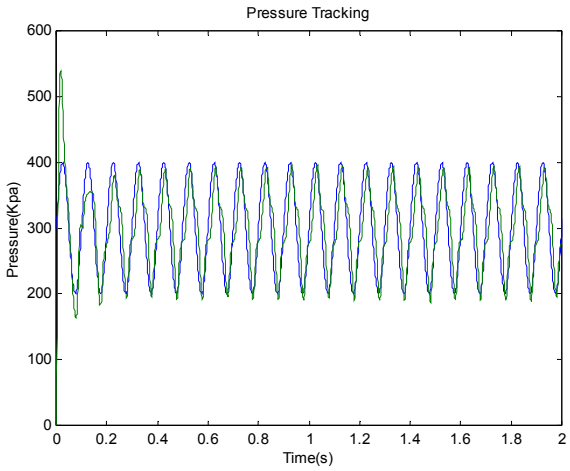

Figure 3-13. Experimental pressure tracking at 10 Hz. The desired pressure is shown in blue and the actual pressure is shown in green.

B. Motion Tracking in Free Space

Figure 3-14 shows closed-loop impedance control of the actuation system in free-space under tracking a 1.5 Hz sinusoidal motion of ±50 mm.

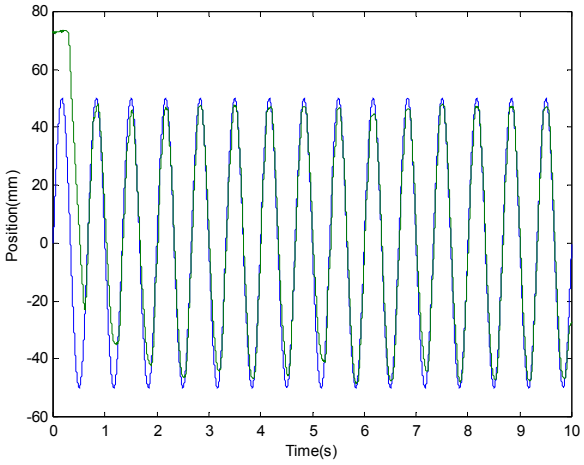

Figure 3-14. Motion tracking at 1.5 Hz under closed-loop impedance control. The desired position is shown in blue and the actual position is shown in green.

C. Non-contact to contact transition

A ramp with slope 30mm/sec was commanded to run the cylinder toward the wall, which is at about 55.6mm. The estimated wall position is at position 60mm (i.e. the ramp is commanded to stop at 60mm). The results of experiments are reported for three sets of impedance parameter combinations. Each set of parameters has the same damping ratio $\xi = 5$ and natural frequency $\omega_n = 40\, rad/\sec$. $P_{sum} = 400\, Kpa$ for all three cases. The position tracking performance and contact force profiles for each case are shown in Figures 3-15, 3-16, and 3-17. Figure 3-15 has target inertia, damping and stiffness of m = 0.5 kg, b = 200 N/(m/s), and k = 800 N/m. Figure 3-16 has target inertia, damping and stiffness of m = 1 kg, b = 400 N/(m/s), and k = 1600 N/m. Figure 3-17 has target inertia,

damping and stiffness of m = 2 kg, b = 800 N/(m/s), and k = 3200 N/m. Position tracking is good for all three cases, while the peak contact force is seen to increase as the target inertia of the system is increased (17 N for m = 0.5 kg, 23 N for m = 1 kg, and 44 N for m = 2 kg). The final steady state contact force is not zero because there is error between the actual wall position and estimated one.

As a conclusion, a method for the impedance control of a pneumatic linear actuator for tasks involving contact interaction was presented. By exploiting the natural compliance properties of a pneumatic actuator, the impedance control method presented does not require the use of a load cell to measure the interaction force, but rather allows the use of a low-bandwidth acceleration feedback signal instead. A controller to achieve desired pressure tracking in each side of the pneumatic cylinder was also presented. Experimental results show good pressure tracking, good motion tracking in free-space, and a predictable trend of lower contact forces for lower target inertias of the system.

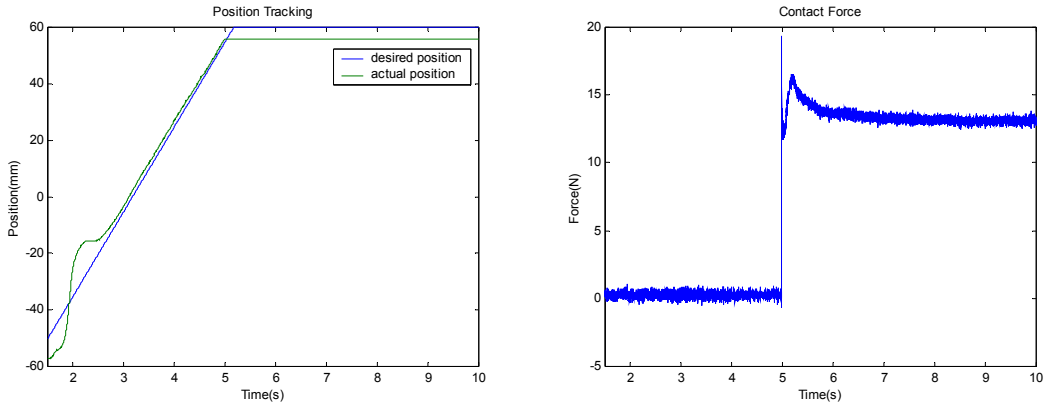

(a) (b)

Figure 3-15. Non-contact to contact transition showing (a) the commanded motion and tracking and (b) the contact force. Target values: m = 0.5 kg, b = 200 N/(m/s), and k = 800 N/m.

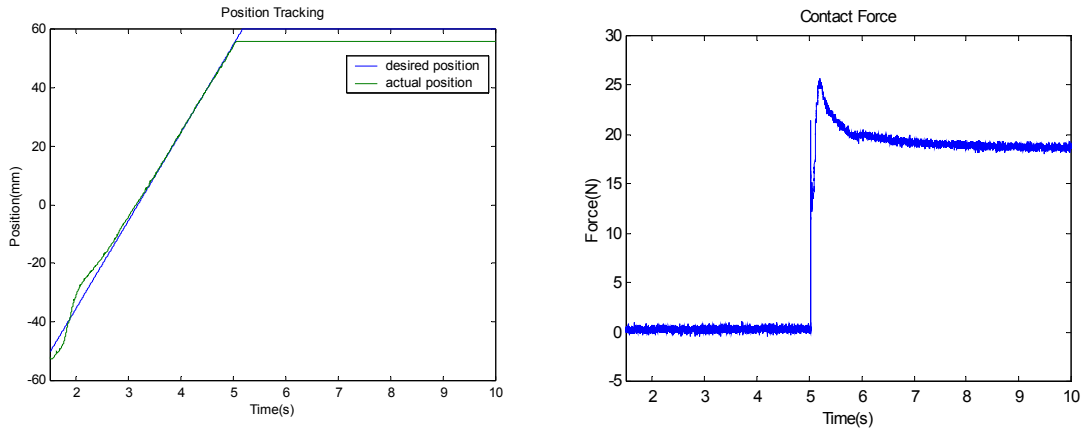

(a) (b)

Figure 3-16. Non-contact to contact transition showing (a) the commanded motion and tracking and (b) the contact force. Target values: m = 1 kg, b = 400 N/(m/s), and k = 1600 N/m.

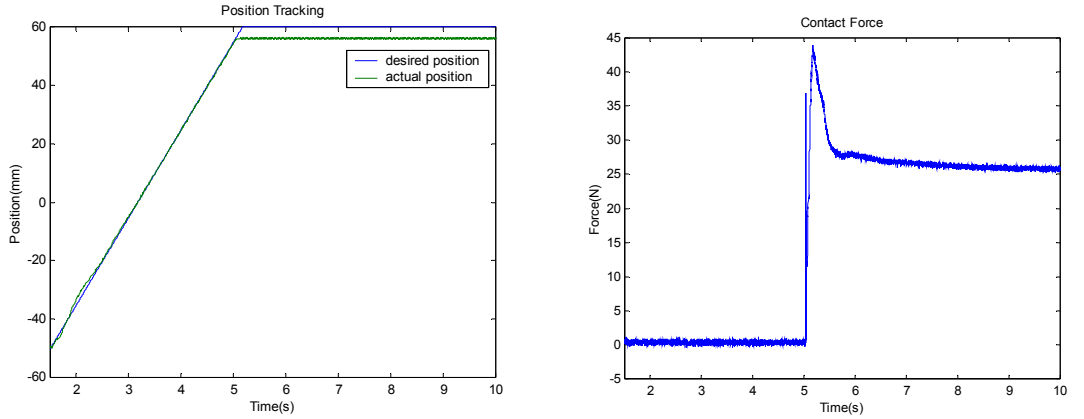

(a) (b)

Figure 3-17. Non-contact to contact transition showing (a) the commanded motion and tracking and (b) the contact force. Target values: m = 2 kg, b = 800 N/(m/s), and k = 3200 N/m.

CHAPTER IV

MANUSCRIPT III

AN ENERGETIC CONTROL METHODOLOGY FOR PNEUMATIC HOPPING ROBOTS

Yong Zhu and Eric J. Barth

Department of Mechanical Engineering
Vanderbilt University
Nashville, TN 37235

Submitted as a Full Paper to the *IEEE/ASME Transactions on Mechatronics*

Abstract

This paper presents an energetically derived control methodology to specify and regulate the oscillatory motion of a pneumatic hopping robot. A lossless pneumatic actuation system with an inertia is energetically shown to represent an oscillator with a stiffness, and hence frequency, related to the equilibrium pressures in the actuator. Following from an analysis of the conservative energy storage elements in the system, a control methodology is derived to sustain a specified frequency of oscillation in the presence of energy dissipation. The basic control strategy is to control the pressure in the upper chamber of the pneumatic cylinder to specify the contact time of the piston, while controlling the total conservative energy stored in the system to specify the flight time and corresponding flight height of the cylinder. The control strategy takes advantage of the natural passive dynamics of the upper chamber to provide much of the required actuation forces and natural stiffness, while the remaining forces needed to overcome the energy dissipation present in a non-ideal system with losses are provided by a nonlinear control law for the charging and discharging of the lower chamber of the cylinder. This control methodology is demonstrated through simulation and experimental results to provide accurate and repeatable energetically efficient hopping motion for pneumatically actuated robots in the presence of dissipative forces.

1. Introduction

The goal of this work is to design a control methodology that takes advantage of the passive dynamics of pneumatic actuation that will result in energetically efficient oscillatory motion when dissipation is present. Recent work [1] on high energy-density

monopropellant power supply and actuation systems for untethered robotics motivates an energetically savvy approach to the control of such systems with application to legged robots. The basic control strategy will be to control the pressure in one side of a pneumatic hopper to specify the contact time, while controlling the energy summation to specify the flight time and corresponding flight height.

For an electrically actuated robot, if no active force control is implemented to effectively absorb the energy during contact, oscillations and even instability can occur. For example, joint acceleration feedback was used to control the contact transition of a three-link direct-drive robot [2]. Aiming at control and energetics, a monopod running robot with hip and leg compliance was controlled by taking advantage of the "passive dynamic" operation close to the desired motion without any actuation [3]. 95% hip actuation energy saving was shown at 3 m/s running speed. This idea is similar to the approach taken here, except here the compliance and hence passive dynamics will be specified by the compressibility of gas in a pneumatic actuator.

Suffering from highly nonlinear dynamics, varying environment conditions and frequent phase transitions between free space and constrained motions, legged robot researchers generally face the challenge of motion planning and control in real time simultaneously. Changing interactions with the environment present extreme challenges for such systems. Looking to nature, the compliance of tendons show great advantages for interaction tasks such as legged locomotion. Series elastic actuators have been applied to walking robot applications [4]. A hopping robot "Kenken" with an articulated leg and two hydraulic actuators as muscles and a tensile spring as a tendon was studied, although stability problems remained for higher speeds [5]. Mckibben artificial muscles were used

for a hopping robot to pursue higher power-to-weight ratio [6]. The end-effects of the McKibben actuators limited their application. A dynamic walking biped "Lucy" actuated by pneumatic artificial muscles was investigated out in Brussel [7]. Although artificial muscles can be used as actuators for legged robots and provide high power-to-weight ratio and shock absorption, they have many limitations such as hysteresis and short stroke.

Pneumatic actuators can be used directly as legs to drive a legged robot, which provide much higher power-to-weight ratio than their electrically actuated competitors. Raibert was a pioneer in legged robot locomotion research using pneumatic cylinders. He first presented the design and control of a pneumatic hopping robot in [8]. The hopping motion is generated in an intuitive manner. The upper chamber is charged when the foot is on the ground and exhausted as soon as it leaves the ground until it reaches a predefined low pressure (15 psi). There is a monotonic mapping between hopping height and thrust value, but this relationship can not be simply characterized. The hopping height can only be chosen based on a set of experimental data empirically. There is also a unique frequency associated with each thrust value, which can only be implicitly regulated also.

Raibert used another leg actuation method for better efficiency [8] when the hopping machine works in 3D. The upper chamber works as a spring and the lower chamber works as an actuator. The upper chamber is connected to the supply pressure through a check valve. The lower chamber is charged when the foot is in flight and discharged when it is on the ground through a solenoid valve. By controlling the length of charging time during flight, the hopping height and frequency can be implicitly

controlled. Energetic efficiency was not the main concern in Raibert's work and the contact time and flight time can not be explicitly specified either.

Many other researches on legged robots using pneumatic systems were also carried out after Raibert. A small six-legged pneumatic walking robot named Boadicea was designed using customized lightweight pneumatic actuators and solenoid valves [9]. The performance clearly showed high force and power density, which means that the robot can walk faster with larger payloads. Other advantages such as energy storage, and natural compliance for shock absorption, provide latitude for stable and energy efficient controller design with pneumatically actuated systems. The absorbed energy can be stored as the internal energy of compressed air and can be released again when the hopper is in flight. Fast gaits are generated for the control of a pneumatically actuated robot in [10]. The control system generates the desired trajectories on line and generates proper control inputs to achieve the desired trajectories. An energy-based Lyapunov function was chosen to generate the controlled limit cycles. This is similar to the approach taken here, except that this work will generate a desired velocity based on the current position and direction of motion. The compliance of pneumatic actuators has been proven to be of great importance when a robot interacts with unknown environment perturbations [11].

The paper is organized as follows. In Section 2, it is energetically shown that a lossless pneumatic actuation system is a natural oscillator. Section 3 presents how system parameters are specified. Basically, desired hopping period and flight time are achieved through control of kinetic and potential energy of the system. Section 4 presents the control law to specify the desired kinetic and potential energy so that the desired hopping

motion can be generated. Simulation results are shown in Section 5. The continuous control inputs are provided by proportional valves. Section 6 presents experimental results of the pneumatic hopper. Instead of using proportional valves, solenoid on/off valves are used to carry out the same control approach. Conclusions are drawn in section 7.

2. Energetic Analysis of a Pneumatic Oscillator

The conservative energy stored in a simple mass-spring linear oscillator not influenced by gravity (Figure 4-1a) can be expressed as:

$$E = \tfrac{1}{2} m\dot{x}^2 + \tfrac{1}{2} kx^2 \tag{1}$$

For a system with no losses, taking the time rate of change of this expression and setting it equal to zero,

$$\dot{E} = (m\ddot{x} + kx)\dot{x} = 0 \tag{2}$$

yields not only the equation of motion of the system, but also reveals that the work rate, or power, injected into the system is always zero ($F_{net}\,\dot{x} = 0$). The resulting equation of motion necessary to keep the conservative energy constant, and the solution $x(t) = A\sin(\omega t)$, $\dot{x}(t) = A\omega\cos(\omega t)$, $\ddot{x}(t) = -A\omega^2\sin(\omega t) = -\omega^2 x(t)$, $\omega = \sqrt{k/m}$, both reveal an algebraic relationship between acceleration and position. From a pole location standpoint, this relationship results in the system having a complex conjugate pole pair on the imaginary axis (marginally stable) and the system is thereby subject to sustained oscillations.

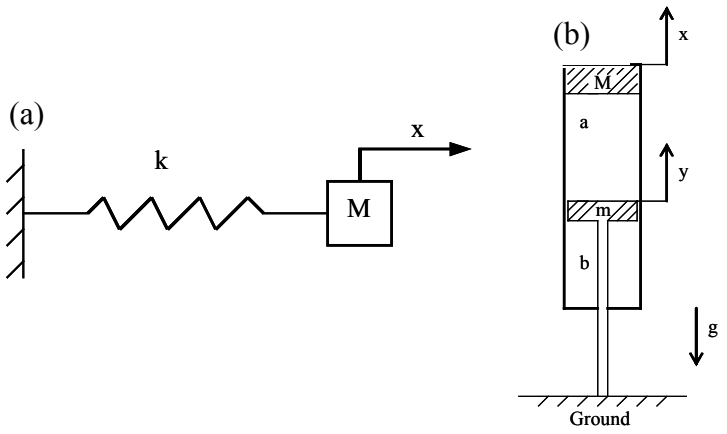

Figure 4-1. Schematic diagrams of (a) a linear mass-spring system, and (b) a vertical pneumatic system. An analysis of energetically lossless versions of both systems reveal equations of motion with an algebraic relationship between acceleration and position.

A similar energetic analysis of the vertical pneumatic system shown in Figure 4-1b also reveals an oscillatory system with a frequency of oscillation dependent upon system parameters. The kinetic and potential energy terms for a leakless, adiabatic (no heat losses), frictionless piston-mass system while in contact with the ground are given as:

$$E = \underbrace{\frac{1}{2}M\dot{x}^2}_{KE(\dot{x})} + \underbrace{\frac{P_a V_a}{1-\gamma}\left[\left(\frac{P_a}{P_{atm}}\right)^{\frac{1-\gamma}{\gamma}} - 1\right]}_{PEa(x)} + \underbrace{\frac{P_b V_b}{1-\gamma}\left[\left(\frac{P_b}{P_{atm}}\right)^{\frac{1-\gamma}{\gamma}} - 1\right]}_{PEb(x)} + \underbrace{P_{atm} A_r x}_{PEr(x)} + Mgx \qquad (3)$$

where $V_{a,b}$ represents the volume of chamber a or b, and $A_r = A_a - A_b$ represents the cross sectional area of the piston rod. The potential energy of each chamber of the actuator is derived using standard thermodynamic relationships as the ability of the pressure in the chamber, P_a or P_b, to do work adiabatically with respect to an environment at atmospheric pressure P_{atm}, where the ratio of specific heats is denoted by

γ. The term, $PE_r(x)$ is a term similar to a gravitational potential energy term due to the unequal piston areas of the two sides of the actuator. If the system has no losses, the system will maintain a constant energy E by shuttling energy between potential and kinetic energy storage in the form of a well defined oscillation.

Akin to the analysis for the simple mass-spring system subject to no energetic losses, the time rate of change of conservative energy storage is taken and set to zero:

$$\dot{E} = [M\ddot{x} + P_b A_b - P_a A_a + P_{atm} A_r + Mg]\dot{x} = 0 \tag{4}$$

The correct equation of motion is evident from this conservation of energy:

$$M\ddot{x} = P_a A_a - P_b A_b - P_{atm} A_r - Mg \tag{5}$$

Substituting the following adiabatic relationships into the equation of motion, and defining static equilibrium pressures: P_{a0}, P_{b0} and volumes: V_{mida}, V_{midb} at $x = 0$,

$$P_a V_a^{\gamma} = \text{constant} = P_{a0} V_{mida}^{\gamma} \tag{6}$$

$$P_b V_b^{\gamma} = \text{constant} = P_{b0} V_{midb}^{\gamma} \tag{7}$$

$$P_{a0} A_a - P_{b0} A_b - P_{atm} A_r - Mg = 0 \tag{8}$$

results in:

$$M\ddot{x} + \left\{ P_{a0} A_a \left[\left(\frac{V_{midb}}{V_{midb} - A_b x} \right)^{\gamma} - \left(\frac{V_{mida}}{A_a x + V_{mida}} \right)^{\gamma} \right] + (P_{atm} A_r + Mg) \left[1 - \left(\frac{V_{midb}}{V_{midb} - A_b x} \right)^{\gamma} \right] \right\} = 0 \tag{9}$$

where

$$V_a = A_a x + V_{mida} \tag{10}$$

$$V_b = V_{midb} - A_b x \tag{11}$$

As seen in Equation (9), the pneumatic system shows a direct algebraic relationship between acceleration and position. Although nonlinear, the second term (contained in

brackets { }) of Equation (9) plays a similar role as the position-dependent spring return force *kx* of the linear oscillator. Denote this return force as F_R,

$$F_R = P_{a0}A_a\left[\left(\frac{V_{midb}}{V_{midb}-A_bx}\right)^{\gamma}-\left(\frac{V_{mida}}{A_ax+V_{mida}}\right)^{\gamma}\right]+(P_{atm}A_r+Mg)\left[1-\left(\frac{V_{midb}}{V_{midb}-A_bx}\right)^{\gamma}\right] \quad (12)$$

Taking the partial derivative of F_R evaluated at $x = 0$ gives the linearly approximated stiffness of the pneumatic actuator:

$$K_{stiff} = \left.\frac{\partial F_R}{\partial x}\right|_{x=0} = \gamma\left[P_{a0}A_a\left(\frac{A_a}{V_{mida}}+\frac{A_b}{V_{midb}}\right)-(P_{atm}A_r+Mg)\frac{A_b}{V_{midb}}\right] \quad (13)$$

This linear approximation and the following linearized equation of motion will be used in the subsequent development of specifying and controlling the hopping robot:

$$M\ddot{x}+K_{stiff}x \cong 0 \quad (14)$$

It should also be noted that a rearrangement of Equation (13) gives the equilibrium pressure P_{a0} in terms of a desired linear stiffness:

$$P_{a0} = \frac{K_{stiff}/\gamma+(P_{atm}A_r+Mg)A_b/V_{midb}}{A_a(A_a/V_{mida}+A_b/V_{midb})} \quad (15)$$

A plot of the nonlinear stiffness due to the compressibility present in a pneumatic system shows that it has the effect of a hardening spring, given that the slope increases as *x* increases. Further, it can also be seen that all potential energy terms in Equation (3) are a function solely of position, and therefore represent true path-independent conservative energy potentials. Substitutions of Equations (6) and (7), in addition to Equations (10) and (11), result in expressions for these position-dependent potentials:

$$PEa(x) = \left(\frac{P_{a0}(V_{mida}+A_ax)}{1-\gamma}\right)\left(\frac{V_{mida}}{V_{mida}+A_ax}\right)^{\gamma}\left\{\left[\frac{P_{a0}}{P_{atm}}\left(\frac{V_{mida}}{V_{mida}+A_ax}\right)^{\gamma}\right]^{\frac{1-\gamma}{\gamma}}-1\right\} \quad (16)$$

$$PEb(x) = \left(\frac{P_{b0}(V_{midb} - A_b x)}{1-\gamma} \right) \left(\frac{V_{midb}}{V_{midb} - A_b x} \right)^{\gamma} \left\{ \left[\frac{P_{b0}}{P_{atm}} \left(\frac{V_{midb}}{V_{midb} - A_b x} \right)^{\gamma} \right]^{\frac{1-\gamma}{\gamma}} - 1 \right\} \quad (17)$$

$$PEr(x) = P_{atm} A_r x \quad (18)$$

Given that the stiffness of the pneumatic system increases as P_{a0} and P_{b0} increase, the frequency of oscillation is dependent upon these system parameters (in addition to being amplitude-dependent as determined by the total conservative energy stored in the system). Simple dynamic simulations of the system verify this claim.

3. Specification of System Parameters

This section will establish approximate relationships between the linearized stiffness and total conservative energy of the system, and the resulting time of flight and time on the ground of the hopping motion. This will provide a way to specify the two independent quantities of the system in terms of a desired dynamic behavior.

3.1 Defining the Hopping Cycle

For the system shown in Figure 4-1b undergoing a representative hopping motion as shown in Figure 4-2, the following critical moments and periods are defined:

$t_0 = 0$: defines the starting point of a **full hopping cycle** ($x = 0$).
t_1 : defines the **lift-up** moment of the foot ($y = 0$).
$T_1 = t_1 - t_0$ is defined as the **launch period**.
T_2 is defined as the **compression period (** $x \le 0$).
T_{air} is defined as the **flight time**.
T_3 is defined as the **recovery period**.
T_{hop} is defined as the **full hopping period**.

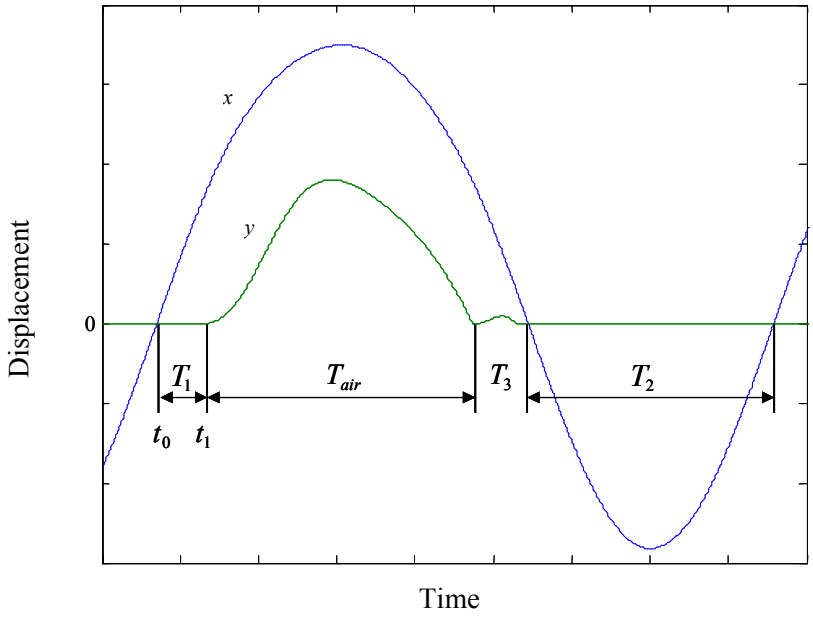

Figure 4-2. Representative hopping trajectory.

In the sections that follow, the hopping cycle will be analyzed according to the following decomposition,

$$T_{hop} \cong T_1 + T_3 + T_{air} + T_2 \tag{19}$$

where T_{hop} and T_{air} are to be specified, and $T_3 \cong T_1$. This relationship will then be utilized to determine the two independently specifiable quantities K_{stiff} and E_d (or alternatively P_{a0} and E_d given that the relationship between P_{a0} and K_{stiff} is a one-to-one mapping provided by Equation (15)). Unfortunately, due to the coupling and nonlinearities present in the system, it is not possible to write closed-form expressions for K_{stiff} and E_d in term of T_{hop} and T_{air}. Equation (19) will therefore be cast as a function solely of the intermediate parameter T_2 (the compression period) by pursuing the functional

relationship $T_1(T_2)$. Once the parameter T_2 is determined, approximate closed-form expressions for K_{stiff} and E_d will be possible. This will allow a designer to specify T_{hop} and T_{air} according to a desired gait, or other criteria, and arrive at initial values of system parameters K_{stiff} and E_d. These values can then be subsequently adjusted if further precision on T_{hop} and T_{air} is required.

3.2 Launch Period T_1

This section will express the launch period T_1 as a function of the compression period T_2. It should be first recognized that during the launch period, the system is in contact with the ground and approximately obeys the linear equation of motion $M\ddot{x} \cong -K_{stiff}x$ given in Equation (14). The solution of this approximate equation of motion is:

$$x(t) \cong A\sin(\omega t) \tag{20}$$

Evaluated at the moment of lift-off, t_1, and utilizing the fact that $\omega_{n,contact} = \sqrt{K_{stiff}/M} = \pi/T_2$ results in an expression that will provide the sought after relationship between T_1 and T_2:

$$x(t_1) \cong A\sin\left(\frac{\pi}{T_2}T_1\right) \tag{21}$$

The task is now to determine expressions for $x(t_1)$ and A as functions of the variable T_2 and specifiable parameters T_{hop} and T_{air}.

To obtain an expression for $x(t_1)$ as a function of T_2, consider the idealized lossless model of the hopping system:

$$M\ddot{x} = P_a A_a - P_b A_b - P_{atm} A_r - Mg \tag{22}$$

$$m\ddot{y} = P_b A_b - P_a A_a + P_{atm} A_r + F_{ground} - mg \tag{23}$$

Utilizing Equation (23) with conditions immediately before contact is lost at time t_1, namely $\dot{y}(t_1) = 0$, $\sum Forces = 0 \;\Rightarrow\; \ddot{y}(t_1) = 0$, and $F_{ground} = 0$, leads to the relationship,

$$P_b A_b - P_a A_a + P_{atm} A_r - mg = 0 \tag{24}$$

Substituting Equation (24) into Equation (22) with $\dot{y} = 0$ results in,

$$\ddot{x}(t_1) = -\left(\frac{M+m}{M}\right)g \tag{25}$$

which is the acceleration condition on *x* for the foot to break contact with the ground. Based on Equation (25), the approximate linear equation of motion $M\ddot{x} = -K_{stiff}x$ given in Equation (14), and the fact that $\omega_{n,contact} = \sqrt{K_{stiff}/M} = \pi/T_2$ leads to the following:

$$K_{stiff} \cong \left(\frac{\pi}{T_2}\right)^2 M \tag{26}$$

$$x(t_1) \cong \frac{(M+m)g}{M \cdot (\pi/T_2)^2} \tag{27}$$

To obtain an expression for *A* in Equation (21) as a function of T_2, consider the velocity $\dot{x}(t_1)$ immediately before the foot breaks contact. Since both chambers are sealed when the foot is in the air, and by assuming the friction influence between the piston and cylinder wall is sufficient enough that relative motion between *x* and *y* can be neglected (a mild assumption given most commercially available pneumatic cylinders),

the time it takes for the cylinder body to reach the its highest point is given by the simple free flight ballistics equation:

$$\dot{x}(t_{peak}) = \dot{x}(t_1) - g(t_{peak} - t_1) \tag{28}$$

Given that $\dot{x}(t_{peak}) = 0$, and assuming that $(t_{peak} - t_1) = \frac{1}{2}T_{air}$, the launch velocity can be expressed in terms of T_{air}:

$$\dot{x}(t_1) = \frac{T_{air}g}{2} \tag{29}$$

Equating the kinetic energy at lift-off $\frac{1}{2}(M+m)\dot{x}(t_1)^2 = \frac{1}{8}(M+m)T_{air}^2 g^2$, with the potential energy at the peak $(M+m)gh$, with height h as the distance above the datum $x(t_1)$, results in the hopping height:

$$h = \frac{1}{8}gT_{air}^{\ 2} \tag{30}$$

The maximum position of the cylinder housing $x_{\max}$ can therefore be represented as the following by combining Equation (30) with Equation (27),

$$x_{\max} = x(t_1) + h = \frac{(M+m)g}{M \cdot (\pi / T_2)^2} + \frac{1}{8}gT_{air}^{\ 2} \tag{31}$$

Although $x_{\max}$ is slightly higher than the absolute value of the minimum distance the cylinder housing can reach, it will be used as an approximation of the amplitude during contact:

$$A \cong x_{\max} = \frac{(M+m)g}{M \cdot (\pi / T_2)^2} + \frac{1}{8}gT_{air}^{\ 2} \tag{32}$$

Ideally, one would use the relationship $A \cong |x_{\min}|$ to more accurately approximate the amplitude of Equation (21), but unfortunately such an expression is not expressible as

a function solely of the compression period T_2 but instead depends upon both K_{stiff} and the total conservative energy *E*. It will be shown that the approximation of Equation (32) is acceptably accurate. Returning to Equation (21), and armed with expressions for $x(t_1)$ and *A* given by Equations (27) and (32), the launch period can be expressed as:

$$T_1 \cong \frac{T_2}{\pi} \arcsin\left(\frac{8(M+m)g}{8(M+m)g + M \cdot (\pi / T_2)^2 g T_{air}^2} \right) \tag{33}$$

From both simulation and experimental results, it was seen that although the trajectory of *x* is quite symmetric, the trajectory of *y* is not as symmetric. To be able to specify the time the foot is in flight, it has been assumed that the *y* trajectory is symmetric about the highest point reached by *x*. However, since the foot generally bounces slightly when it lands on the ground, the time the foot is in the air cannot be easily determined. Due to this, the recovery period T_3 is not strictly equal to the launch period T_1, but equating these two quantities in Equation (19) will offer a reasonable approximation.

3.3 Solving for K_{stiff} and the Total Desired Conservative Energy

Utilizing Equation (33), Equation (19) can be expressed as:

$$T_{hop} \cong \frac{2T_2}{\pi} \arcsin\left(\frac{8(M+m)g}{8(M+m)g + M \cdot (\pi / T_2)^2 g T_{air}^2} \right) + T_{air} + T_2 \tag{34}$$

Equation (34) is unfortunately a transcendental nonlinear equation that does not offer a closed-form solution for T_2. Standard nonlinear solvers, such as MATLAB's `fzero` routine, can be used to solve for T_2 given known or specified values for *M*, *m*, T_{hop} and T_{air}. Once the value of T_2 has been determined, the sought after parameters K_{stiff} and P_{a0} can be determined from Equations (26) and (15) respectively. The desired total

conservative energy of the system to support the desired T_{hop} and T_{air} can be obtained from the expression:

$$E_d = \tfrac{1}{2} M\dot{x}(t_1)^2 + PEa(x(t_1)) + PEb(x(t_1)) + P_{atm} A_r x(t_1) + Mgx(t_1) \qquad (35)$$

utilizing Equations (29), (27), (16), and (17) for quantities $\dot{x}(t_1)$, $x(t_1)$, $PEa(x(t_1))$, and $PEb(x(t_1))$ respectively.

4. The Controlled Pneumatic Hopping Robot

This section presents the system equations and control strategy for a vertical, gravity influenced pneumatic piston carrying an inertial load, serving as a hopping robot, as shown in Figure 4-3. This system contains two exogenous control inputs in the form of control valves that influence the flow of mass into or out of each chamber *a* or *b*. The cylinder position and piston positions are defined as *x* and *y*, respectively with separate origins as shown.

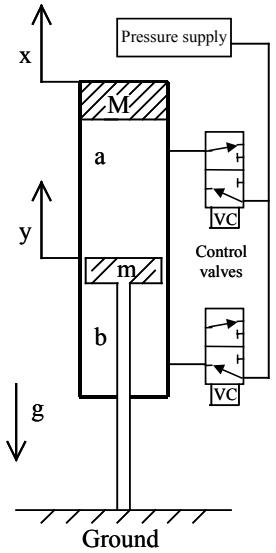

Figure 4-3. Schematic of a pneumatic hopping robot showing inertial coordinates for the cylinder housing (*x*) and piston (*y*) positions. (*x* = 0 at equilibrium pressures with *y* = 0 when the piston is in contact with the ground).

By neglecting friction, leakage and other losses, the dynamics of the vertical pneumatic cylinder housing (while the system is in contact with the ground, or during flight) can be represented by the following equation:

$$M\ddot{x} = P_a A_a - P_b A_b - P_{atm} A_r - Mg \tag{36}$$

Expressions for the time rates of change of the pressures can be derived from the following constitutive relations for the rate of internal energy storage $\dot{U}$, rate of heat input $\dot{Q}$, enthalpy rate $\dot{H}$, and work rate $\dot{W}$, of each control volume associated with side *a* and side *b*:

$$\dot{U} = \dot{Q} + \dot{H} - \dot{W} \tag{37}$$

$$\dot{U} = \frac{\dot{P}V + P\dot{V}}{\gamma - 1} \tag{38}$$

$$\dot{H} = \dot{m} c_p T_{flow} \tag{39}$$

$$\dot{W} = P\dot{V} \tag{40}$$

These result in the following for $\dot{Q} = 0$ (adiabatic):

$$\dot{P}_a = \frac{\gamma R T_{flow}}{V_a}\dot{m}_a - \frac{\gamma P_a \dot{V}_a}{V_a} \tag{41}$$

$$\dot{P}_b = \frac{\gamma R T_{flow}}{V_b}\dot{m}_b - \frac{\gamma P_b \dot{V}_b}{V_b} \tag{42}$$

Taking the derivative of Equation (36) and substituting Equations (41) and (42) yield:

$$\dddot{x} = \frac{1}{M}\left(\frac{\gamma P_b A_b \dot{V}_b}{V_b} - \frac{\gamma P_a A_a \dot{V}_a}{V_a} + \frac{\gamma R T_{flow} A_a}{V_a}\dot{m}_a - \frac{\gamma R T_{flow} A_b}{V_b}\dot{m}_b \right) \tag{43}$$

This system (43) contains two inputs, $\dot{m}_a$ and $\dot{m}_b$, which can be specified arbitrarily by the two control valves and an adequate supply pressure [12, 13, 14, 15, 16].

In practice, the pneumatic system shown in Figure 4-3 will be subject to non-ideal energetic losses including friction, leakage, heat losses, and losses due to impact with the ground when hopping. The aim of this work is to control the pneumatic system to oscillate and hop using the two control valves in order to inject energy to account for the energetic losses in the system. The control strategy will be to exploit the natural resonate dynamics of the pneumatic piston-mass system. Furthermore, it would be desirable to do so in a way to be able to specify and then regulate the time-of-flight and the total period of oscillation.

One imaginable control approach would be to create a time dependent position trajectory from a simulation or analytical solution of the ideal lossless system, and then create a controller to have the controlled system follow this desired trajectory. This however would not take full advantage of the natural passive dynamics of the system, which can be utilized to help achieve this task in an energetically savvy manner by storing and returning energy among its conservative energy storage elements. Hence, the strategy taken here will be to regulate the stiffness of the system and the total amount of conservative energy stored in the system such that predictable and repeatable dynamic behavior is achieved in the face of dissipative losses. In brief, regulation of the stiffness of the system will be attained by using the control valve for chamber *a* (see Figure 4-3) in order to maintain the ideal position-dependent potential energy given by Equation (16). It should be reiterated that the equilibrium pressure P_{a0} present in Equation (16) uniquely specifies the system's stiffness (as given in Equation (13)). Maintenance of this stiffness will essentially scale time (natural frequency) while in contact with the ground. The control valve for chamber *b* (see Figure 4-3) will be used to maintain the kinetic energy

of the system. Due to the fact that all terms except the kinetic energy of Equation (3) are position-dependent or a specified constant (E_d), the desired velocity will be derived *as a function of position*. In this manner, the passive dynamics of the system will contribute constructively to a specified hopping motion. This strategy will be justified in the remainder of the paper.

It should be noted that this strategy is based on the conservative energy storage expression of Equation (3), which is valid only while contact with the ground is maintained. In order to include the case where ground contact is lost (and regained, implying hopping), it will be sufficient to control the energy storage during contact only. The strategy is to therefore control the actuator only while it is in contact with the ground, and seal off the actuator while in flight (both mass flow rates equal zero). Since it is known that the energy of the system when leaving and re-contacting with the ground will be identical except for losses, controlling the energy profile while in contact will serve to compensate for the energy dissipation the system undergoes during both contact and flight.

4.1 Controlling the Potential Energy and Natural Frequency

The natural frequency of the pneumatic oscillator is specified via the dependence of the potential energy storage on position. It has been shown in Equation (16) that the scaling of this potential energy is dependent upon the equilibrium pressure P_{a0}. Therefore, utilizing Equation (6), the correct energy profile as a function of position is maintained if P_a is driven to the following desired pressure:

$$P_{ad}(x) = P_{a0}\left(\frac{V_{mida}}{V_{mida} + A_a x}\right)^{\gamma} \tag{44}$$

where P_{a0} is determined from the desired periods T_{hop} and T_{air} according to Section 3.3. Tracking this desired pressure as a function of position will compensating for leakage and heat losses and ensure that the correct amount of potential energy is stored in the system. In a manner akin to a spring, the correct amount of potential energy at each position will in turn ensure that the natural frequency of the passive dynamics contribute constructively to the desired hopping motion.

To drive P_a to P_{ad}, the following first order error dynamic with pole location $-\lambda_1$ on the real axis is enforced during contact:

$$e = P_a - P_{ad}(x) = P_a - P_{a0}\left(\frac{V_{mida}}{V_{mida} + A_a x}\right)^{\gamma} \tag{45}$$

$$\dot{e} + \lambda_1 e = 0 \tag{46}$$

$$\dot{P}_a - \dot{P}_{ad}(x) = -\lambda_1 (P_a - P_{ad}(x)) \tag{47}$$

Substituting in Equation (41) for $\dot{P}_a$, and its idealized form for $\dot{P}_{ad}(x)$,

$$\dot{P}_{ad}(x) = -\frac{\gamma P_a A_a \dot{x}}{(V_{mida} + A_a x)} \tag{48}$$

results in the following control law for chamber *a*,

$$\dot{m}_a = \left(-\frac{\lambda_1 (V_{mida} + A_a x)}{\gamma R T_{flow}} + \frac{A_a \dot{x}}{R T_{flow}}\right)\left(P_a - P_{a0}\left(\frac{V_{mida}}{V_{mida} + A_a x}\right)^{\gamma}\right) \tag{49}$$

where T_{flow} is approximated to be room temperature.

4.2 Controlling the Kinetic Energy

Merely maintaining the proper potential energy profile as a function of position is not sufficient to sustain a cyclic motion in the face of dissipation. By additionally ensuring the correct amount of kinetic energy as a function of position, a well regulated cyclic motion while in contact with the ground can be achieved. During flight, and as evidenced by Equation (29), the flight time is dependent upon the launch velocity at the critical lift-off position $x(t_1)$. Therefore, in controlling the hopping robot subject to losses, it will be critical to maintain the correct velocity at each position during contact.

The total desired conservative energy of the system, E_d, in terms of the desired periods T_{hop} and T_{air} is specified in Section 3.3. By utilizing this quantity for E in Equation (3), the following position-dependent desired velocity can be defined to maintain the desired conservative energy while in contact:

$$\begin{aligned} \dot{x}_d(x) = sign(\dot{x})\sqrt{\left|\tfrac{2}{M}\left(E_d - PEa(x) - PEb(x) - PEr(x) - Mgx\right)\right|} \\ \times sign\left(\tfrac{2}{M}\left(E_d - PEa(x) - PEb(x) - PEr(x) - Mgx\right)\right) \end{aligned} \tag{50}$$

where $PEa(x)$, $PEb(x)$, and $PEr(x)$ are evaluated according to Equations (16), (17) and (18) respectively with the value of P_{b0} evaluated according to Equation (8). The resulting shape of the desired position-dependent velocity profile according to Equation (50) is shown in Figure 4-4.

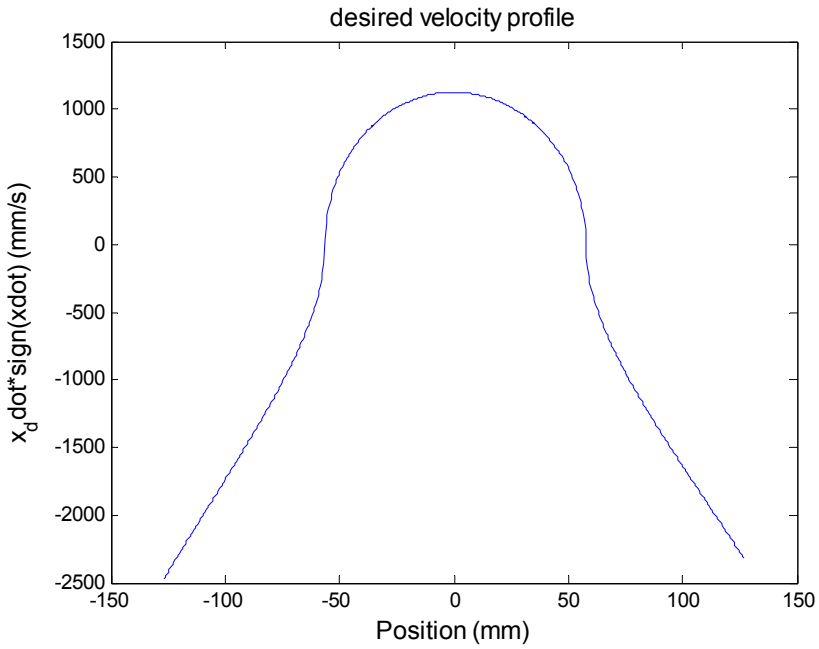

Figure 4-4. Representative position-dependent velocity profile.

Note that this position-based desired velocity also depends on the sign of the current velocity. Based on Equation (9), the desired acceleration can also be expressed as a function of position,

$$\ddot{x}_d(x) = \frac{1}{M}\left\{P_{a0}A_a\left[\left(\frac{V_{mida}}{A_a x + V_{mida}}\right)^{\gamma} - \left(\frac{V_{midb}}{V_{midb} - A_b x}\right)^{\gamma}\right] + (P_{atm}A_r + Mg)\left[\left(\frac{V_{midb}}{V_{midb} - A_b x}\right)^{\gamma} - 1\right]\right\} \tag{51}$$

As will be seen, the desired jerk is required as a feedforward term in the control law:

$$\dddot{x}_d(x, \dot{x}_d) = \frac{1}{M}\left[-\frac{\gamma A_a^2 P_{a0} V_{mida}^{\gamma}}{(V_{mida} + A_a x)^{1+\gamma}} - \frac{\gamma A_b (P_{a0}A_a - P_{atm}A_r - Mg) V_{midb}^{\gamma}}{(V_{midb} - A_b x)^{1+\gamma}}\right]\dot{x}_d \tag{52}$$

The desired position-dependent acceleration profile is shown in Figure 4-5. It should also be noted that the relationship between acceleration and position revealed by Equation

(51), and shown in Figure 4-5 below, is very nearly linear for a large range of positions (80% of the total stroke of the actuator). This large linear range substantiates the use of the approximate equation of motion $M\ddot{x} + K_{stiff}x \cong 0$ given in Equation (14) and the linear stiffness term given in Equation (13).

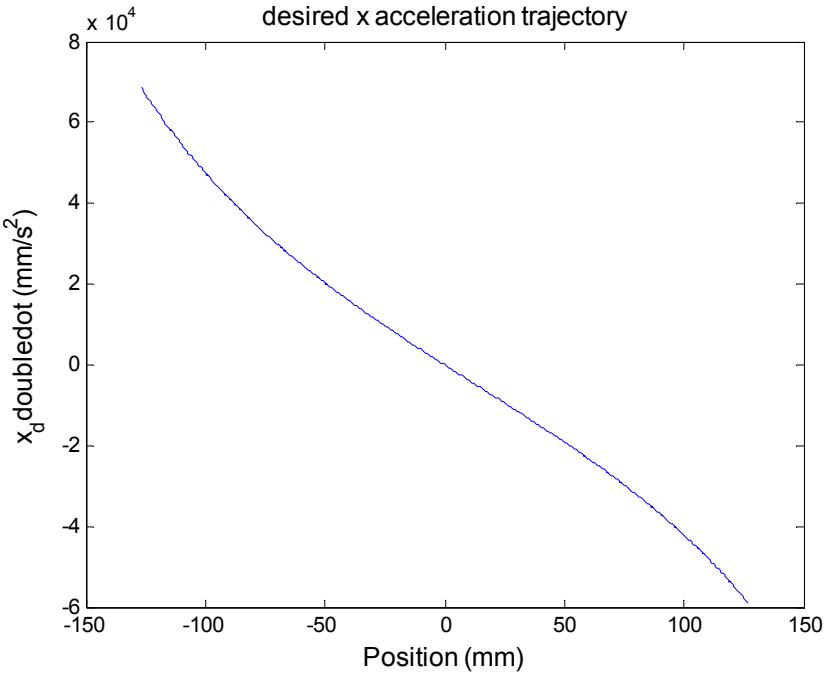

Figure 4-5. Representative position-dependent acceleration profile.

The desired velocity can be achieved through a simple nonlinear control law to track the desired position-dependent velocity through valve *b*. The Lyapunov-based control law derivation can be summarized as follows:

$$V = \tfrac{1}{2}s^2 \tag{53}$$

$$s = (\ddot{x} - \ddot{x}_d) + \lambda_2(\dot{x} - \dot{x}_d) \tag{54}$$

$$\dot{V} = s\dot{s} = -k_2 s^2 \tag{55}$$

$$\dot{s} = -k_2 s \tag{56}$$

$$\dot{s} = (\dddot{x} - \dddot{x}_d) + \lambda_2(\ddot{x} - \ddot{x}_d) = -k_2 s \tag{57}$$

$$\dddot{x} = \dddot{x}_d - \lambda_2(\ddot{x} - \ddot{x}_d) - k_2 s \tag{58}$$

where λ_2 and k_2 specify the dynamics on and off the sliding surface respectively. Substitution of Equation (43) into Equation (58) with $\dot{m}_a = 0$ yields the control law for side *b*,

$$\dot{m}_b = -\frac{MV_b}{\gamma R T_{flow} A_b}\left[\frac{\gamma P_a \dot{V}_a A_a}{MV_a} - \frac{\gamma P_b \dot{V}_b A_b}{MV_b} + \dddot{x}_d - (\lambda_2 + k_2)(\ddot{x} - \ddot{x}_d) - k_2\lambda_2(\dot{x} - \dot{x}_d)\right] \tag{59}$$

where T_{flow} is again approximated to be room temperature.

Achieving the control mass flow rates specified in Equations (49) and (59) can be done with two three-way valves (one per side *a* and *b*) to charge or discharge the piston chambers. In the case of proportional valves that modulate the flow orifice area, there is a direct algebraic relationship between orifice area and mass flow rate [12, 13, 14, 15, 16]. This relationship can be utilized to command the valve orifice area. For a sufficiently high bandwidth valve, the dynamics associated with achieving the needed orifice can be, and is commonly, neglected.

5. Hopping Simulation Results Using Proportional Valves

A simulation of a controlled pneumatic hopping robot involving frictional losses is presented below. The hopping system was modeled as the following,

$$M\ddot{x} = P_a A_a - P_b A_b - P_{atm} A_r - Mg - b(\dot{x} - \dot{y}) \tag{60}$$

$$m\ddot{y} = P_b A_b - P_a A_a + P_{atm} A_r + F_{ground} - mg - b(\dot{y} - \dot{x}) \tag{61}$$

with M = 0.54 kg and m = 0.05 kg, and viscous friction effects representing the sliding piston and rod seals modeled by b = 2 N.sec/m. The mass parameters are the same as the experimental setup, which will be described in Section 6. The pressure dynamics were modeled as Equations (41) and (42). The ground model was approximated as a very stiff spring and damping to represent losses upon collision,

$$F_{ground} = -k_{ground} y - b_{ground} \dot{y} \qquad \text{if } y < 0 \tag{62}$$

where k_{ground} = 1.0×10^6 N/m and b_{ground} = 1000 N.sec/m. The control laws for each side of the piston are given by Equations (49) and (59) respectively, with λ_1 = 1000, λ_2 = 400, and k_2 = 40, during contact ($y \le 0$); and $\dot{m}_a = \dot{m}_b = 0$ during flight ($y > 0$).

Figures 4-6 to 4-11 show simulations of the hopper for three cases. Case I: designed periods of T_{hop} = 0.5 and T_{air} = 0.3 seconds. Case II: designed periods of T_{hop} = 0.4 and T_{air} = 0.2 seconds. Case III: designed periods of T_{hop} = 0.3 and T_{air} = 0.1 seconds. Figures 4-6, 4-7 and 4-8 show the position response of the system for each case. Hopping is present as evidenced by the piston position y becoming non-zero. From the figures, it can be seen that the approximations of Section 3.3 provided parameters P_{a0} and E_d that result in reasonably close approximations of the desired periods T_{hop} and T_{air}. Figure 4-9 shows the velocity tracking for Case II where, again, this is only achieved or expected during contact. Figure 4-10 shows the resulting pressures in the two sides of the cylinder for Case II. Figure 4-11 shows the mass flow rates during Case II.

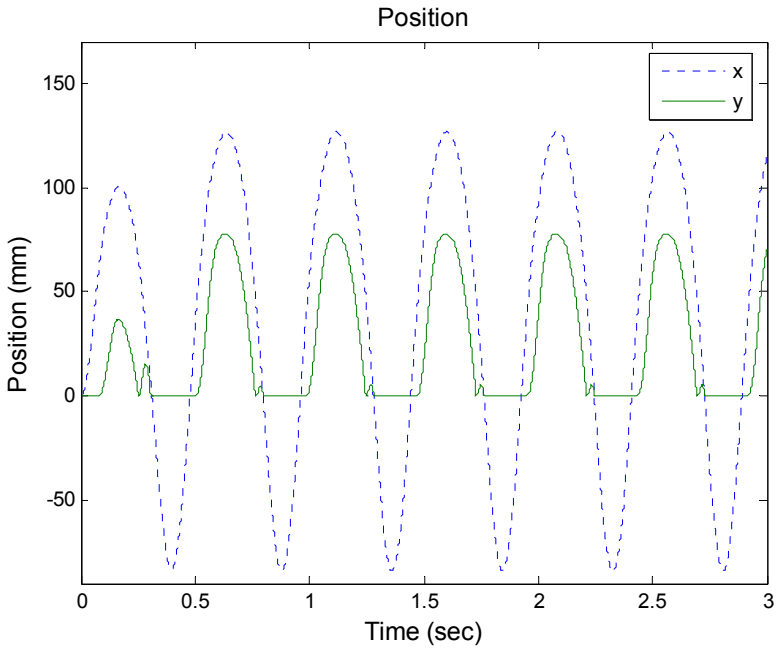

Figure 4-6. Case I: Hopping results for designed periods of T_{hop} = 0.5 seconds and T_{air} = 0.3 seconds. Actual periods in simulation are T_{hop} = 0.48 seconds and T_{air} = 0.26 seconds.

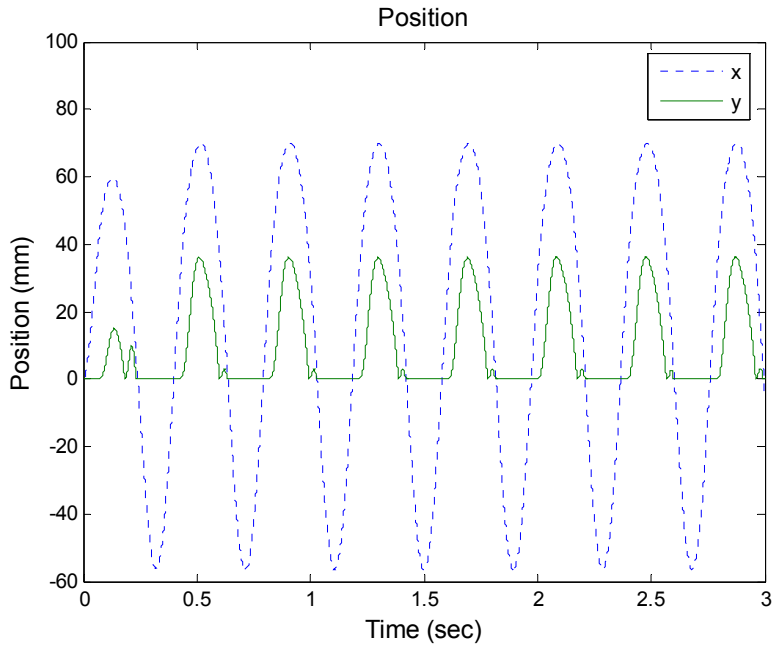

Figure 4-7. Case II: Hopping results for designed periods of T_{hop} = 0.4 seconds and T_{air} = 0.2 seconds. Actual periods in simulation are T_{hop} = 0.39 seconds and T_{air} = 0.18 seconds.

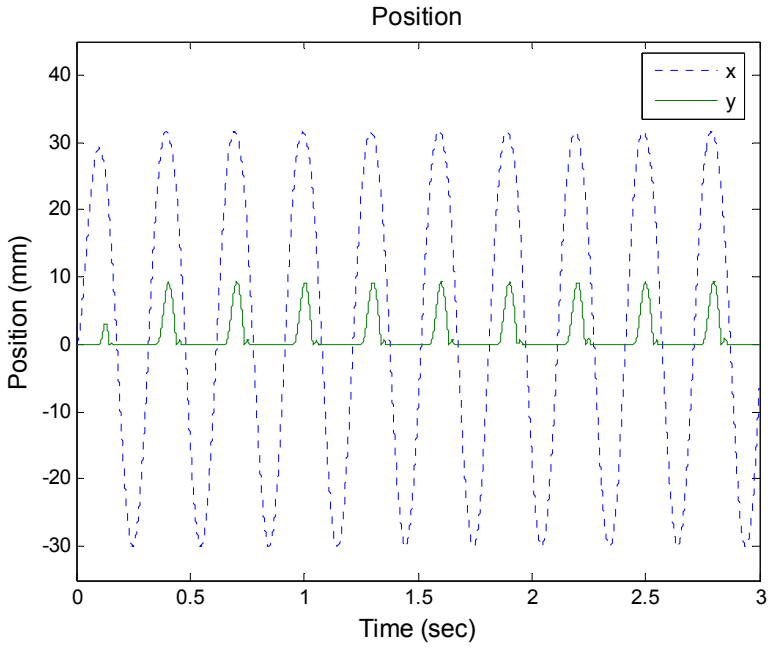

Figure 4-8. Case III: Hopping results for designed periods of T_{hop} = 0.3 seconds and T_{air} = 0.1 seconds. Actual periods in simulation are T_{hop} = 0.3 seconds and T_{air} = 0.09 seconds.

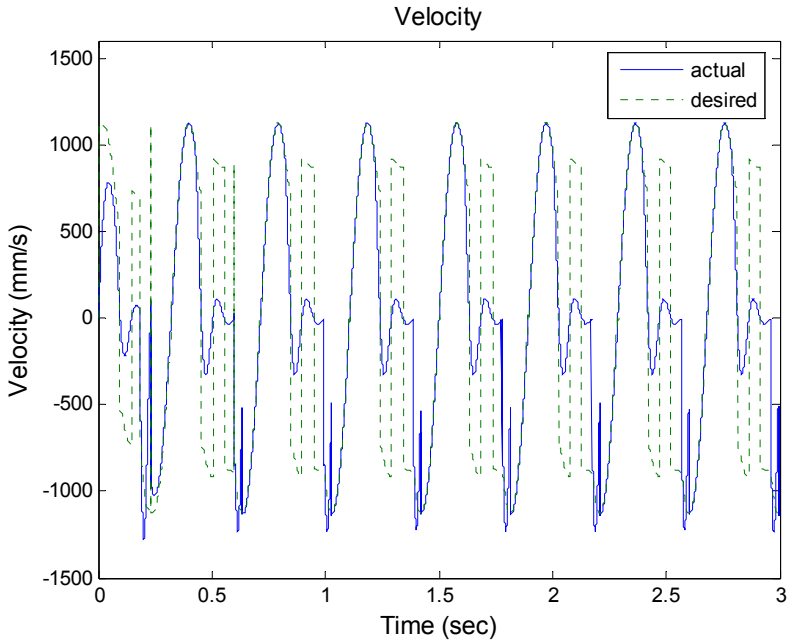

Figure 4-9. Case II: Desired velocity ($\dot{x}_d$) and actual velocity ($\dot{x}$). Velocity tracking is achieved during contact only.

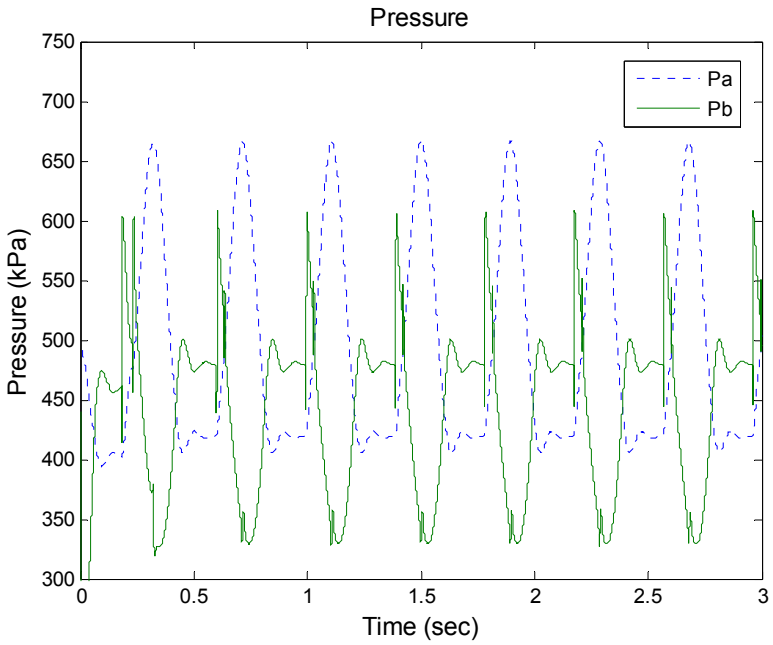

Figure 4-10. Case II: Pressures P_a and P_b.

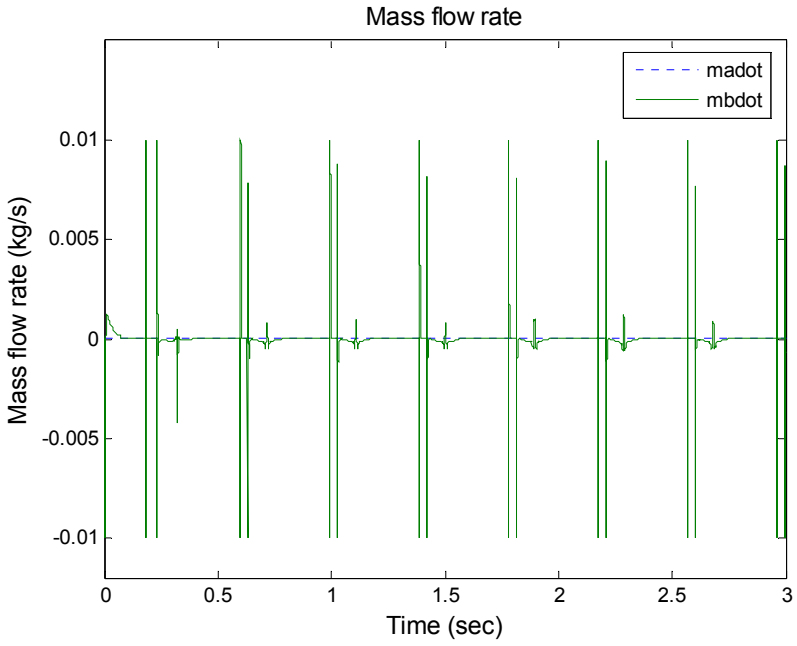

Figure 4-11. Case II: Control mass flow rates $\dot{m}_a$ and $\dot{m}_b$.

6. Experimental Implementation using Solenoid Valves

To implement the proposed hopping control, the use of proportional valves presents a costly and bulky option for a system that is ideally lean and inexpensive. If the proposed hopping control is to be part of a multi-legged robot where the vertical frequency of gait at each limb is addressed with the proposed methodology, the number of valves needed quickly becomes prohibitive in terms of both cost and size. More importantly, proportional spool valves are not necessary to implement the proposed control methodology given that the method takes advantage of the passive dynamics of the system for the majority of the control task and only utilizes mass flow to maintain the correct passive dynamics. As seen in Figure 4-11, the required mass flow comes only in short shots. Therefore, to make future pneumatic powered walking machines more feasible, while exploiting the energetic approach of the proposed controller, simple on/off three-way solenoid valves are used in the experiments.

To carry out the proposed control approach with on/off three-way valves, some modification of the control laws (49) and (59) is required. As an alternative to the control of side *a*, consider the error signal of Equation (45). Instead of specifying a particular error dynamic as done in Equation (46), consider instead the positive definite Lyapunov function below:

$$V = \tfrac{1}{2} e^2 \tag{63}$$

At the simplest level, it is desired to ensure the following:

$$\dot{V} = e\dot{e} = (P_a - P_{ad})(\dot{P}_a - \dot{P}_{ad}) \leq 0 \text{ while } e \neq 0 \tag{64}$$

Furthermore, as stated previously, the control of side *a* is compensating mostly for leakage and it is realistically only required to occasionally pressurize the chamber. This

corresponds to the actual pressure being lower than the desired pressure $(P_a - P_{ad}) < 0$. Upon substitution of Equations (41) and (48) for the case of $(P_a - P_{ad}) < 0$, the following condition arises:

$$\dot{m}_a \geq (P_a - P_{ad})\left(\frac{A_a \dot{x}}{RT_{flow}}\right) \text{ while } (P_a - P_{ad}) < 0 \tag{65}$$

Since Equation (65) simply states that the mass flow rate must be greater than some number when the chamber is under pressurized, the following on/off control law will be used for side *a* while in contact with the ground:

$$\text{Charge chamber } a \text{ if } P_a < P_{a0}\left(\frac{V_{mida}}{V_{mida} + A_a x}\right)^{\gamma} \text{ and } y \leq 0 \tag{66}$$

To control side *b* using an on/off valve, the on/off control methodology of [17] will be used. The derivation of this control law is summarized briefly here. With V and s defined as before in Equations (53) and (54), $\dot{s}$ can still be represented as:

$$\dot{s} = (\dddot{x} - \dddot{x}_d) + \lambda_2(\ddot{x} - \ddot{x}_d) \tag{67}$$

It will be necessary to enforce the following condition:

$$\dot{V} = s\dot{s} = [(\ddot{x} - \ddot{x}_d) + \lambda_2(\dot{x} - \dot{x}_d)][(\dddot{x} - \dddot{x}_d) + \lambda_2(\ddot{x} - \ddot{x}_d)] \leq 0 \tag{68}$$

Taking the derivative of Equation (36) gives,

$$M\dddot{x} = \dot{P}_a A_a - \dot{P}_b A_b \tag{69}$$

Substitution of Equation (41) with $\dot{m}_a = 0$ and a linearized form of the pressure dynamics $\dot{P}_b = \frac{u_b - P_b}{\tau_b}$ [17] yields:

$$M\ddot{x} = -\frac{\gamma P_a \dot{V}_a}{V_a} A_a - \frac{u_b - P_b}{\tau_b} A_b \tag{70}$$

where τ_b is a time constant determined by pressure response. In accordance to the three positions of the valves (charge, seal, or discharge) the input term of Equation (70) is only a finite set of discrete values,

$$u_b \in \{Ps, Pb, Patm\} \tag{71}$$

Substitution of Equation (70) into Equation (68) yields a candidate $\dot{V}$ associated with each input value. Each $\dot{V}$ candidate can be computed on-line in real-time.

$$\dot{V} \in \{\dot{V}_{Ps}, \dot{V}_{Pb}\, \dot{V}_{Patm}\} \tag{72}$$

To track the desired position based velocity trajectory by enforcing Equation (68) and utilize the least amount of compressed air from the supply, the following switching control law is implemented while in contact with the ground:

IF ($\dot{V}_{Pb} \le 0$**) THEN**
    $u_b = P_b$
ELSE
    IF ($\dot{V}_{Ps} \le 0$) THEN
        $u_b = P_s$
    ELSE
        if ($\dot{V}_{Patm} \le 0$) then
            $u_b = P_{atm}$
        else
            u_b = input associated with min($\dot{V}$)
        end if
    END IF
END IF

That is, sealing off the chamber is the first priority if this option presents a negative definite candidate $\dot{V}_{Pb} \le 0$. If this candidate is not negative definite, then

charging the chamber is the second consideration for velocity tracking convergence. If both of these control options cannot make the velocity tracking converge, then discharge is used. If none of these can enforce a negative definite $\dot{V}$, which means that $\dot{V} > 0$ for any of the three possible inputs, the one associated with the minimum $\dot{V}$ is chosen as the input. This slight violation of Equation (68) is discussed in [17].

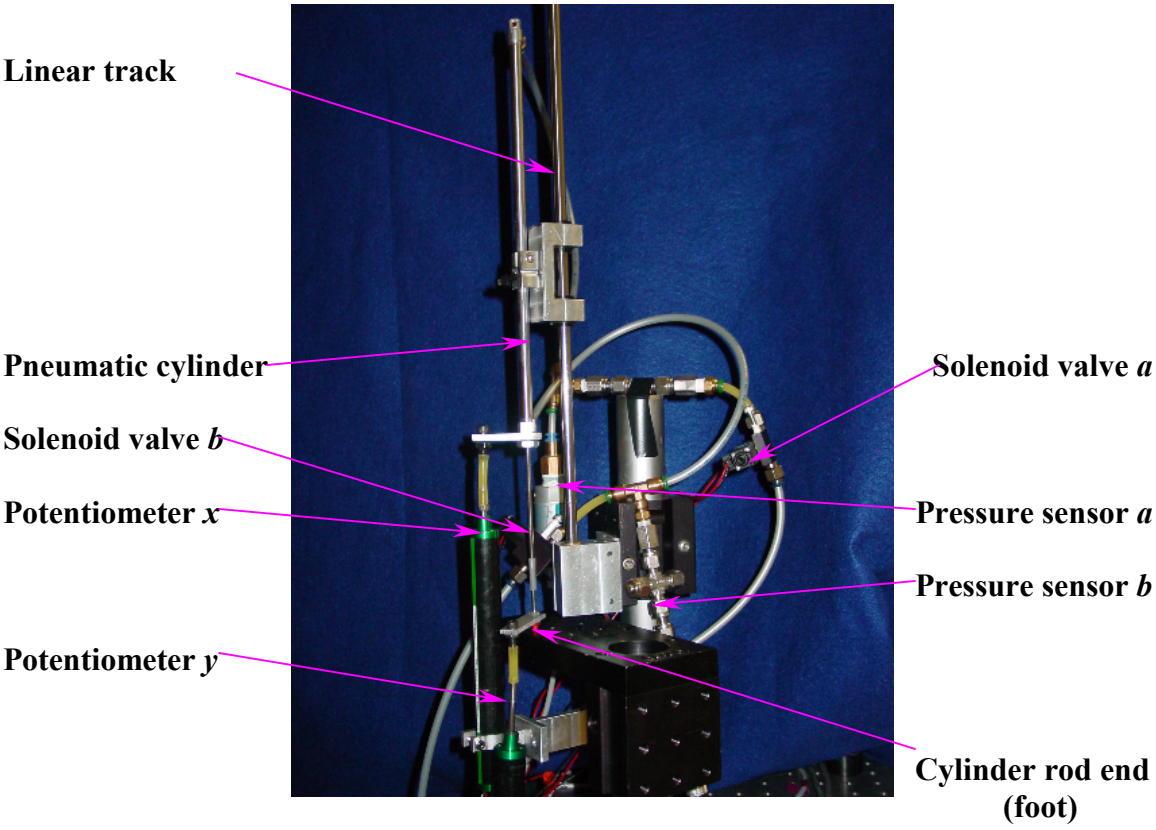

Figure 4-12. Photograph of the experimental setup.

The experimental setup is shown in Figure 4-12. The pneumatic actuator is a long, small diameter double acting cylinder (Bimba 0078-DXP) stroke length of 10 inches, piston diameter 0.39 inches and piston rod diameter of 1/8 inch). A linear potentiometer

(Midori LP-150F) with 150 mm maximum travel is used to measure the vertical position of the cylinder housing, and a linear potentiometer (Midori LP-100F) with 100 mm maximum travel is used to measure the vertical position of the piston. The velocity of the cylinder was obtained from position by utilizing a differentiating filter with a 20 dB roll-off at 100 Hz. The acceleration signal was obtained from the velocity signal with a differentiating filter with a 20 dB roll-off at 30 Hz. Given the range of desired frequencies of operation, these differentiating filters added negligible phase lag. Two pressure transducers (Festo SDE-16-10V/20mA) are attached to each cylinder chamber, respectively. Control is provided by a Pentium 4 computer with an A/D card (National Instruments PCI-6031E), which controls the two solenoid valves through two digital output channels. The moving mass is about 0.54 kg. Two two-way, three-position (charge, discharge, sealed) solenoid valves (Numatics M10SS600M00006) are attached to the chambers.

Three sets of experimental results are included in Figures 4-13 to 4-18 below to show that the hopping frequency can be explicitly controlled and hopping height can be implicitly regulated. These three cases are the following. Case I: designed periods of T_{hop} = 0.35 and T_{air} = 0.1 seconds. Case II: designed periods of T_{hop} = 0.4 and T_{air} = 0.2 seconds. Case III: designed periods of T_{hop} = 0.45 and T_{air} = 0.15 seconds. Figures 4-13, 4-14 and 4-15 show the position response of the system for each case. Figure 4-16 shows the velocity tracking for Case II where, again, this is only achieved or expected during contact. Figure 4-17 shows the pressure tracking in chamber *a* for Case II where, this is only achieved during contact. Figure 4-18 shows the discrete valve control signals during Case II. Comparing the experimental result shown in Figure 4-14 with the simulation

result shown in Figure 4-7 for the same desired T_{hop} = 0.4 and T_{air} = 0.2 seconds, it can be seen that the solenoid valves provide very similar experimental results that matches the simulation results well in terms of hopping height (x and y) and time periods (T_{hop} and T_{air}). Although the velocity tracking shown in Figure 4-16 is not very accurate, the total conservative energy is still compensated during contact, this is verified by the consistent hopping height shown in the position trajectories.

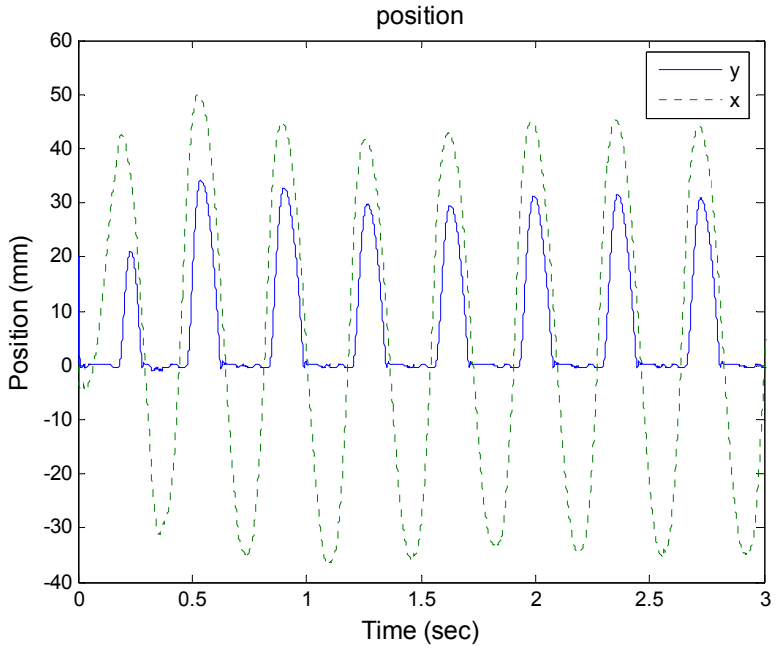

Figure 4-13. Case I: Hopping results for designed periods of T_{hop}=0.35 seconds and T_{air} = 0.1 seconds. Actual experimental periods are T_{hop} = 0.36 seconds and T_{air} = 0.14 seconds.

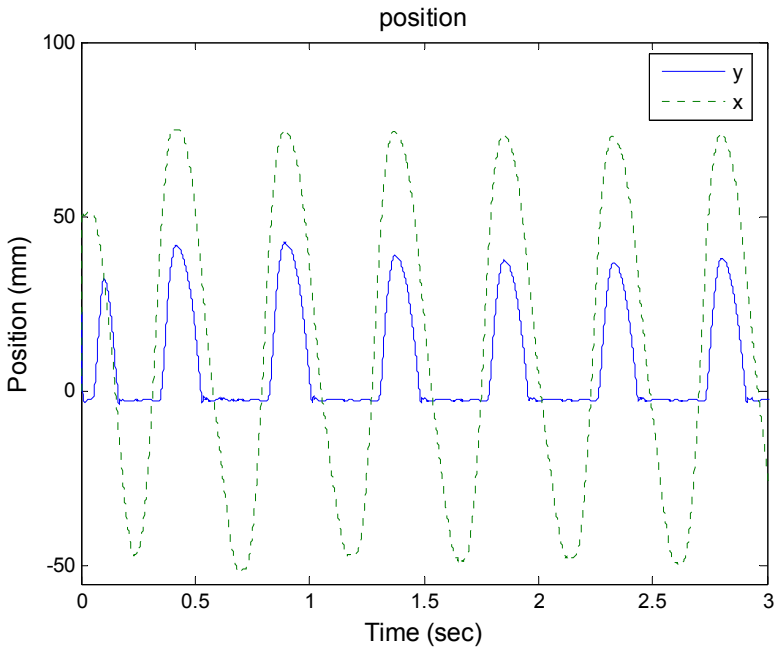

Figure 4-14. Case II: Hopping results for designed periods of T_{hop}=0.4 seconds and T_{air} = 0.2 seconds. Actual experimental periods are T_{hop} = 0.46 seconds and T_{air} = 0.18 seconds.

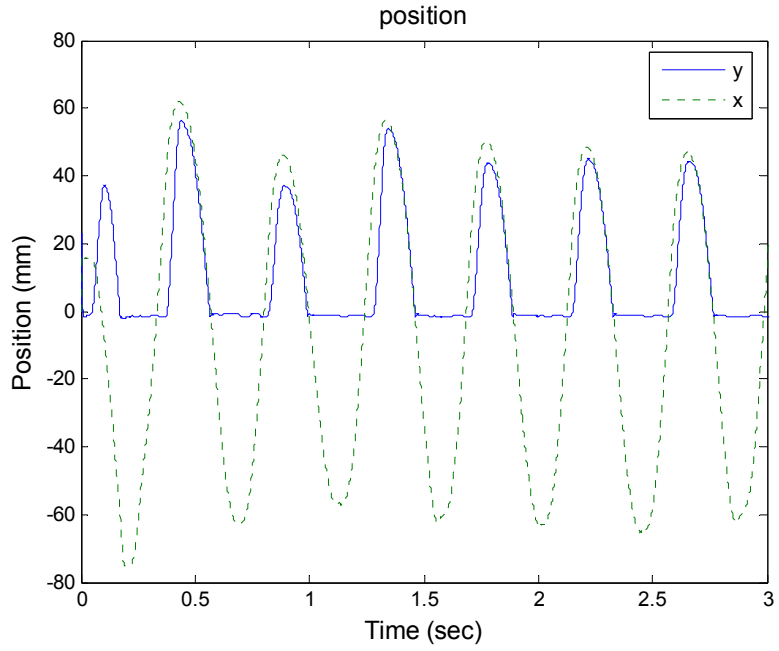

Figure 4-15. Case III: Hopping results for designed periods of T_{hop}=0.45 seconds and T_{air} = 0.15 seconds. Actual experimental periods (consistent after the fourth hop) are T_{hop} = 0.44 seconds and T_{air} = 0.17 seconds.

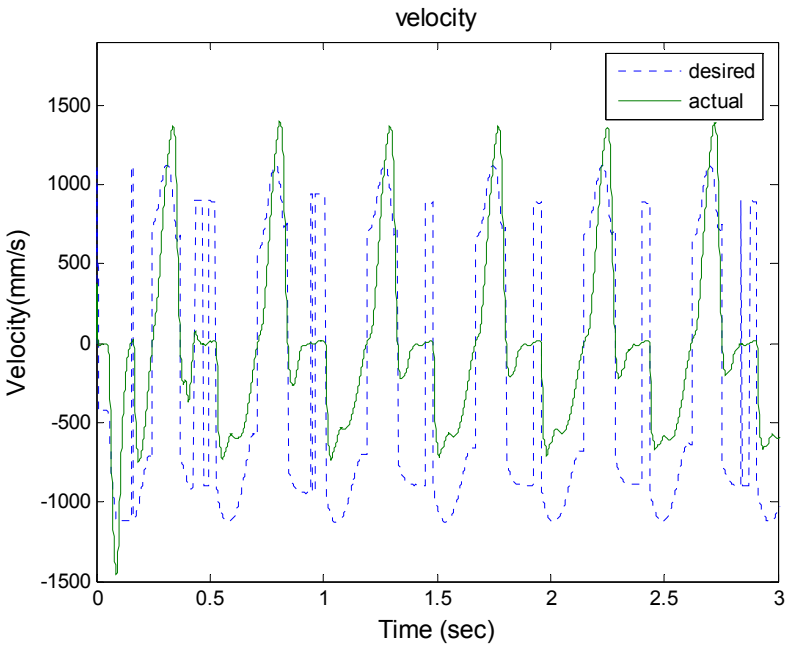

Figure 4-16. Case II: Desired velocity ($\dot{x}_d$) and actual velocity ($\dot{x}$). Velocity tracking is achieved during contact only.

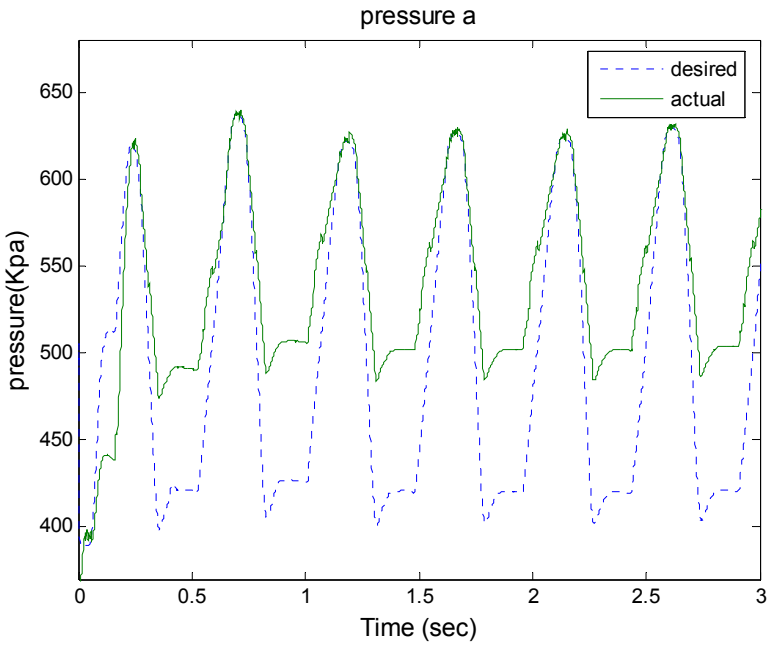

Figure 4-17. Case II: Desired pressure (P_{ad}) and actual pressure (P_a) in chamber a. Pressure tracking is achieved during contact only.

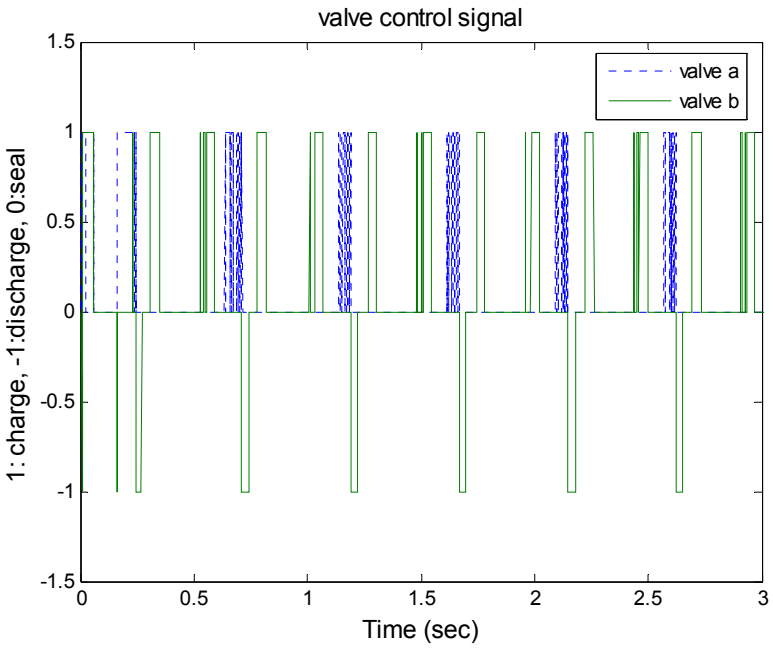

Figure 4-18. Case II: Discrete valve control signals.

7. Conclusions

This paper presents the design of a "natural" pneumatic hopping robot that exploits the passive dynamics of the system to achieve a desired period of oscillation and a desired time-of-flight. The desired pressure as a function of *position* is generated for one chamber of the actuator and tracked to regulate the natural frequency of the pneumatic cylinder. Desired velocity, acceleration and jerk is scheduled as a function of *position* and then tracked using the pressure of the rod-side of the actuator to regulate the kinetic energy of the system and hence hopping amplitude and flight time. Analysis showed that the *position dependent desired behavior* ensures that the passive dynamics of the system are energetically exploited to achieve the desired motion. Control is activated only during contact. During flight, the energy of the system is stored and returned as additional gravitational energy. Given that the control methodology is position based,

variations in flight time or disturbances during flight will not affect the degree to which the passive dynamics are beneficially exploited. Finally, the control laws were modified for the use of simple solenoid valves. Simulation and experimental results demonstrated the accuracy and consistency of the proposed control methodology.

References

[1] Goldfarb, M., Barth, E. J., Gogola, M. A., and Wehrmeyer, J. A., "Design and Energetic Characterization of a Liquid-Propellant-Powered Actuator for Self-Powered Robots," *IEEE/ASME Transactions on Mechatronics*, vol. 8, no. 2, pp. 254-262, June 2003.

[2] Xu, W. L., Han, J.D. and Tso, S. K., "Experimental Study of Contact Transition Control Incorporating Joint Acceleration Feedback," *IEEE/ASME Transaction on Mechatronics*, vol. 5, no. 5, September 2000.

[3] Hmadi, M. and Buehler, M., "Stable Control of a Simulated One-legged Running Robot with Hip and Leg Compliance," *IEEE Transactions on Robotics and Automation*, vol. 13, no. 1, pp. 96-104, 1997.

[4] Williamson, M. M., *Series Elastic Actuators*, Master's thesis, MIT, Cambridge, MA, 1995.

[5] Hyon, S. H. and Mita, T., "Development of a Biologically Inspired Hopping Robot – 'Kenken'," *Proceedings of the 2002 IEEE International Conference on Robotics & Automation*, Washington DC, pp. 3984-3991, 2002.

[6] Delson, N., Hanak, T., Loewke, K. and Miller, D. N., "Modeling and Implementation of McKibben Actuators for a Hopping Robot," *Proceedings of the 12th Annual International Conference on Advanced Robotics (ICAR)*, Seattle, Washington, pp. 833-840, 2005.

[7] Verrelst, B., A Dynamic Walking Biped Actuated by Pleated Pneumatic Artificial Muscles: Basic Concepts and Control Issues, Ph.D dissertation, Vrije Universiteit Brussel, 2005.

[8] Raibert, M., Legged Robots that Balance, MIT Press, Cambridge, MA, 1986.

[9] Binnard, M. B., *Design of a Small Pneumatic Walking Robot*, master's thesis, MIT, Cambridge, MA, 1995.

[10] M'sirdi, N. K., Manamani, N. and Nadjar-Gauthier, N., "Methodology based on CLC for Control of Fast Legged Robots," *Proceedings of the 1998 IEEE/RSJ International Conference on Intelligent Robotics and Systems,* Victoria, B.C., Canada, pp. 71-76, 1998.

[11] Guihard, M. and Gorce, P., "Dynamic Control of a Large Scale of Pneumatic Multichain Systems," *Journal of Robotic Systems*, vol. 21, no. 4, pp. 183-192, 2004.

[12] Richer, E. and Hurmuzlu, Y., "A High Performance Pneumatic Force Actuator System: Part I - Nonlinear Mathematical Model," *ASME Journal of Dynamic Systems, Measurement and Control*, vol. 122, no. 3, pp. 416-425, 2000.

[13] Richer, E. and Hurmuzlu, Y., "A High Performance Pneumatic Force Actuator System: Part II - Nonlinear Control Design," *ASME Journal of Dynamic Systems, Measurement and Control*, vol. 122, no. 3, pp. 426-434, 2000.

[14] Zhu, Y. and Barth, E. J., "Impedance Control of a Pneumatic Actuator for Contact Tasks," in *Proceedings of the 2005 IEEE international Conference on Robotics and Automation*, pp. 999-1004, 2005.

[15] Al-Dakkan, K., Goldfarb, M., Barth, E. J., "Energy Saving Control for Pneumatic Servo Systems," *Proceedings of the 2003 IEEE/ASME International Conference on Advanced Intelligent Mechatronics*, pp. 284-289, 2003.

[16] Fite, K. B. and Goldfarb, M., "Design and Energetic Characterization of a Porportional-injector Monopropellant-powered Actuator," *IEEE/ASME Transactions on Mechatronics*, vol. 11, no. 2, pp. 196-204, 2006.

[17] Barth, E. J. and Goldfarb, M. "A Control Design Method for Switching Systems with Application to Pneumatic Servo System", *2002 ASME International Mechanical Engineering Congress & Exposition*, New Orleans, Louisiana, November 2002.

ADDENDUM TO MANUSCRIPT III

A1. The Controlled Horizontal Pneumatic Oscillator

An energetic analysis of the linearly actuated pneumatic system shown in Figure 4-19 reveals an oscillatory system with a frequency of oscillation dependent upon system parameters.

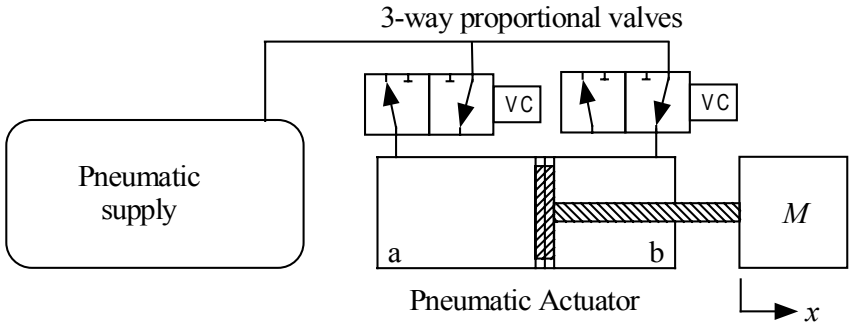

Figure 4-19. Schematic of a pneumatically actuated system.

The kinetic and potential energy terms for a leakless, adiabatic, frictionless horizontal piston-mass system are given as:

$$E = \underbrace{\frac{1}{2}M\dot{x}^2}_{KE(\dot{x})} + \underbrace{\frac{P_a V_a}{1-\gamma}\left[\left(\frac{P_a}{P_{atm}}\right)^{\frac{1-\gamma}{\gamma}} - 1\right]}_{PEa(x)} + \underbrace{\frac{P_b V_b}{1-\gamma}\left[\left(\frac{P_b}{P_{atm}}\right)^{\frac{1-\gamma}{\gamma}} - 1\right]}_{PEb(x)} + \underbrace{P_{atm}A_r(x-x_0)}_{PEr(x)} \qquad (73)$$

A horizontal pneumatic system can be described by the following equations:

$$M\ddot{x} = P_a A_a - P_b A_b - P_{atm} A_r \qquad (74)$$

Taking derivative of this equation and substituting the pressure dynamics show that this system contains two inputs, $\dot{m}_a$ and $\dot{m}_b$, which can be specified arbitrarily by two three-way proportional valves. The strategy for controlling the frequency and amplitude of oscillation while taking advantage of the natural dynamics of the pneumatic system will

be twofold. First, the pressure in chamber a will be controlled to track the pressure necessary to specify a desired $PEa(x)$ as a function of position. This desired potential in side a will be specified by selecting a particular value for P_{a0}. The natural frequency of the lossless pneumatic resonator scales in proportion to this equilibrium pressure. Second, the amplitude of oscillation will be influenced by controlling the mass flow rate in and out of side b such that the position dependent desired velocity is tracked.

The control laws for pressure tracking in chamber *a* and velocity tracking are exactly the same as the vertical pneumatic hopper. Except that the expression of desired conservative energy E_d is slightly different. The kinetic energy can be represented as:

$$\tfrac{1}{2} M\dot{x}_d^2 = E_d - PEa(x) - PEb(x) - PEr(x) \tag{75}$$

From this, a position-dependent velocity can be defined:

$$\dot{x}_d(x) = sign(\dot{x})\sqrt{\left|\tfrac{2}{M}\left(E_d - PEa(x) - PEb(x) - PEr(x)\right)\right|} \times sign\left(\tfrac{2}{M}\left(E_d - PEa(x) - PEb(x) - PEr(x)\right)\right) \tag{76}$$

The selection of two parameters is required to specify the frequency and amplitude of oscillation. The amplitude of oscillation is governed by the total amount of conservative energy E_d desired to be in the system. The frequency of amplitude is indirectly specified via P_{a0}, knowing that the frequency will be regulated through this. The desired amplitude of oscillation $\pm x_{\max}$ can then be used to determine the desired energy by substituting $x_{\max}$, $\dot{x} = 0$, $P_a = P_{a0}\left(\dfrac{V_{mida}}{V_{mida} + A_a x_{\max}}\right)^{\gamma}$ and $P_b = \dfrac{1}{A_b}(P_{a0}A_a - P_{atm}A_r)\left(\dfrac{V_{midb}}{V_{midb} - A_b x_{\max}}\right)^{\gamma}$ into the energy expression (73):

$$E_d = \frac{P_{a0}(V_{mida} + A_a x_{\max})}{1-\gamma}\left(\frac{V_{mida}}{V_{mida} + A_a x_{\max}}\right)^{\gamma}\left[\left(\frac{P_{a0}}{P_{atm}}\left(\frac{V_{mida}}{V_{mida} + A_a x_{\max}}\right)^{\gamma}\right)^{\frac{1-\gamma}{\gamma}} - 1\right]$$
$$+ \frac{(P_{a0}A_a - P_{atm}A_r)(V_{midb} - A_b x_{\max})}{A_b(1-\gamma)}\left(\frac{V_{midb}}{V_{midb} - A_b x_{\max}}\right)^{\gamma}$$
$$\times\left[\left(\frac{(P_{a0}A_a - P_{atm}A_r)}{A_b P_{atm}}\left(\frac{V_{midb}}{V_{midb} - A_b x_{\max}}\right)^{\gamma}\right)^{\frac{1-\gamma}{\gamma}} - 1\right] + P_{atm}A_r x_{\max} \quad (77)$$

This desired energy E_d and equilibrium pressure P_{a0} is then used to determine the desired velocity, acceleration and jerk schedules as given in the pneumatic hopper case.

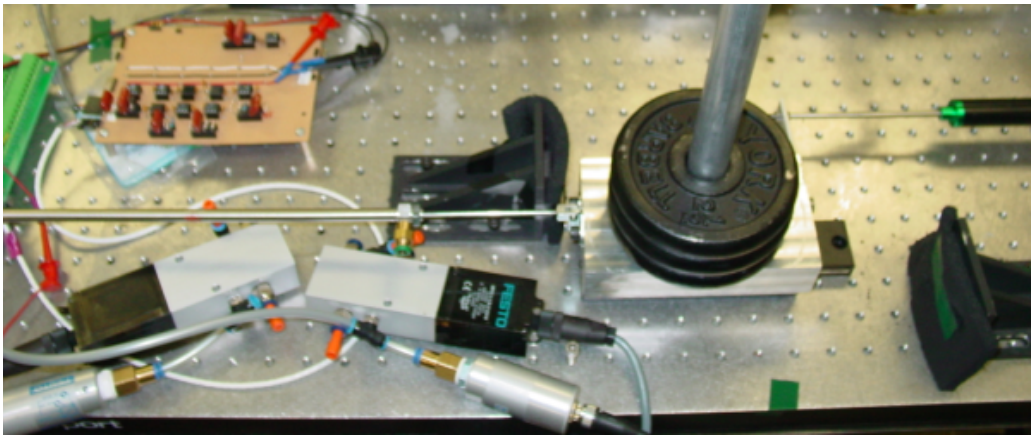

Figure 4-20. Photograph of the experimental setup.

The experimental setup is shown in Figure 4-20. The pneumatic actuator is a small cylinder (Bimba 0078-DXP) with a stroke length of 10 inches, piston diameter 0.39 inches and piston rod diameter of 1/8 inch. A linear potentiometer (Midori LP-150F) with 150 mm maximum travel is used to measure the linear position of the cylinder and cart/mass. Two four-way proportional valves (Festo MPYE-5-1/8-LF-010-B) are attached

to the chambers, but they were configured to function as two three-way valves. Two pressure transducers (Festo SDE-16-10V/20mA) are attached to each cylinder chamber, respectively. Control is provided by a Pentium 4 computer with an A/D card (National Instruments PCI-6031E), which controls the two proportional valves through two analog output channels. The payload is about 5.7 kg.

The equilibrium pressure in side a was selected as $P_{a0} = 450\,\text{kPa}$, and the amplitude of oscillation was set as $x_{\max} = 40$ mm. Figure 4-21 shows the resulting controlled position. It should be noted that the amplitude of oscillation and period of oscillation were very regular. Additionally, when the system was subject to an external disturbance, such as letting the piston rod slide between two pinched fingers, the amplitude and frequency of oscillation remained quite accurate with higher resulting commanded mass flow rates to compensate for the energy dissipation caused by the disturbance.

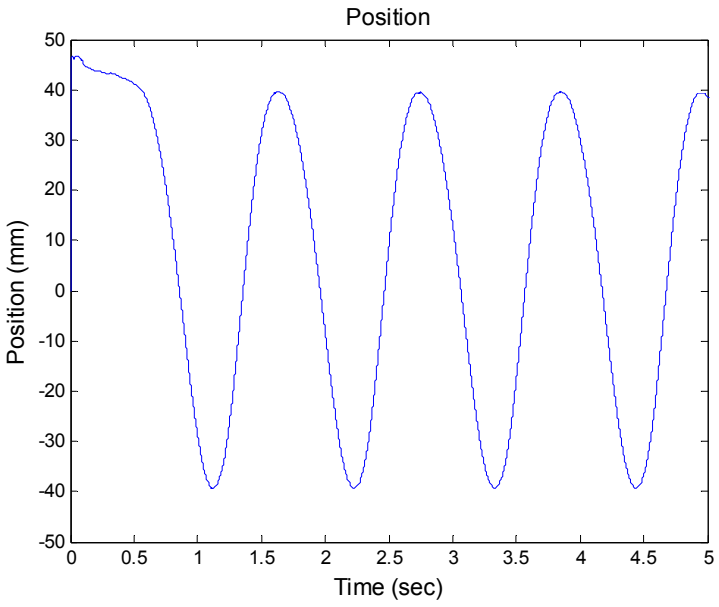

Figure 4-21. Position response.

Figure 4-22 shows the mass flow rates for chambers *a* and *b*. It should be noted that the mass flow rate from the pressure control law was only executed for positive mass flow rates given the leakage present in the system. Figure 4-23 shows the pressures in chamber *a* and *b*, while Figure 4-24 shows the desired and actual velocity.

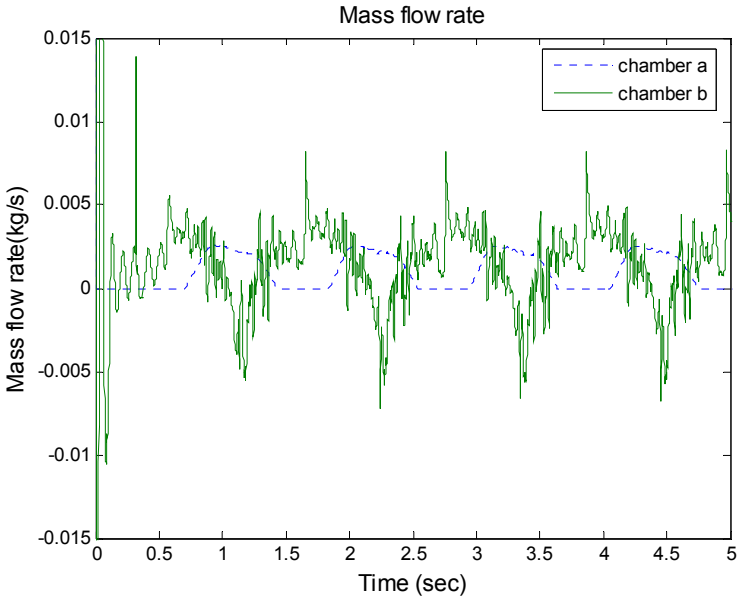

Figure 4-22. Controlled mass flow rates for chamber *a* and *b*.

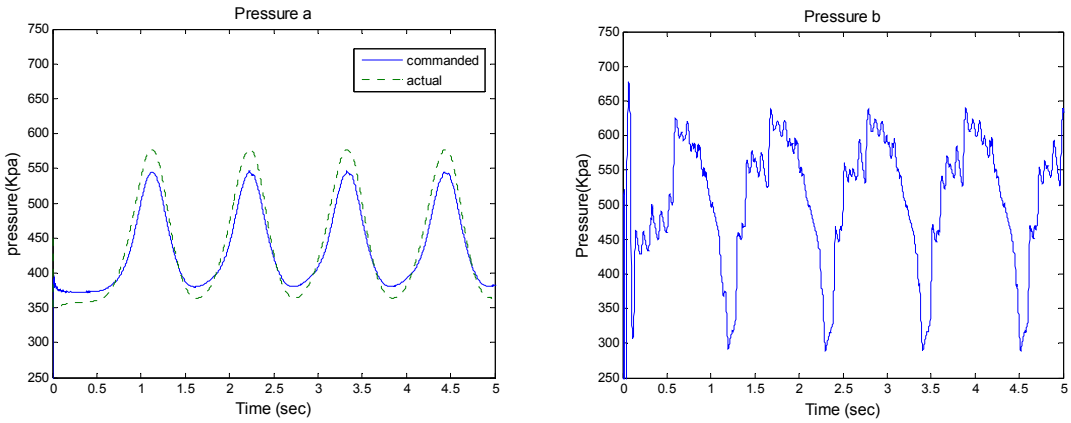

(a) (b)

Figure 4-23. (a) Pressure and scheduled pressure in chamber *a*. (b) Pressure in chamber *b*.

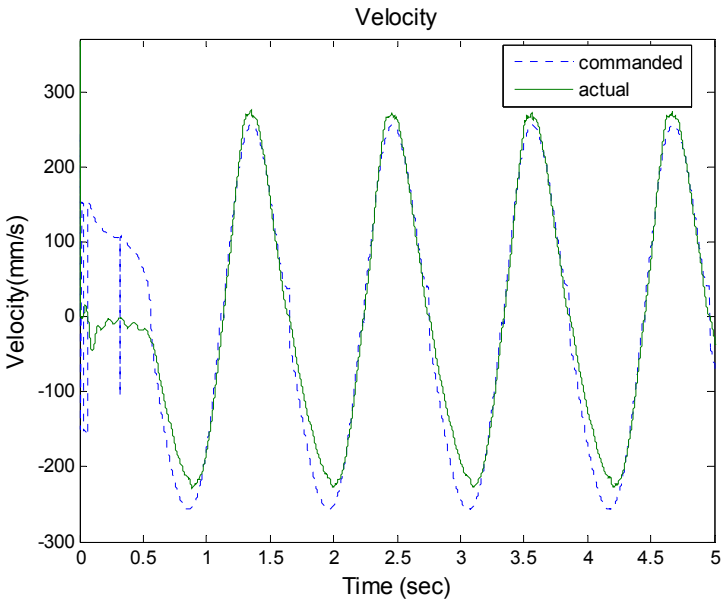

Figure 4-24. Desired and actual velocity.

It is interesting to note that the control laws inject mass into each chamber during the part of the stroke where that chamber has a smaller volume. This verifies the notion that the control laws act to increase or decrease the potential energy of each chamber with knowledge of what effect and when such energy storage will be converted into work. This is a consequence of the energetic approach to the control of the system taken.

APPENDIX A

MATLAB SIMULINK BLOCKS FOR MANUSCRIPT I

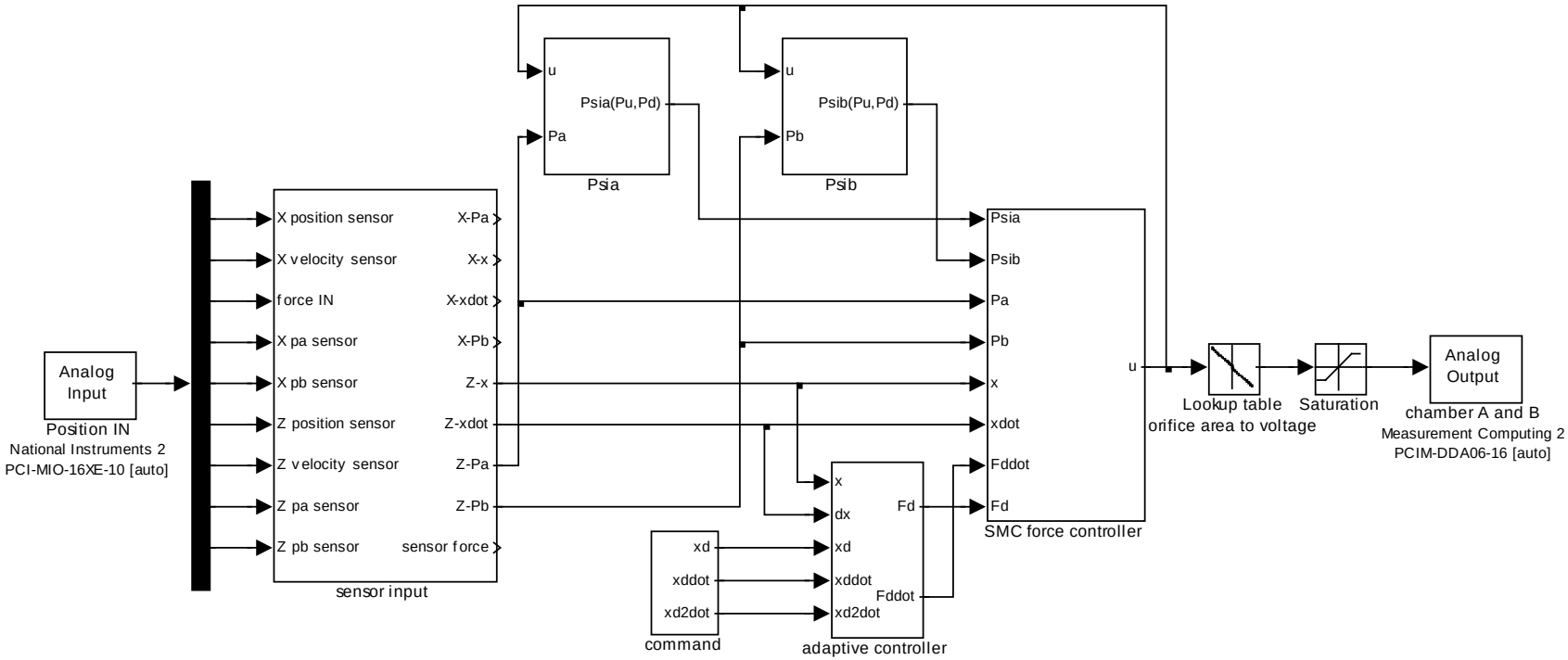

Figure A-1. Block diagram of the controller implemented in manuscript 1.

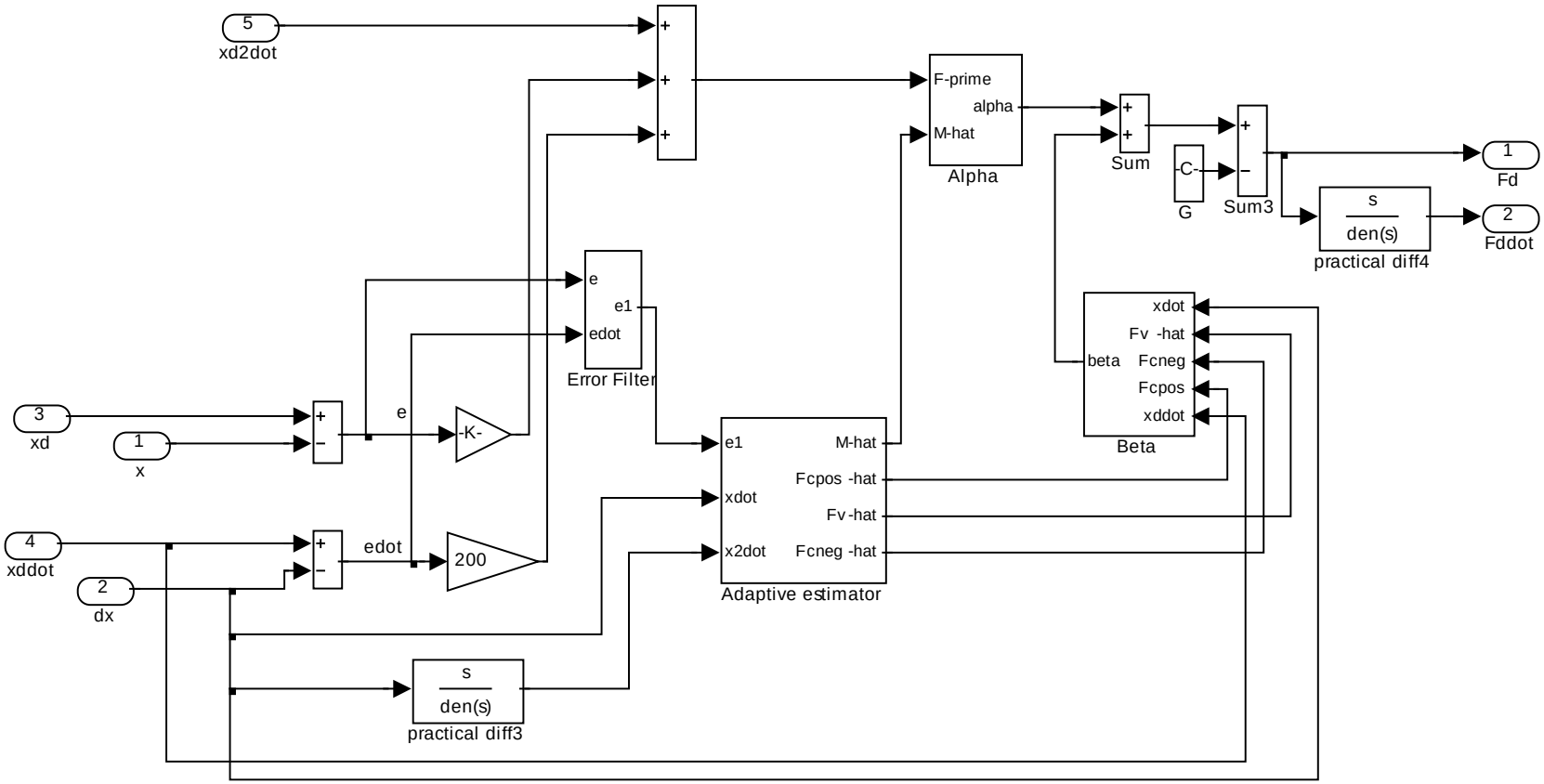

Figure A-2. Block diagram of the *adaptive controller* subsystem implemented in manuscript 1.

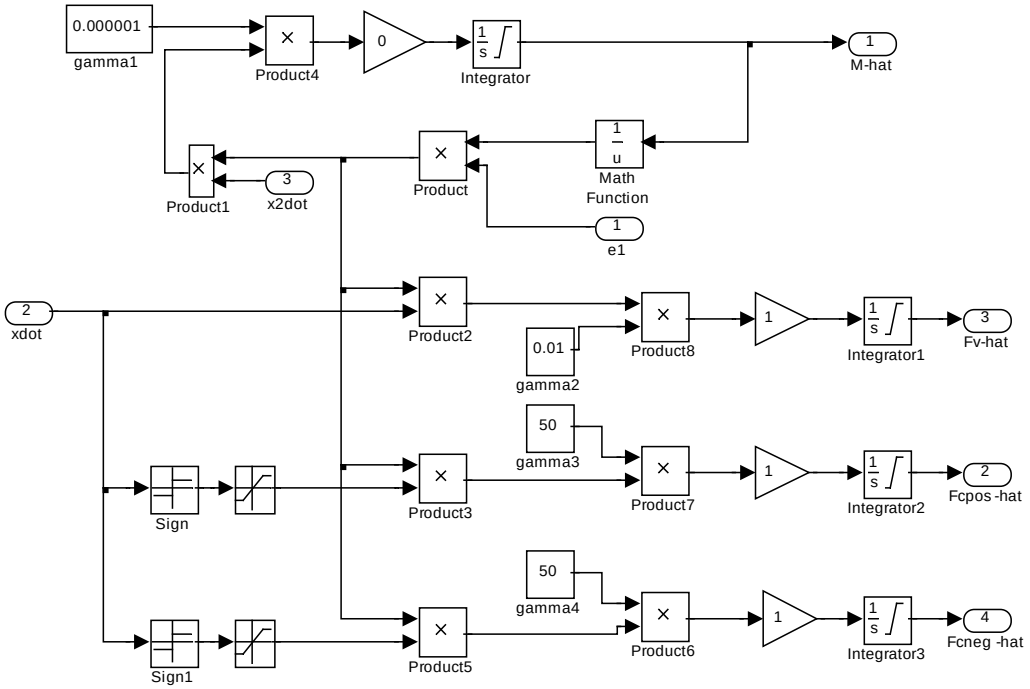

Figure A-3. Block diagram of the *adaptive estimator* subsystem implemented in manuscript 1.

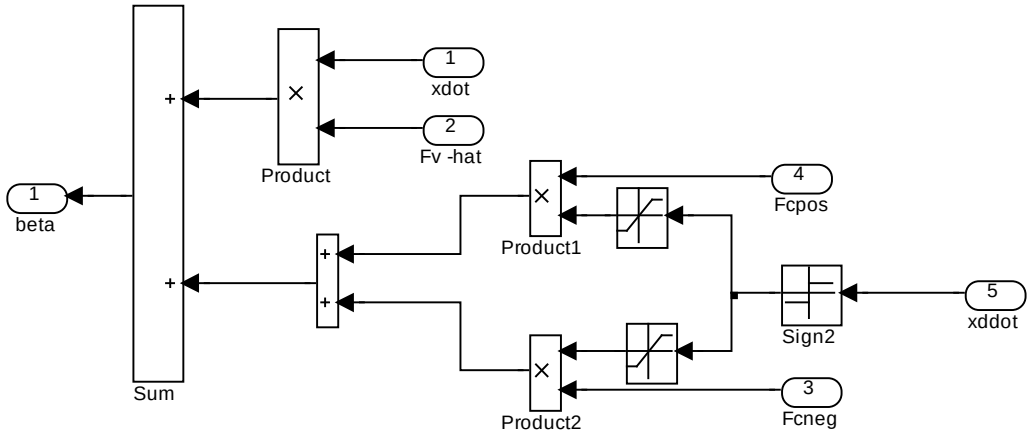

Figure A-4. Block diagram of the *Beta* subsystem implemented in manuscript 1.

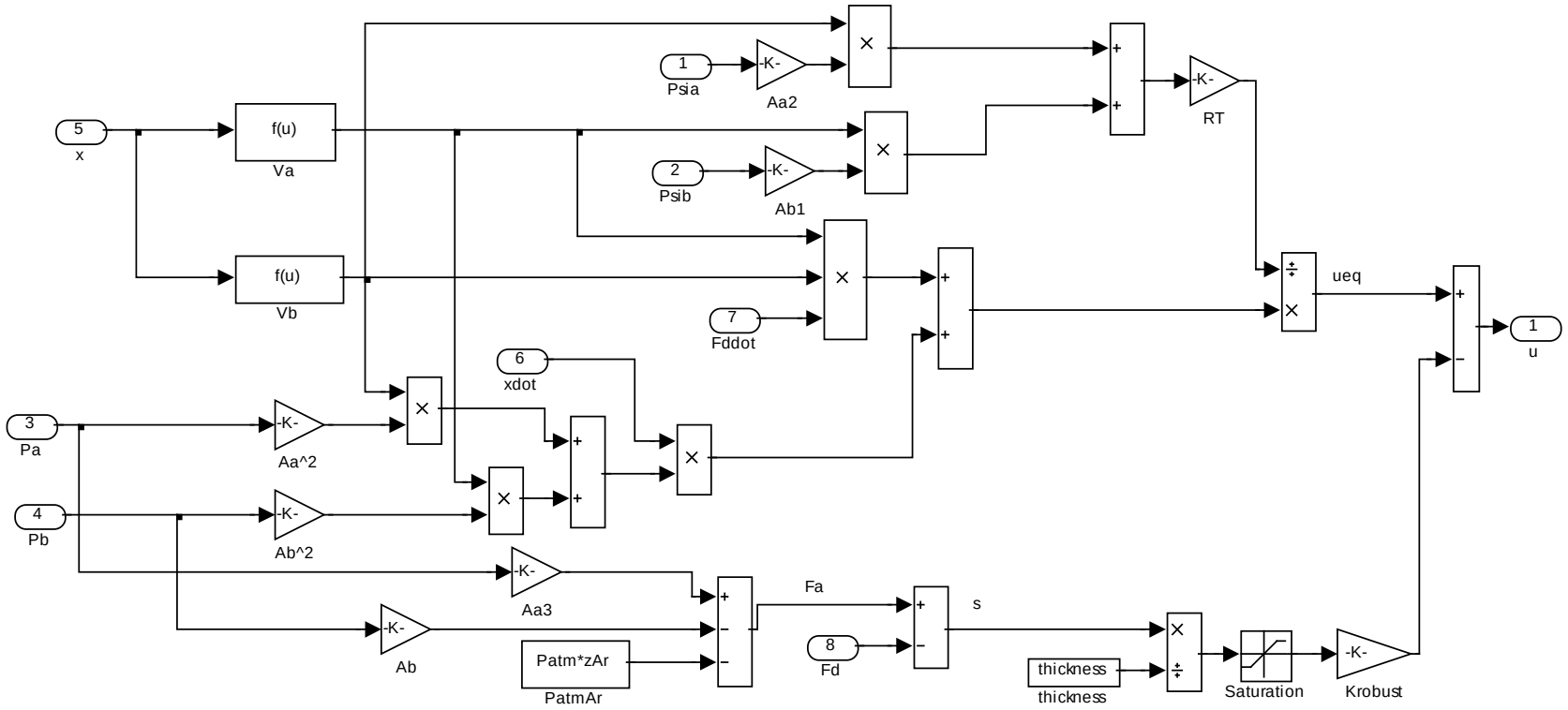

Figure A-5. Block diagram of the *SMC force controller* subsystem implemented in manuscript 1.

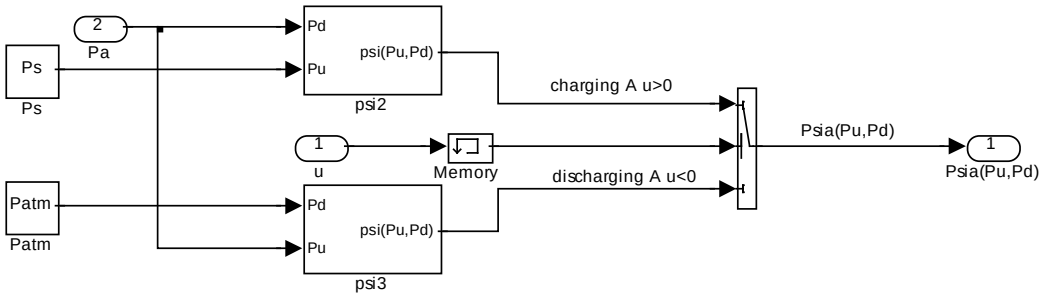

Figure A-6. Block diagram of the *psia (or psib)* subsystem implemented in manuscript 1.

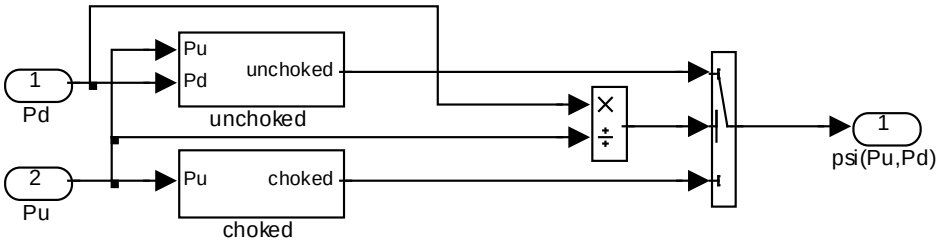

Figure A-7. Block diagram of the *psi* subsystem implemented in manuscript 1.

APPENDIX B

MATLAB SIMULINK BLOCKS FOR MANUSCRIPT II

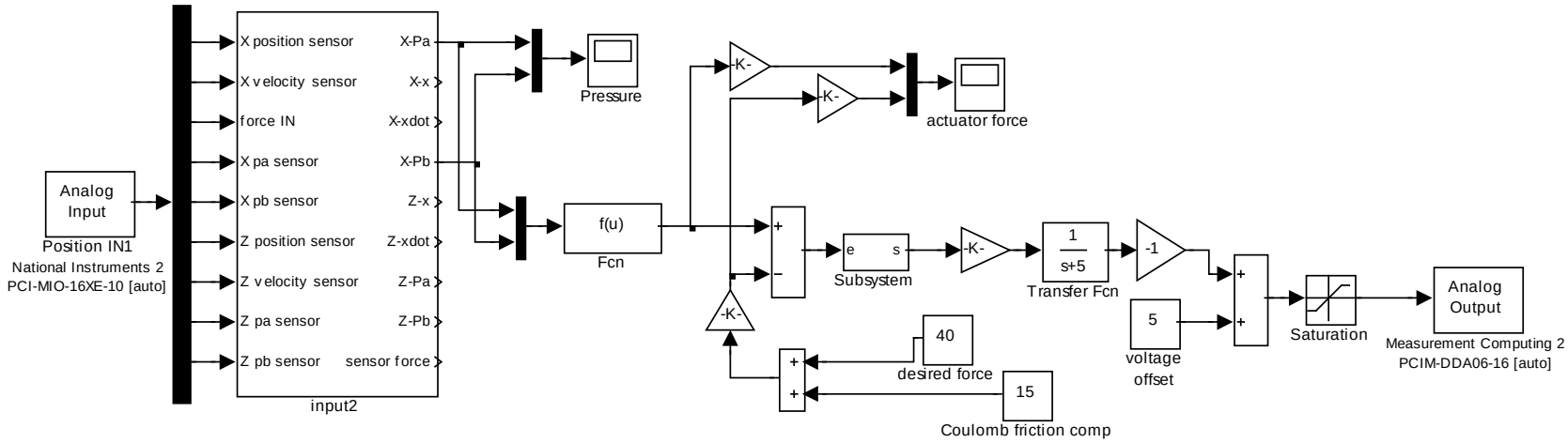

Figure B-1. Block diagram of the passivity-based controller implemented in manuscript 2.

APPENDIX C

MATLAB SIMULINK BLOCKS FOR MANUSCRIPT III

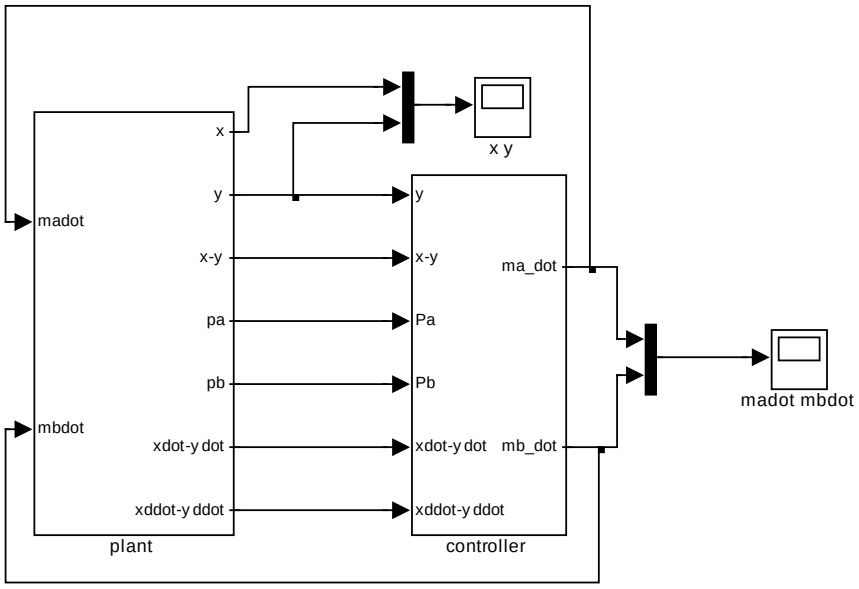

Figure C-1. Block diagram of the hopping robot simulation implemented in manuscript 3.

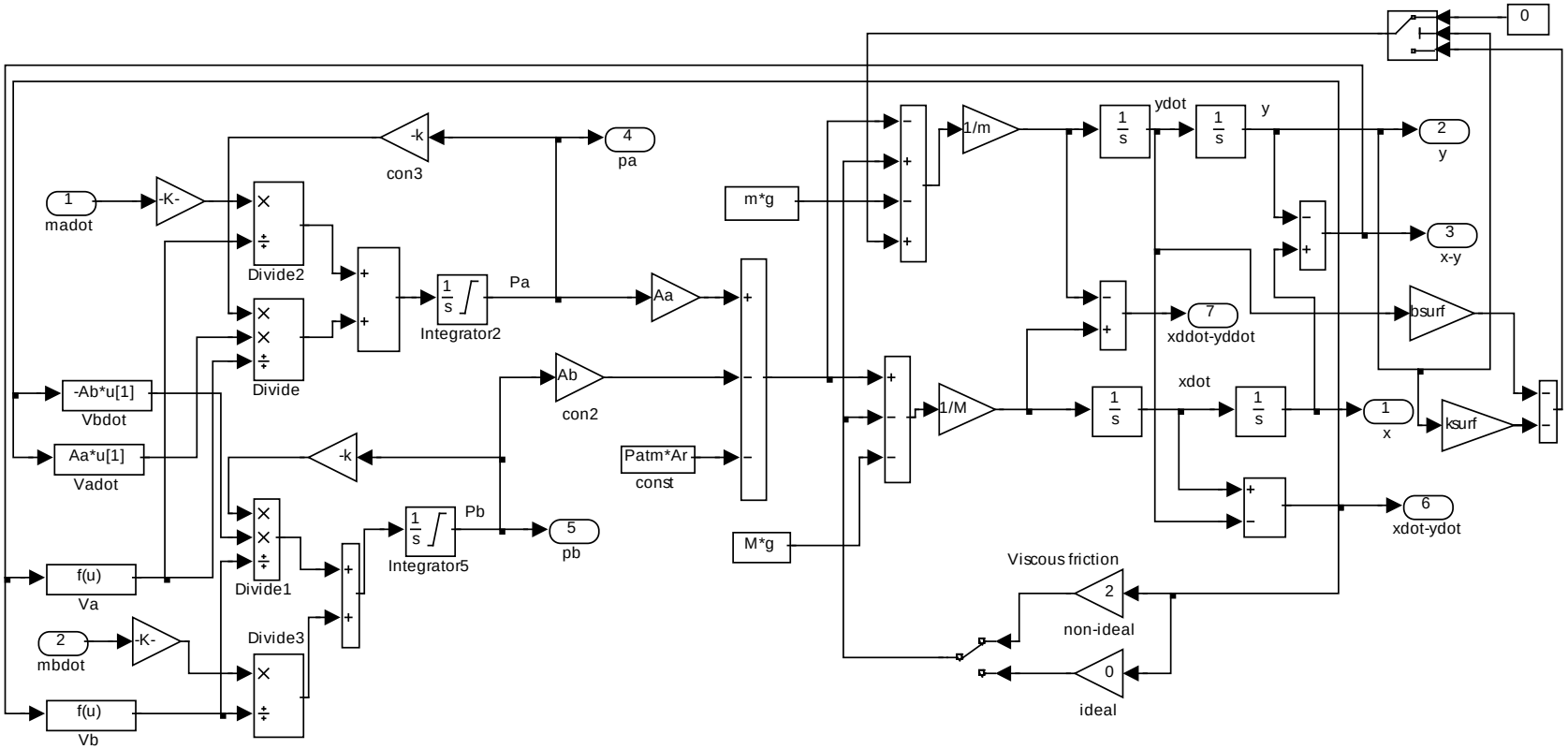

Figure C-2. Block diagram of the *plant* subsystem of hopping simulation implemented in manuscript 3.

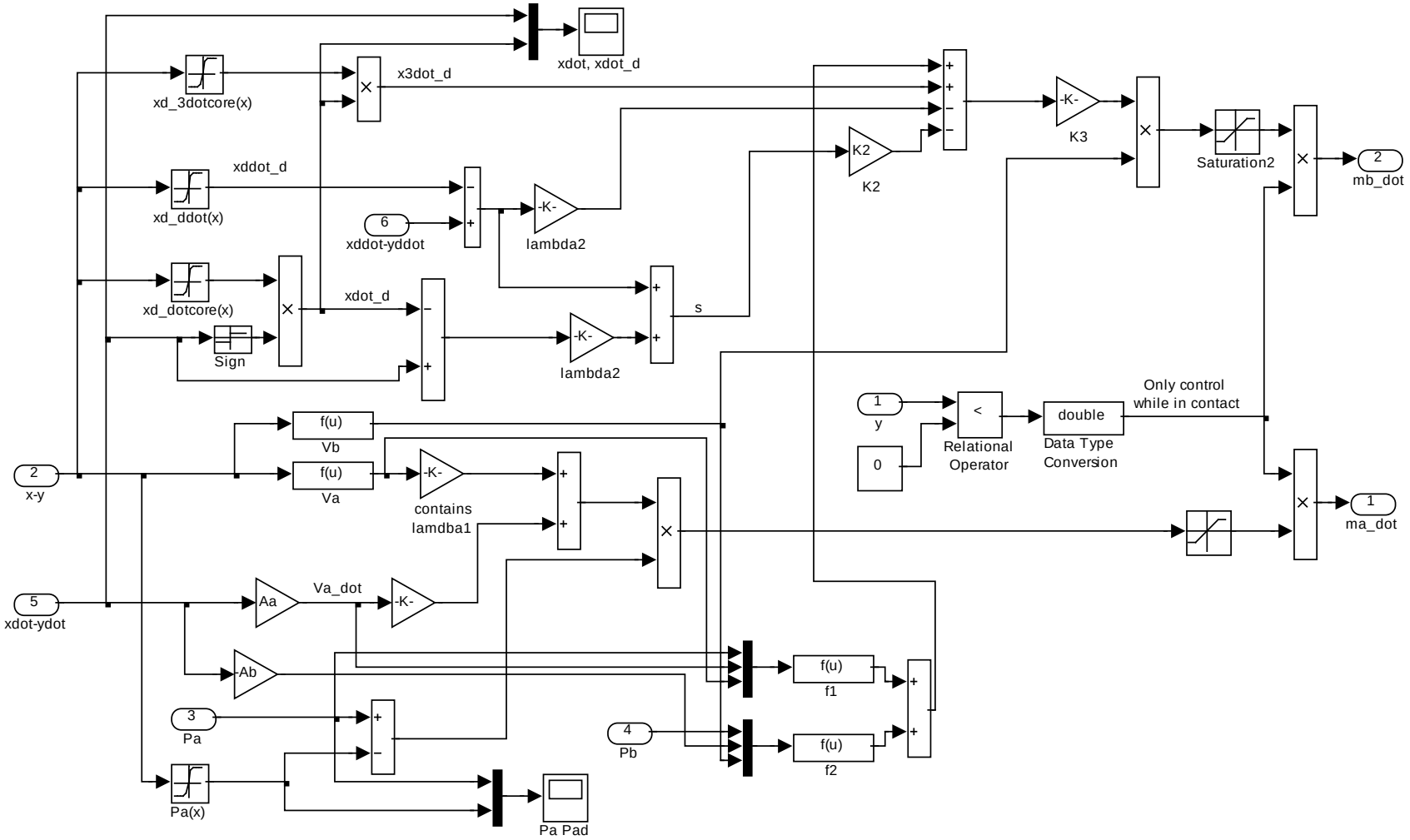

Figure C-3. Block diagram of the *controller* subsystem of hopping simulation implemented in manuscript 3.

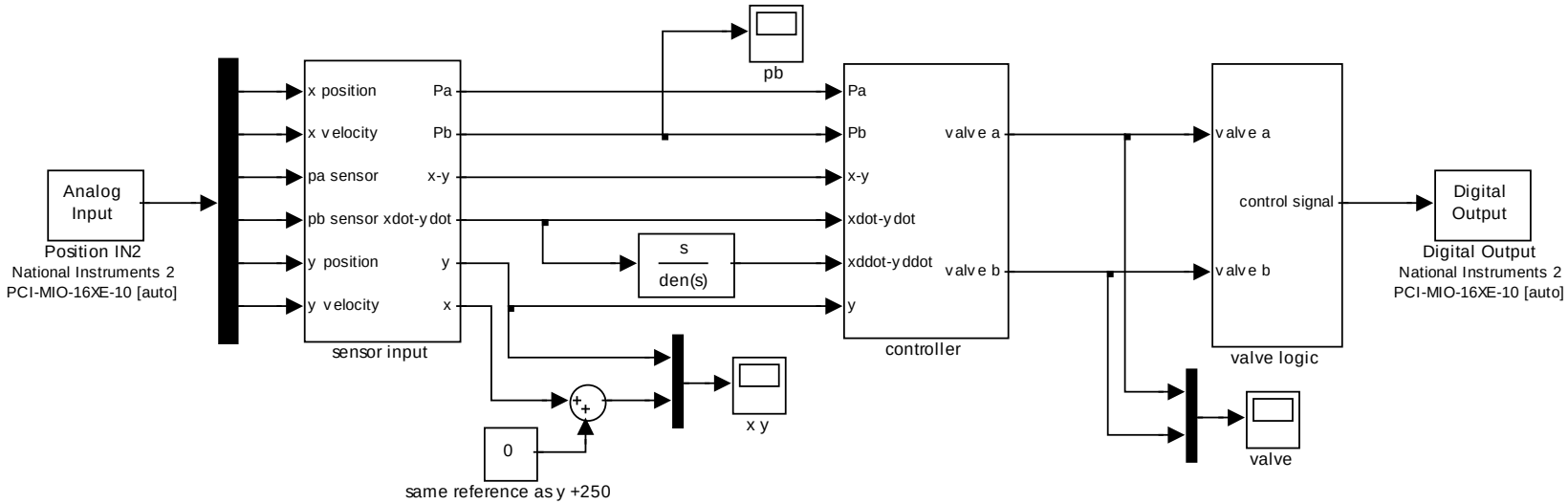

Figure C-4. Block diagram of the controller of hopping experiments using on/off solenoid valves implemented in manuscript 3.

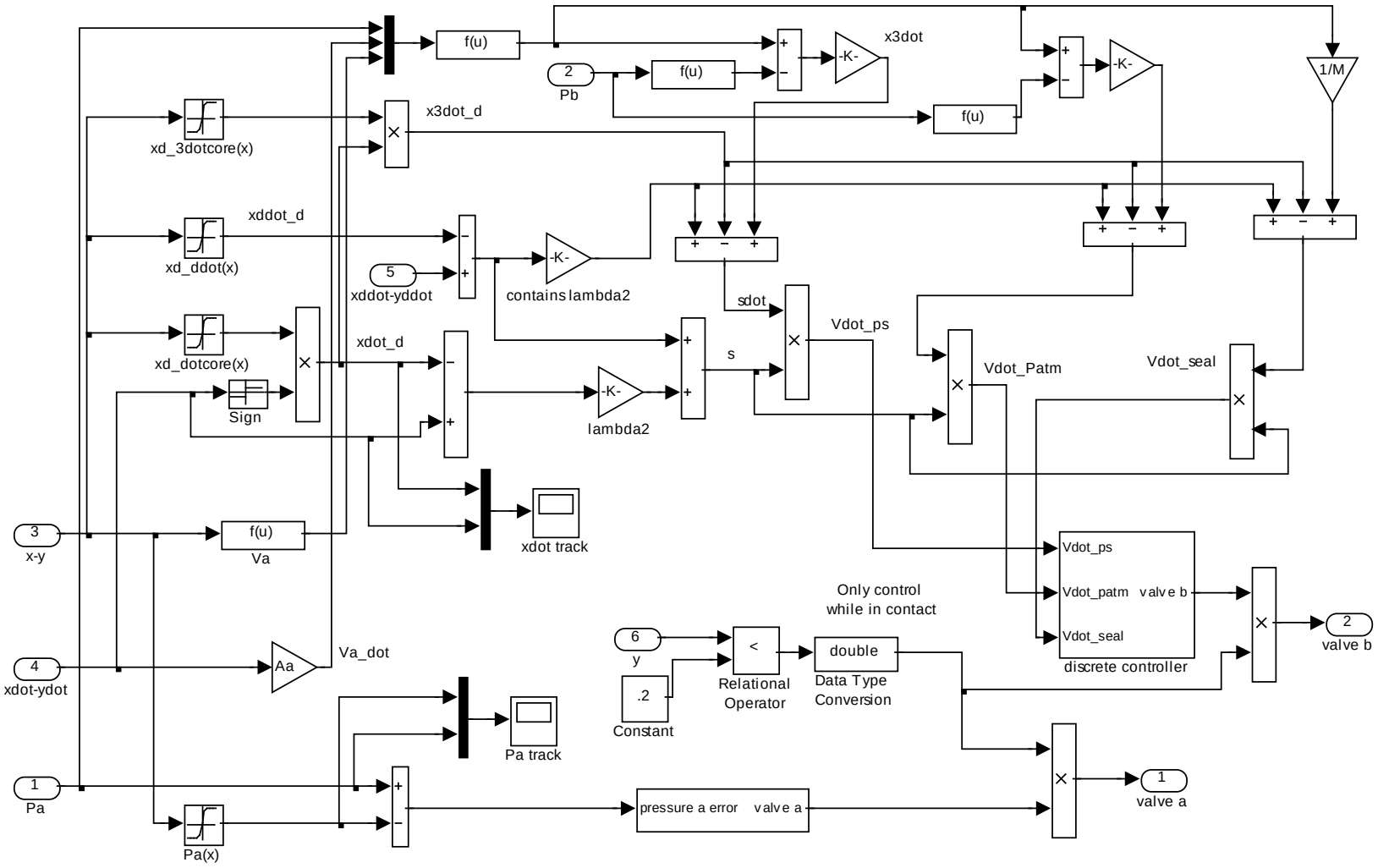

Figure C-5. Block diagram of the *controller* subsystem of hopping experiments implemented in manuscript 3.

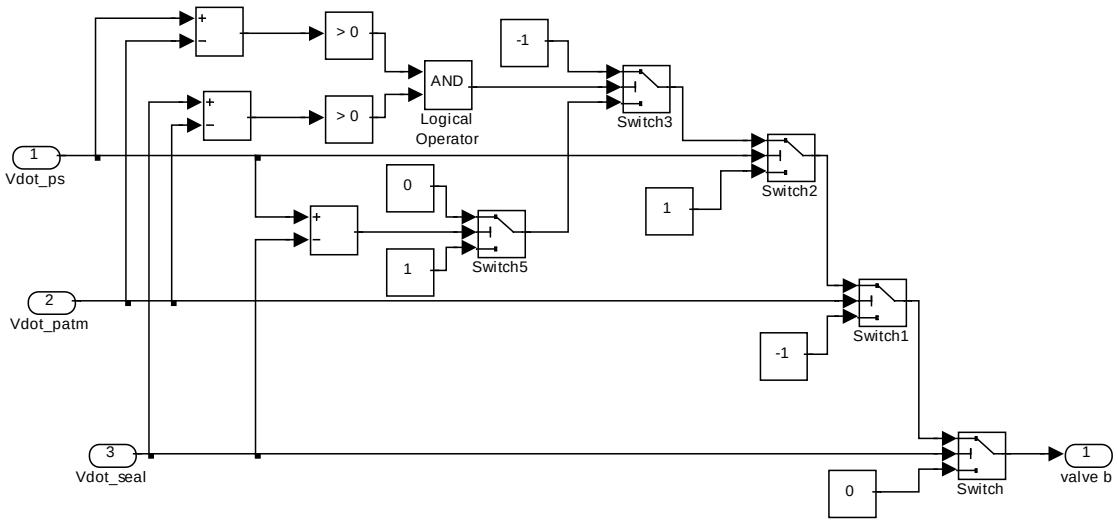

Figure C-6. Block diagram of the *discrete controller* subsystem of the hopping experiments implemented in manuscript 3.

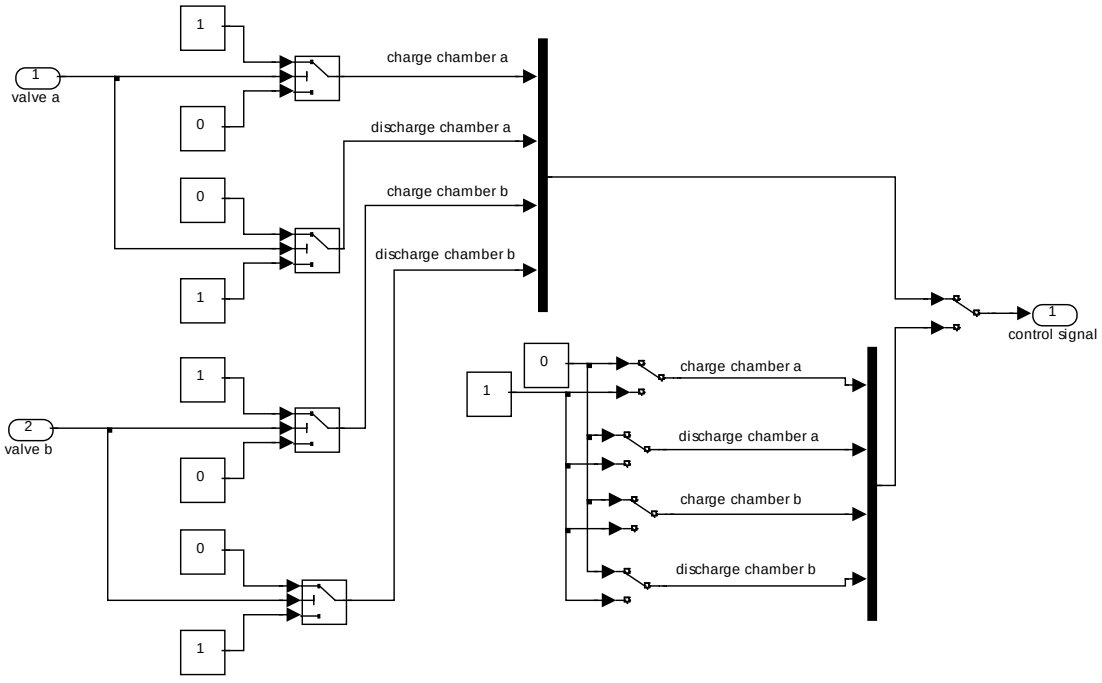

Figure C-7. Block diagram of the *valve logic* subsystem of the hopping experiments implemented in manuscript 3.